# MODELLING THERMAL CONDUCTIVITY OF OXIDE NANOFLUIDS

## A

## THESIS

**Submitted in partial fulfillment of the requirement for the award of degree of**

**Master of Engineering**

**In**

**Thermal Engineering**


**Submitted by**

**AKANKSHA MISHRA**

**(ROLL NO. 801083029)**



**UNDER THE GUIDANCE OF**

**DR. S.S. MALLICK**

**(ASSISTANT PROFESSOR)**

**Department of Mechanical Engineering**

**Thapar University, Patiala**

# CERTIFICATION

I, Akanksha Mishra, declare that this thesis report, submitted toward fulfillment of the requirements for the award of Master's degree in Thermal engineering, in the Mechanical Department, Thapar University, Patiala, is wholly my own work. This document has not been submitted for any degree at any other institution.

Akanksha

**Date:** 29/6/12

**Place:** Patiala

**Akanksha Mishra**

**801083029**

**Thapar University, Patiala**

This is to certify that the above statement made by the candidate is correct and true to the best of my knowledge

29/6/12

**Guide:**
**Dr. S.S. Mallick**
Assistant Professor
Mechanical Engineering Department
Thapar University, Patiala

**Countersigned by**

**Dr. Ajay Batish**
Professor and Head
Mechanical Engineering Department
Thapar University, Patiala

**Dr. S. K. Mahopatra**
Dean
Academic Affairs
Thapar University, Patiala

# ACKNOWLEDGEMENT

I wish to express my deep sense of gratitude to Dr. S.S. Mallick, Department of Mechanical Engineering, Thapar University, Patiala, for introducing the present topic and for their inspiring guidance, constructive criticism and valuable suggestion during thesis work.

Akanksha Mishra

801083029

Thapar University, Patiala.

**CONTENT** **PAGE NO.**

# Chapter 1: Introduction and Objectives

## 1.1 Introduction

Conventional heat transfer fluids widely used in industries (e.g. water, ethylene glycol and oil) generally suffer from inherently poor heat transfer characteristics, due to the lower values of thermal conductivity of these fluids (Choi, 1999). With an aim to enhance the thermal conductivity of conventional heat transfer fluids, Maxwell (1873) dispersed micrometer sized particles into conventional base fluids (Choi, 1999; Chon et al., 2005 and Chopkar et al., 2008). However, the problems occurring from the micrometer size particles are: rapid settlement, abrasion, fouling of components and clogging of flow passages (Kwak and Kim, 2005; Chon et al., 2005; Chopkar et al., 2008 and Das et al., 2007). In 1995, Choi created the concept of nanofluids (Choi, 1999) by suspending nano-sized metals, metal oxides, metal carbides and carbon nanotubes in conventional base fluids (such as water, ethylene glycol and oil) using techniques, e.g. ultrasonication and magnetic stirring (Sundar et al., 2007 and Das et al., 2007). Mainly due to their smaller sizes, nanofluids offer several advantages over conventional heat transfer fluids, such as superior thermal conductivity (due to large surface to volume ratio), long time stability, homogeneity and minimum clogging of flow passages (Xie et al., 2002 and Gallego et al., 2011). These novel properties make nanofluids attractive to various industries requiring heat transfer applications - such as microelectronics, transportation, biomedical, micro fluids, nuclear, automobile, power generation, x-ray, refrigerators etc (Chandrasekar et al., 2010 and Khanafer and Vafai, 2011).

In spite of such merits and wide spread potential applications of nanofluids, this technology is still limited for commercial use because there is yet no proven standardized design process for

accurately predicting important heat transfer properties, such as the nanofluids thermal conductivity. Certain theories have been proposed over the years by different researchers to explain the thermal conductivity enhancement, such as heat transfer due to Brownian motion of particles (Jang and Choi, 2004; Chon et al., 2005; Teng et al., 2010) and interfacial layer formation at solid-liquid interface (Murshed et al., 2008), but there seems to be no agreement between these different postulates. Because of the influence of various particle and fluid properties, such as the shape/size distribution of nanoparticles (Chon et al., 2005; Mintsa et al., 2007**;** Murshed et al., 2008 and Tang et al., 2010), volume concentration of nanoparticles in base fluids (Wang et al., 1999; Li and Peterson, 2006**;** Murshud et al., 2008 and Timofeeva et al., 2007), ultrasonication and storage time to prepare nanofluids (Timofeeva et al., 2007), use of surfactants (Murshed et al., 2008 and Lin et al., 2011), pH value (Xie et al., 2002) and temperature (Das et al., 2003; Li and Peterson, 2006; Mintsa et al., 2007; Murshud et al., 2008), developing accurate fundamental model for the thermal conductivity of nanofluids has always been a challenging task. There are few existing models to predict the thermal conductivity of solids-liquid mixture and nanofluids, such as Maxwell (1873); Bruggeman (1935); Jeffrey (1973); Yu and Choi (2003); Koo and Kleinstreuer (2004); Xie et al. (2005) are theoretical models and Chon et al. (2005); Li and Peterson (2006); Mintsa et al. (2009) and Teng et al. (2010) are empirical models. However, these models have not been tested for their scale-up accuracy and stability against a wide range of experimental data if they are to be used for future applications (especially, under industrial scale of operation). Hence there is because of these present limitations, for better understanding the heat conduction mechanism and systematically study of the effect of different parameters on thermal conductivity of nanofluids more studies have to be carried out.

## 1.2 Objectives

Specific objectives include:

i. To evaluate the effects of different particle properties and experimental conditions on nanofluids thermal conductivity.

ii. To evaluate the accuracy of existing models for thermal conductivity of nanofluids/ two phase system by comparing the calculated values with available experimental data.

iii. Development of new model of thermal conductivity of $Al_2O_3/TiO_2$-water nanofluid by using wide range of available experimental data in literature.

# Chapter 2: Literature Review

This chapter consist the brief review of concept of nanofluids, materials for nanoparticles and fluids, preparation of nanoparticles and nanofluids, characterization of nanoparticles and nanofluids, methods of measuring thermal conductivity of nanofluids and an extensive literature review of several research papers of nanofluids. Although the theoretical and empirical models of thermal conductivity of nanofluids are the part of literature review, these models are discussed in chapter 4.

## 2.1 Concept of nanofluids as existing technology

The thermal conductivity of heat transfer fluids has an essential role in the development of energy efficient heat transfer fluids (Das et al., 2007). The conventional heat transfer fluids (oils, water and ethylene glycol) suffer from poor thermal conductivity than those of solids. Many scientists and engineers have made many efforts towards poor thermal conductivity of conventional base fluids (Das et al., 2007). In 1873, Maxwell dispersed micrometer or millimeter size particles in liquids for better heat transfer property, this approach has two major technical problems i.e. micrometer or millimeter size particles settle rapidly in base fluids and at low particle concentration thermal conductivity of these suspensions are low (Das et al., 2007, Choi, 1999). So to overcome these problems a modern nanotechnology has come into picture. In 1995, Choi proposed the novel concept of suspension of nano-sized particles in a base fluid (commonly known as “nanofluids”) to improved thermal characteristics (such as thermal conductivity) of base fluids (Das et al., 2007 and Choi, 1999). Nanoparticles in base fluids overcome the

problems offered by micrometer or millimeter size particles such as rapid settlement, clogging, abrasion and fouling due to small size of particles (Das et al., 2007 and Choi, 1999).

### 2.2 Different nanoparticles and base fluids

Nanoparticles are the particles with average size below 100 nm. Nanopaericles have superior mechanical, electrical, optical, magnetic and thermal properties than that of conventional bulk materials due to coarse grain structure (Das et al., 2007).

(i) *Nanoparticle materials:* Nanoparticles which are used in nanofluids have made up of different materials such as meals (Al, Cu, Ag, Au, Fe), metal oxides ($Al_2O_3$, CuO, $TiO_2$, $WO_3$, $Fe_3O_4$, ZnO), nitride ceramics (AIN, SiN), carbide ceramics (SiC, TiC), carbon nanotubes and composite materials such as nanoparticle core polymer shell composites or alloyed nanoparicles $Al_{70}Cu_{30}$ (Das et al., 20007; Choi, 1999; Yoo et al., 2007; Zhu et al., 2006 and Yu et al., 2009).

(ii) *Base fluids:* Water, oil and ethylene glycol are commonly used as base fluid (Das et al., 2007, Choi, 1999; Yoo et al., 2007 and Timofeeva et al., 2007).

### 2.3 Synthesis of nanoparticles and nanofluids

Several nanoparticles have been prepared by physical process and chemical process (Kimoto et al., 1963; Granqvist and Buhrman, 1976; Gleiter 1989). Physical process includes inert gas condensation. In the gas phase condensation process evaporation of source material and very

quick condensation of vapor into nanometer size particles or loosely agglomerated clusters is done in inert, cool and reduced pressure atmosphere (Kimoto et al., 1963; Granqvist and Buhrrnan, 1976). A chemistry-based solution-spray conversion process proceeds with water-soluble salts of materials. This solution is then converted into an aerosol and a spray drying system is used for drying. Very quick vaporization of the solvent and Very quick precipitation of the solute remains the composition similar to that of the starting solution. The precursor powder is kept in a fluidized-bed reactor to evenly pyrolyze the mixture, drive out volatile constituents and make porous powders of a uniform fine homogeneous structure (Ashly, 1994).

If nanoparticles are made up of any of these methods there is some formation of agglomeration of individual particles. There is a technique for producing non-agglomerated nanoparticles involves condensing nanophase powders from the vapor phase directly into flowing low-vapor-pressure fluids. This approach is called the VEROS (Vacuum Evaporation onto a Running Oil Substrate) technique and this approach is developed by Akoh et al. (1978). VEROS has been essentially avoided by the nanocrystalline-materials community because of difficulties in subsequently separating the particles from the fluids to make bulk materials or dry powders. A modification of the VEROS technique developed in Germany (Wagener et al., 1997), Eastman et al. (1997) developed a direct evaporation system which is based on the modification of VEROS technique (Das et al., 2007 and Chon, 1999).

Stable suspension of nanoparticles into conventional base fluids (water, oil and ethylene glycol) i.e. nanofluids are prepared by two techniques: the single step technique and the two step technique (Das et al., 2007 and Chon, 1999). The single step method simultaneously prepare and disperse nanoparticles directly into conventional base fluids. The two step method first prepare

nanoparticles using physical or chemical process to prepare nanoparticles and disperses these nanoparticles into conventional base fluids (Das et al., 2007 and Choi, 1999). Ultrasonicator (Das et al., 2007) and magnetic stirrer (Sundar et al., 2007) are used to prepare nanofluids by two step technique, commonly bath or prob type ultrasonicator is used to prepare nanofluids (Das et al., 2007).

## 2.4 Characterization of nanoparticles and nanofluids

Characterization of nanoparticles after synthesis is very important step. Characterization of nanoparticles is done by following major steps:

**(i) X-ray Diffraction Analysis (XRD):** X-ray diffraction is an important technique to understand the properties of synthesis materials. X-ray diffraction is a fast technique and for XRD small amount of sample is required which is non destructive. With the help of data base of known structure XRD is used for the phase identification and XRD is also used to determine crystal structure of unknown materials, strain, crystal size, orientation of single crystal or polycrystalline materials (Cullity and Stock 2001; Suryanarayana and Norton 1998 and Waseda et al., 2001).

Cullity and Stock 2001; Suryanarayana and Norton 1998 and Waseda et al., 2001 explained the principle of operation of X-ray diffraction analysis, when X-rays are directed on the sample, electrons present in the material scatter the X-rays. Scattering results in maxima and minima of different intensity, if the material is crystalline. Bragg's law provides the conditions that must be satisfy for the reflected X-ray waves to be in phase with each other (constructive interference).

If conditions of Bragg's law are not satisfied, destructive interference reduces the reflected intensity to zero. Bragg's law is $m'\lambda = 2D\sin\Theta$. Here $\lambda$ is the X-ray wavelength, m' is an integer, $\Theta$ is the diffraction angle and D is the distance between crystal lattice planes. For each lattice spacing D, Bragg's law predicts a maximum at diffraction angle $\Theta$. An X-ray diffraction pattern is obtained when the intensity of detected X-rays is plotted as a function of diffraction angle $\Theta$. To identify the phase of tested sample XRD Patten is matched with the pure substance. The plot obtained from XRD analysis shows the characteristic of the sample material.

**(ii) Scanning Electron Microscopy (SEM):** Scanning Electron Microscopy is a powerful method to investigate the surface structures of mollicutes. SEM is standardized method for imaging and the measuring the dimensions of nanometer and micrometer size particles because of high imaging speed and high resolution of SEM (Buhr et al., 2009). This technique provides a large depth of field. SEM has relatively wide range of magnification which allows the investigator to easily focus in an area of interest on a specimen; an investigator may easily interpret SEM images (Stadtlander, 2007).

Gabriel (1985) discussed about the operating conduction and operation of SEM: the basic operating condition for SEM involves high vacuum with minimum contagion, properly aligned column and saturated filament to its effective operating temperature. After setting the basic operating condition, for a given specimen the optimal imaging conditions are controlled by spot size, accelerating voltage and focus. Prepared specimen should be clean and conductive. Sometimes the filament is not heated until high vacuum is maintained. The alignment of column is evaluated, after filament has been saturated. Alignment of electron gun is evaluated in reduced rapid or TV scan rate. In both the scanning mode, manipulate the gun X and Y electronic

controls until uniform bright and centered image in CRT is obtained. Focus the image at about 1000X in rapid or TV mode. Select a view field where symmetrical object is able to be seen. If the image is not expanding symmetrically from its centre, correct its asymmetry by manipulating the stigmators. If the stigmator is not able to correct the asymmetry, the final aperture is off axis. Then again correct the stigmators by moving the aperture X and Y. After correcting the asymmetry, set the magnification and evaluate the specimen. A series of images from low to high magnification is obtained to examine the specimen. After finishing the examination, filament should be cooled for minimum 3 minutes before chamber is subjected to atmospheric pressure.

**(iii) Transmission Electron Microscopy (TEM)**: Transmission electron microscopy (TEM) is also a standardized method for imaging and measurements of dimension of nano and micro size structures due to their high imaging speed and high resolution (Buhr et al., 2009). The advantage of TEM over SEM is that the specimen's cellular structures can be viewed at extremely high magnifications (Stadtlander, 2007).

Cullity and Stock (2001) explained the operation of TEM. TEM is a complex assembly of magnetic lenses, electron gun, a sample holder, several apertures and image viewing/ recording systems. Magnetic lenses are set into illuminating systems between sample and electron gun and those of imaging system after sample. There are three lenses in the imaging system and two condenser lenses in the illumination system. The traditional TEM mode adjusts condense lenses to illuminate the sample with approximately parallel beam. Beam covers sample area of several micrometer diameters at magnification lies between 20,000X and 100,000X. To control beam position or angle pre-specimen scanning or deflection coils are often used. In TEM to view the

diffraction pattern, the intermediate lens is set to focus on the back focal plane of objective lens. In the case of viewing the image the intermediate lens is adjusted so that its object plane is plane of image of the objective lenses. If all the transmitted beams and diffraction beams were directed to combine in the first intermediate image plane, resultant images would be of little contrast.

## 2.5 Measurement of thermal conductivity of nanofluids

Two types of methods are available for measuring the thermal conductivity of nanofluids: steady state methods and transient methods. Transient methods are best for accurate measurement of thermal conductivity of fluids/nanfluids. Steady state methods are less accurate than transient methods because in steady state methods heat lose cannot be quantified and may provide considerable inaccuracy and natural convection may also set in, which provides apparently higher value of thermal conductivity (Das et al., 2007).

Most popularly used methods of transient and steady state method in literature are discussed in detail:

### 2.5.1 Transient hot-wire method

***Principle of measurement:*** Transient hot wire method is most accurate, fast and widely used method for the measurement of thermal conductivity of. In this method a thin wire of metal is used as both a temperature sensor and a line heat source. Liquid whose thermal conductivity is measured surrounds the thin metallic wire. Thin metallic wire is heated by passing current through it. Now, if the thermal conductivity of the surrounding liquid is higher than there will be

lower rise in the temperature of wire. Experiment is preformed for short duration of time (2 to 8 seconds), so that natural convection cannot set. This is the principle on which this method works. The mathematical model for this method is given in equation 2.1 (Das et al., 2007):

$$K_{n_f} = \frac{Q}{4\pi(T_2 - T_1)} \ln \frac{i_2}{i_1} \tag{2.1}$$

To explain the working of transient hot wire apparatus specifications of Murshed et al. (2005) are considered i.e. platinum wire of 76 micrometer diameter and 215 mm length and container is of 80 ml and diameter of container is 20 mm. A schematic of the transient hot-wire apparatus used by Murshed et al. (2005) is given in Figure 2.1. As shown in Figure 2.1 main experimental cell is a part of the Wheatstone bridge circuit. Thin platinum wire is used as an arm of the Wheatstone bridge circuit. Platinum wire has been used because of higher electrical resistivity and order of higher magnitude than that of any other material and Platinum wire has temperature coefficient of resistance of $0.0039092^{o}$C which is higher than any other material (Das et al., 2007; Murshed et al., 2005). Wire should be of smaller diameter to act as a line heat source. The Wheatstone bridge circuit was balanced by adjusting the adjustable circuit resistance and ground resistance of A/D (analog to digital) converter input panel. Circuit was considered as balance circuit when there is no voltage change observed in A/D converter. When a uniform voltage is supplied to the circuit, the temperature and electric resistance of the wire rises and the output voltage is measured by an A/D convertor. The obtained data of temperature rise is linear against logarithmic time interval. The thermal conductivity is calculated from the slope of the rise in the wire's temperature against logarithmic time interval by the equation 2.1 (Das et al., 2007).

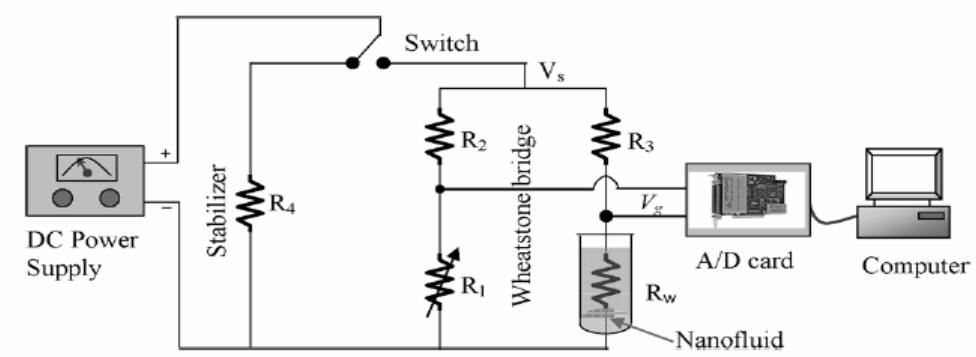


**Figure 2.1:** Schematic of transient hot wire experimental setup by Murshed et al., 2005.

### 2.5.2 Transient short-hot-wire (SHW) method

***Principle of measurement:*** Transient SHW technique is used to measure the thermal conductivity and thermal diffusivity of nanofluids simultaneously (Zhang et al., 2000). Zhang et al. (2000) explained the principle of operation of transient SHW technique in detail. Zhang et al. (2000) explained that (SHW) technique was developed from the conventional transient hot wire method. This technique is also based on the two-dimensional transient heat conduction numerical solution for a short wire of the same length-to-diameter ratio and boundary conditions as those used in the actual measurements. The thermal conductivity of nanofluids in transient SHW technique is calculated by equation 2.2 (Zhang et al., 2000):

$$K_{n_f} = \frac{VI}{2\pi h}.\frac{E}{e} \tag{2.2}$$

Coefficient E is calculated by the least-squares method for a relevant range of Fourier number corresponding to the periods of measurement. Coefficient e is also determined by the least-squares method for time range before the onset of natural convection.

To explain the working of this method specification of Zhang et al. (2000) are considered. Figure 2.2 shows the schematic of transient SHW cell. The SHW probe is set on the Teflon cap of the cell. A short platinum wire of 9.2 mm length and 97 micrometer diameter (1) is welded at the both ends to 1.5 mm diameter platinum lead wire (3) which is supported by a ceramic circular plate (2) and joined with voltage (5) and current (6) platinum lead wires of 0.5 mm diameter. A pure gold crucible (4) of 50 mm diameter and 120 $cm^3$ volume is heated with an electric furnace (8) which is outside covered with a thermal insulator (9). The temperatures at the outside wall of crucible are measured with thermocouples (7) to give a feedback signal for the temperature controller. The measurements have to carry at atmospheric pressure and different temperature levels. Platinum wire is welded to the platinum lead terminals. Alumina is used as a coated material which is 99.99% pure. The sputtering time is 6.4 h for $Al_2O_3$ film thickness of 2 micrometer. Sputtering apparatus provide a thin uniform film on the cylindrical wire. The measuring system of SHW technique is also shown in Figure 2.2. Measuring system is composed of a dc power supply current and voltage measuring system, digital multimeter, power input/output (PI/O) controller and personal computer. A maximum constant current of 1 A with 1.5 mA resolution cab be generated by power supply. When the liquid temperature becomes uniform and constant, a small current of 15 mA, is supplied to the probe for 3 s for the measurement of initial temperature of liquid. The switch is turned on to the dummy circuit. Dummy circuit is having the same resistance as the main circuit including the probe. A heating current of 0.3 to 0.5 A is supplied. When the current becomes stable (After 1 s,), the switch is closed to the main circuit to begin heating the hot wire. In this process, the voltage and current are measured 20 times per sec. All the measurements are carried out automatically using a personal computer.

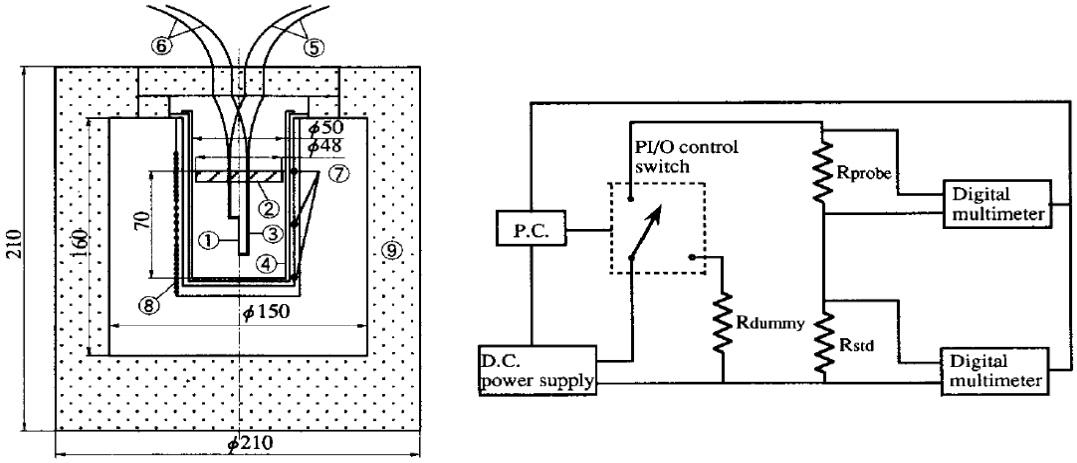


**Figure 2.2:** Schematic of experimental setup and measurement system by Zhang et al., 2000.

### 2.5.3 Temperature oscillation method

***Principle of measurement:*** The principle of thermal conductivity measurement is based on the propagation of temperature oscillation inside a cylindrical liquid volume. The measurement of thermal conductivity is based on energy equation for conduction which is given by equation 2.3:

$$\frac{1}{\alpha}.\frac{\partial T}{\partial t} = \nabla^2 T \tag{2.3}$$

The assumptions for the equation 2.3 in this case are the test fluid is isentropic and thermo physical properties are constant and uniform with time throughout the entire specimen volume. Das et al. (2003) explained the experimental set up and procedure for the measurement of thermal conductivity. Experimental set up by Das et al. (2003) is shown in Figure 2.3. Das et al. (2003) described that this technique consist of a specially fabricated test cell (1) which is cooled by cooling water (2) at both of the ends. Cooling water is coming from a thermostatic bath (3).

Electrical connection provides DC power which is obtained through a converter (4). The temperatures are measured in the test section with the help of number of thermocouples and the responses are amplified with amplifier (5). Amplifier (5) is followed by a filter which is fed to the data acquisition system (6). The data logger in data acquisition system is, in turn connected to a computer (7). Temperature of the fluid is controlled by proper adjustment of the cooling water coming from the thermostatic bath. For higher temperatures, it is sometimes necessary to increase the input voltage to obtain the required temperature level which is then tuned to the required temperature by adjusting or maintain the cooling water temperature. The test section is also shown in Figure 2.3 which is a flat cylindrical cell. The frame of the cell is made of Polyoxymethylene, which acts as the first layer of insulation. The frame consists of a main part with 40 mm hole. Hole act as cavity to hold the test fluid. Frame also consist two end plates which sandwiches the Peltier element and water cooler at both ends. The hole is closed from both sides by disk type reference material of 15 mm thickness and 40 mm diameter. The space formed for the test fluid is 8 mm thickness and 40 mm diameter. The fluid is filled through a small hole in the cell body. The temperatures are measured at three locations—at the interface of the reference layer and the Peltier element, the central axial plane of the test fluid and at the interface of the test fluid and the reference layer. For this purpose, Ni-CrNi thermocouples of 0.1 mm in diameter were used at the interfaces and 0.5 mm in diameter at the central plane, for stability consideration. The thermocouples are put in small groove at the interfaces and welded at the tip, whereas the thermocouple at center is hanging from the wall. The entire cell is insulated. The temperature of the reference material is periodically oscillated by two peltier elements (40 mm×40 mm square) from two ends. For example an oscillated temperature recorded at the locations after reaching steady oscillation. It can be observed that the amplitude of the

temperature oscillation produced by Peltier element gets attenuated and its phase shifts as it crossed the reference material. It is further shifted and attenuated as it reaches the center of the test fluid. Thermal diffusivity of the fluid can be calculated very accurately by considering amplitude attenuating of thermal oscillation from the boundary fluid to the center of the fluid. For direct thermal conductivity measurement one has to consider the attenuation at the reference material. Since the reference material has been worked upon and inhomogenity and microcracks of material brings out uncertainty in its value of thermal conductivity, so the direct evaluation of thermal conductivity of fluid is not very accurate. Hence the value of thermal diffusivity for the nanofluid is evaluated from experiment. Density can be measured and specific heat can be calculated by: $C_{nf} = \frac{m'_p C_p + m' C_f}{m'_p + m'_f}$

Finally the thermal conductivity is calculated by equation 2.4 (Das et al., 2003):

$$K_{nf} = \alpha_{n_f} \rho_{n_f} C_{nf} \tag{2.4}$$

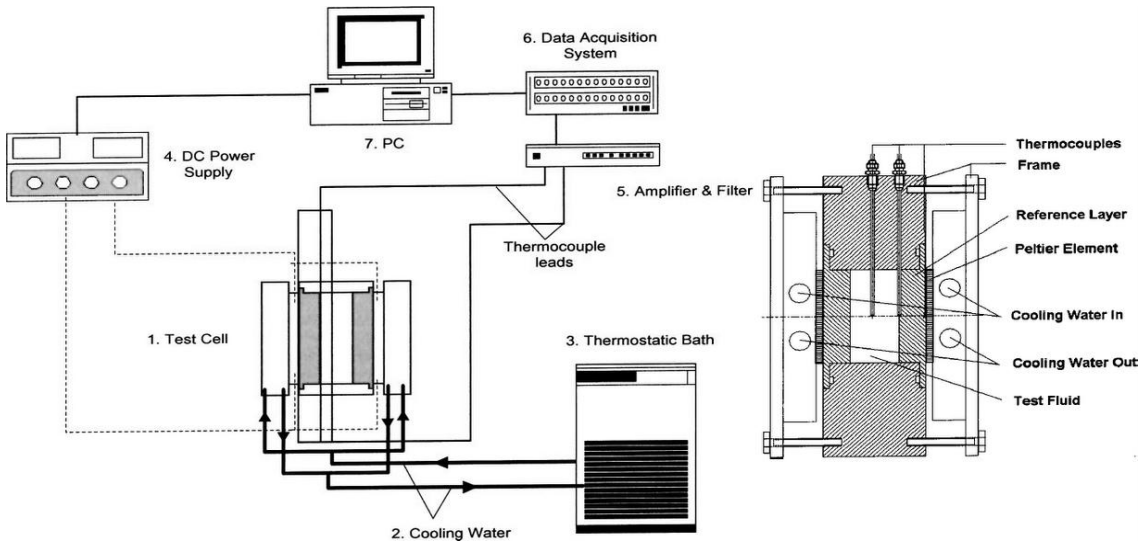


**Figure 2.3:** Schematic of experimental setup and test cell by Das et al., 2003

### 2.5.4 Steady-state parallel-plate method

***Principle of measurement:*** This method is used to measure the thermal conductivity of nanofluids, this method requires very small amount of liquid sample. Wang et al. (1999) used this method to measure the thermal conductivity of $Al_2O_3$ and CuO nanofluids. Figure 2.4 shows the experimental setup. Fluid sample is placed between two parallel round copper plates. The surface of the fluid sample is slightly higher than the lower surface of upper plate. Any gas bubbles are avoided when fluid sample is filled into the cell. The cross-sectional area of the upper plate is 9.552 $cm^2$. Both the copper plates are separated by three small glass spacers. Each glass spacer is of 0.9652 mm in thickness and a total surface area of 13.76 $mm^2$. Liquid cell is housed in a larger aluminum cell to control the temperature of liquid cell. The top copper plate is centered and away from the inside wall of the aluminum cell. There is a hole of 0.89 mm diameter is drilled in aluminum cell and copper plates. Temperature is measured by inserting E-type thermocouples (nickel–chromium/copper– nickel) into these holes. Because the thermal conductivity of copper is much higher than the thermal conductivity of the liquid, thermocouples provide temperatures at the surfaces of the plates. Total 14 thermocouples are used. At the time of experiment heater 1 gives the heat flux from upper plate to lower plate. Uniformity in temperature of the lower copper plate is maintained by heater 4. Heaters 2 and 3 are used to increase the temperature of the aluminum cell to that of the upper plate to eliminate radiation and convection losses from the upper copper plate. The temperature difference between the inside wall of the aluminum cell and upper copper plate is less than $0.05^oC$, during all measurements. The uniformity of temperature in the top and the bottom plates is better than $0.02^oC$. The difference of temperature between the two copper plates varies from 1 to $3^oC$. All the heat

supplied by heater 1 is flows between both the copper plates. The overall thermal conductivity across the two copper plates, adding the effect of the three glass spacers, can be calculated by the one-dimensional heat conduction equation 2.5:

$$K = (P.X_g)/(a_c \Delta T) \tag{2.5}$$

Where, Xg=0.9652 mm, ac=9.552 $mm^2$. Thermal conductivity of nanofluids is calculated by equation 2.6:

$$K_{nf} = \frac{K.a_c - K_g.a_g}{a_c - a_g} \tag{2.6}$$

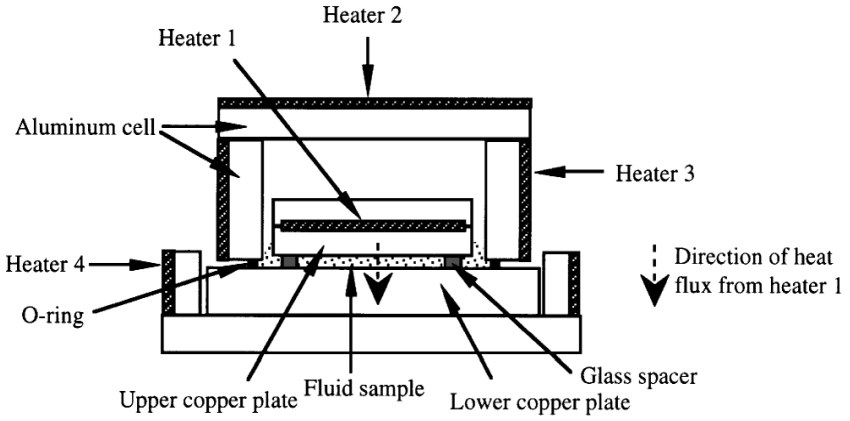


**Figure 2.4:** Schematic of experimental set up by Wang et al., 1999.

### 2.5.5 Steady state method (traditionally referred to as a "Cut-Bar Apparatus")

.

***Principle of measurement:*** This steady state method which is referred as cut-bar apparatus had used for measuring the thermal conductivity of porous media and other materials (Li and

Peterson, 2006). This method could be modified and extended to measure the thermal conductivity of nanofluids. Li and Peterson (2006) used this method to measure the thermal conductivity of $Al_2O_3$ based nanofluds. Figure 2.5 shows the schematic of apparatus. A pair of copper rods of 2.54 cm diameter is separated by O-ring to form a test cell setup. Several thermocouples (6) are located in copper bars to measure the surface temperature and heat flux. Experimental test set up has to place in a vacuum chamber to perform experiments. Vacuum environment should be less than 0.15 Torr. By measuring the temperature differences in the copper bars, the heat flux in a traditional cut-bar apparatus can be determined. Then averaging the computed heat fluxes. Using the heat flux obtains from equation 2.7 and surface temperature calculate by averaging the temperature obtained from thermocouples, the thermal conductivity of nanofluids can be calculated by equation 2.8:

$$Q = K_{copper} a_{bar} \frac{\Delta T_{bar}}{\Delta Z_{bar}} \tag{2.7}$$

$$K_{nf} = [Q(\Delta Z c_{ell} / \Delta T_{cell}) - K_{oring} a_{oring}] / a_{cell} \tag{2.8}$$

The test facility was calibrated to initiating the experimental test program. The two copper bars were aligned vertically and to ensure good contact, a load was applied using a load screw. Hence, an air tight seal for the test cell. The sample was charged through the lower sample charge inlet until the suspension filled the test cell setup and exited the charge outlet shown in Figure 2.5.

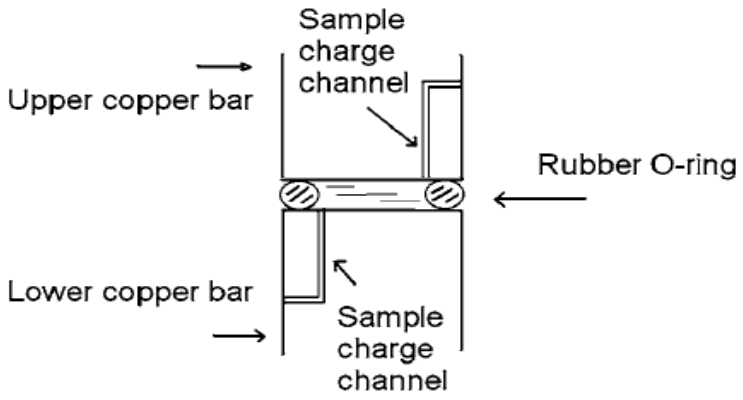


**Figure 2.5:** Schematic of experimental setup by Li and Peterson, 2006.

KD2Pro is a commercially available instrument to measure thermal conductivity of nanofluids. It works on the transient line heat source method to measure thermal conductivity.

## 2.6 Experimental work done by the other researchers

Wang et al. (1999) investigated effective thermal conductivity of nanofluid, $Al_2O_3$ nanoparticles of average diameter 28 nm dispersed in water and ethylene glycol. One-dimensional, steady-state parallel-plate method was used for the measurement of thermal conductivity. Experiments were performed at room temperature (297 K). Thermal conductivity ratio ($K_{nf}/K_f$) was found to increase with increase in volume fraction of nanopowders in base fluid. At volume fraction of approximately 5 and 8% of $Al_2O_3$ powders in ethylene glycol, effective thermal conductivity increased to 26 and 40%, respectively. Three sample preparation techniques were used to disperse $Al_2O_3$ in water: mechanical blending, coating particles with polymers and filtration. Filtration showed largest enhancement in thermal conductivity i.e. 12% at 3% $Al_2O_3$ volume

fraction in water. The enhancement in thermal conductivity was found to be more with ethylene glycol than water at 3% volume fraction.

Xie et al. (2002) investigated the effect of specific surface area of the dispersed $Al_2O_3$ nanoparticles, pH value of aqueous suspension, crystalline phase of $Al_2O_3$ and thermal conductivity of base fluid on the thermal conductivity of nanofluids. Transient hot-wire method was used to measure the thermal conductivity of nanofluids. $Al_2O_3$ nanoparticles of αA5 (302 nm), αA25 (60.4 nm), αA58 (26 nm), αA101 (15 nm), and ϒA58 (26 nm) were used. Water and ethylene glycol are used as base fluids. Experimental results showed that thermal conductivity of αA25/water nanofluid increased with increase in volume fraction, but with different slopes for different pH values (2, 4, 7 and 11.5). It was mentioned in the paper that at lower pH values, rise in thermal conductivity was marginally higher than at the higher pH values. Enhancement in thermal conductivity ratio decreased with an increase in pH value for water as base fluid. Experimental data of $Al_2O_3$ naoparticles dispersed in ethylene glycol showed that thermal conductivity enhancement increased almost linearly with increase in volume fraction of nanoparticles. At 0.05 volume fraction the enhancement of thermal conductivity was more than 29% for αA25/ ethylene glycol nanofluids. At volume fraction 0.05 enhancement of thermal conductivity first increased up to 25 $m^2g^{-1}$ specific surface area and then decreased with increase in surface area.

Das et al. (2003) investigated the thermal conductivity of water based $Al_2O_3$ nanofluid. Nanoparticles were produced by vapor synthesis method Ultrasonic vibration was used to

disperse 38.4 nm size $Al_2O_3$ particles into distilled water. A temperature oscillation technique was used to measure thermal conductivity. Experimental results showed that with 1% volume fraction of $Al_2O_3$ nanoparticles, enhancement in thermal conductivity ratio was about 2% and 10.8% at 21°C and 51°C, respectively. At 4% volume fraction, the enhancement in thermal conductivity ratio was 9.4 to 24.3% with temperature variation from 21 to 51°C. The average rate of increase of enhancement of thermal conductivity in case of 4% volume fraction was much higher than that of 1% volume fraction of $Al_2O_3$ nanoparticles.

Li and Peterson (2006) used steady state method to determine the experimental thermal conductivity of nanofluid. $Al_2O_3$ nanoparticles were prepared by a gas condensation technique. Area weighted diameter and density of $Al_2O_3$ nanoparticle was 36 nm and 3600 $kg/m^3$, respectively in gamma crystal phase. $Al_2O_3$ nanoparticles were dispersed in distilled water at 2, 4, 6 and 10% volume fractions. The powder and base fluid were mixed by immersing the suspension in an ultrasonic bath for 3 hours to get well dispersed suspension of nanoparticles. With increase in volume fraction the rate of increase of thermal conductivity of $Al_2O_3$ /water nanofluid was nearly twice and three times at mean sample temperatures of 32.5±0.3°C and 34.7±0.3°C, respectively compared to that obtained for mean sample temperatures of 27.5±0.3°C. It was concluded in Li and Peterson (2006) paper, the thermal conductivity ratio increased with increase in temperature at each volume fraction. At a temperature of 34°C the effective thermal conductivity of $Al_2O_3$-water was increased by a factor of 1.3. Two-factor linear analysis based on volume and temperature factor was used, which is discussed in detail in chapter 4.

Yoo et al. (2007) provided experimental data for thermal conductivity of $Al_2O_3$ nanoparticles dispersed into deionized water. Two step method was used to disperse the nanoparticles into base fluid. Mean size of $Al_2O_3$ particles was 48 nm. For the dispersion of nanoparticles, ultrasonic cell disrupter generating ultrasonic pulses of 700W at 20 kHz was used. To measure the thermal conductivity of nanofluids, transient hot-wire method was used. To perform experiments 0.3, 0.5, 0.7 and 1% volume fraction of $Al_2O_3$ nanoparticles were used. Experimental results showed that there was only 4% enhancement in thermal conductivity at 1% volume fraction of $Al_2O_3$ nanoparticles.

Mintsa et al. (2007) experimentally investigated the thermal conductivity of water based $Al_2O_3$ nanofluid. Average particle size of 36 and 47 nm were used for the preparation of $Al_2O_3$ nanofluids. Experiments were performed at 3, 6 and 9% volume fractionas of $Al_2O_3$ nanoparticles and at temperature range from 20 to 40ºC. For the measurement of thermal conductivity, KD2Pro thermal analyzer was used. Results showed that thermal conductivity of nanofluids increased with temperature and volume fraction of nanoparticles. Authors observed that between 20 and $40^oC$, an average increase in thermal conductivity of nanofluid was approximately 16% for each type of nanofluids (prepared at 3, 6 and 9% volume fraction).

Zhang et al. (2007) measured the effective thermal conductivity of water based $Al_2O_3$ nanofluid using transient short hot wire technique. Spherical $Al_2O_3$ particles of average diameter 40 nm were dispersed into deionized water. Measurements showed that value of thermal conductivity of nanofluids at low volume concentration did not change over a period of 48 hrs. Measured

effective thermal conductivity ratio as a function of mass fraction (10, 20 and 40%) of $Al_2O_3$ particle was obtained at different temperatures of 10, 30 and 50$^oC$. The effective thermal conductivity of nanofluid increased with increase in temperature and particles concentration.

Li and Peterson (2007) investigated the thermal conductivity of $Al_2O_3$–water nanofluid using steady state method. $Al_2O_3$ nanoparticles of 36 nm and 47 nm were dispersed in distilled water at volume concentration ranges from 0.5 to 6%. Thermal conductivity of nanofluid was measured for a temperature range from 27 to 37°C. It was reported that thermal conductivity enhancement was 3% at 0.5% volume concentration. For $Al_2O_3$ particles of 36 nm, at 2% volume fraction thermal conductivity enhancement of nanofluid was increased from 7.7% at 27.9 °C to 18.1% at 35.0°C. For $Al_2O_3$ particles of 36 nm, at 6% volume fraction the thermal conductivity enhancement of nanofluid was increased from 11% at 27.5°C to 28% at 35.8°C. For $Al_2O_3$ particles of 47 nm, at temperature of 28°C the thermal conductivity enhancement of nanofluid was 2.9, 3.5, 9.7 and 10.9% at 0.5, 2, 4 and 6% volume concentration, respectively. For $Al_2O_3$ particles of 47 nm, at temperature of 35°C thermal conductivity enhancement of nanofluid was 3.4, 9.3, 21.2, and 26% at 0.5, 2, 4, and 6% volume concentration, respectively.

Timofeeva el al. (2007) investigated the thermal conductivity of $Al_2O_3$-water/ethylene glycol nanofluids. $Al_2O_3$ particles of nominal diameters of 11, 20 and 40 nm were dispersed into water and ethylene glycol and mixture was continuously sonicated for 5 to 20 hours in an ultrasonic bath. To measure thermal conductivity KD2Pro thermal analyzer was used. The ranges of volume fraction of $Al_2O_3$ nanoparticles for experimentation were 0.5 to 10 and all the experiments are performed at 23°C. Experimental results showed that thermal conductivity of

water based $Al_2O_3$ nanofluid increased with increase in volume fraction. At a fixed volume fraction, 40 nm size particles showed highest enhancement and 20 nm particles showed smallest enhancement of thermal conductivity for $Al_2O_3$-water nanofluid. Enhancement of thermal conductivity for 11 nm particles size lies between 40 and 20 nm $Al_2O_3$-water nanofluid. For $Al_2O_3$-ethylene glycol nanofluids, the results of thermal conductivity enhancement were almost same for all the particle sizes (11, 20 and 40 nm). So the nominal particle size does not have significant effect on the thermal conductivity enhancement of $Al_2O_3$-ethylene glycol nanofluid. Their results also showed that at the same volume fraction of $Al_2O_3$ particles, higher thermal conductivity enhancement is found in ethylene glycol than in water. They observed the temperature dependence of the thermal conductivity of water and ethylene glycol nanofluids with 5% volume of 40 nm $Al_2O_3$ particles in the range from 10 to 65°C. It concluded that the enhancement in nanofluids relative to base fluids is essentially temperature independent.

Zhu et al. (2009) investigated the thermal conductivity of $Al_2O_3$-water nanofluid at different pH and sodium dodecylbenzenesulfonate (SDBS) concentration. Two-step method was used for the preparation of $Al_2O_3$-water nanofluid. Dispersion of nanoparticles was good in the presence of sodium dodecylbenzenesulfonate (SDBS) dispersant. Good dispersion of $Al_2O_3$ nanoparticles was found at pH value of 8. Thermal conductivity of nanofluid increased with an increase in concentration of nanopartcles with maximum enhancement of thermal conductivity up to 10.1% at 0.15% weight fraction. Thermal conductivity of $Al_2O_3$-water nanofluid was improved by adding sodium dodecylbenzenesulfonate (SDBS) dispersant.

Beck et al. (2009) investigated the thermal conductivity of $Al_2O_3$-water/ethylene glycol nanofluids. Nanofluids were prepared by dispersing $Al_2O_3$ nanoparticles of diameter 8-282 nm in water/ethylene glycol and pH value of the solution was adjusted to 4 by adding Hydrochloric acid. It was reported that below 50 nm particle size enhancement of thermal conductivity decreased as particle size decreases.

Chandrasekar et al. (2010) investigated the thermal conductivity of $Al_2O_3$–water nanofluid. Microwave assisted chemical precipitation method was used to synthesis $Al_2O_3$ nanoparticles. $Al_2O_3$ nanoparticles of diameter 43 nm were dispersed into water at different volume concentration i.e upto 3% at room temperature. For the measurement of thermal conductivity KD2Pro was used. Thermal conductivity enhancement of $Al_2O_3$-water nanofluids were 1.64, 3.28, 3.43, 7.52 and 9.7% at 0.33, 0.75, 1, 2 and 3% volume fraction. They developed a theoretical model which is discussed in chapter 4.

Gallego et al. (2011) investigated the thermal conductivity of $Al_2O_3$- ethylene glycol nanofluid. Nanofluid sample was prepared by dispersing dry $Al_2O_3$ nanoparticles in ethylene glycol. The nanoparticles had diameter distribution from 40 to 50 nm and a crystal phase composition of 70:30 of $\Upsilon$ and $\delta$ phases, respectively. The Decagon devices KD2Pro Thermal Properties analyzer was used to measure thermal conductivity. Thermal conductivity of ethylene glycol-based $Al_2O_3$ nanofluids was measured at temperatures of 283.15, 303.15, and 323.15 K. The volume fractions had varied between 1.5 to 8.6%. Thermal conductivity increased with an increase in nanoparticle volume fraction Average enhancement of thermal conductivity of

nanofluid was varied from 3% at the lowest volume fraction up to 19% for the highest concentration.

### 2.7 Different mechanisms for change in thermal conductivity for nanofluids

Jang and Choi (2004) postulated that Brownian motion of nanoparticles is a key mechanism at molecular and nanoscale level to govern the thermal behavior of nanofluids. They derived theoretical model (which is discussed in chapter 4) that accounts for the fundamental role of dynamic nanoparticles in nanofluids.

Chon et al. (2005) used $Al_2O_3$ nanoparticles of 11, 47 and 150 nanometer diameter to prepare $Al_2O_3$–water nanofluids. Miniaturized thermal conductivity device which is based on transient hot wire method is used to measure thermal conductivity of nanofluids. Experiments to measure thermal conductivity of nanofluids were performed at 1 and 4% volume concentration of $Al_2O_3$ nanoparticles and temperature range from 21 to 71$^{o}$C. Authors developed an empirical correlation for nanofluid thermal conductivity ratio (discussed in detail in chapter 4). Data obtained from measured $Al_2O_3$ nanofluid thermal conductivity normalized by base fluid thermal conductivity at specified temperature and experimental correlation was shown at different particle size and volume fraction. They observed that thermal conductivity ratio ($K_{nf}/K_f$) increased with increase in temperature and decrease in size of nanoparticles. This paper described that Brownian velocity is considered as the key mechanism describing the temperature dependency of nanoparticle thermal conductivity than any other factor. So it was stated that at

higher temperature, thermal conductivity of nanofluid increases due to increased nanoparticle Brownian velocity.

Murshed et al. (2008) used $Al_2O_3$ nanoparticles of 80 and 150 nm diameters to prepare nanofluids. Water and ethylene glycol were used as base fluids. For the better stability of any dispersion of nanoparticles into base fluids Cetyl Trimethyl Ammonium Bromide (CTAB) surfactant (about 0.01 mm) was used. Transient hot wire method was used to measure the thermal conductivity. From the experimental data it was stated that at a temperature of 60$^o$C, the effective thermal conductivity of ethylene glycol based $Al_2O_3$ (80 nm) nanofluid increased by 9 and 12% for 0.5 and 1% volume fraction of nanoparticles, respectively. Authors developed theoretical models for thermal conductivity of nanofluids by considering the effect of interfacial layer (discussed in chapter 4). They concluded that other than particle size and volume fraction, the interfacial layer has significant role to enhance the thermal conductivity of nanofluids.

Teng et al. (2010) investigated the effect of temperature, weight fraction and size on thermal conductivity ratio of water based $Al_2O_3$ nanofluid. $Al_2O_3$ particles of diameter 20, 50 and 100 nm were dispersed in water using ultrasonic vibration technique at different weight fraction of 0.5, 1, 1.5 and 2% to prepare nanofluids. To measure the thermal conductivity of nanofluid at 10, 30 and 50$^o$C KD2Pro was used. This paper represented the Brownian diffusion coefficient $D_0$ expressed by the Einstein Stokes equation:

$$D_o = \frac{K_B T}{3\pi\mu(d_p/10^9)} \tag{2.9}$$

Equation shows that Brownian diffusion coefficient is directly proportional to the temperature and reciprocal to diameter of particles. It implied that the added particles of smaller diameter and at higher temperatures would result in more severe collisions among particles, which led to better thermal conduction. It also implied that the thermal conductivity increment under high temperature and small particle size would be higher than that under low temperature and large particle size. When the temperature of experimental sample was $10^{o}$C, the thermal conductivity ratios of nanofluid could be enhanced by 1.8 to 6.5% at 20 nm, 0.8 to 6.0% at 50 nm and 0.4-5.6% at 100 nm, as the temperature of the samples rise to $30^{o}$C the thermal conductivity ratios could be enhanced by 5.1-12.8% at 20 nm, 1.4-6.9% at 50 nm and 0.7-5.3% at 100 nm and as the temperature of the samples rise to $50^{o}$C the thermal conductivity ratios could be enhanced by 6.7 to14.7% 20 nm, 2.3 to 7.3% at 50 nm, and 1.2 to5.6% at 100 nm. Using these experimental data, the enhanced thermal conductivity ratio for water based $Al_2O_3$ nanofluid could be expressed in terms of temperature, weight fraction and particle size. Empirical equation which showed the results of regression analysis is discussed in chapter 4.

# Chapter 3: Evaluation of Effects of Different Particle Properties and Experimental Conditions on Nanofluids Thermal Conductivity

Following work has been carried out using experimental data obtained from various past researches work on $Al_2O_3$ based nanofluids. For this purpose, digitize software has been used to create data bank of thermal conductivity of nanofluids from several research papers. Efforts are done to obtain useful and comparative results from digitize data.

Experimental data obtain from Chon et al. (2005) is shown in Figure 3.1.

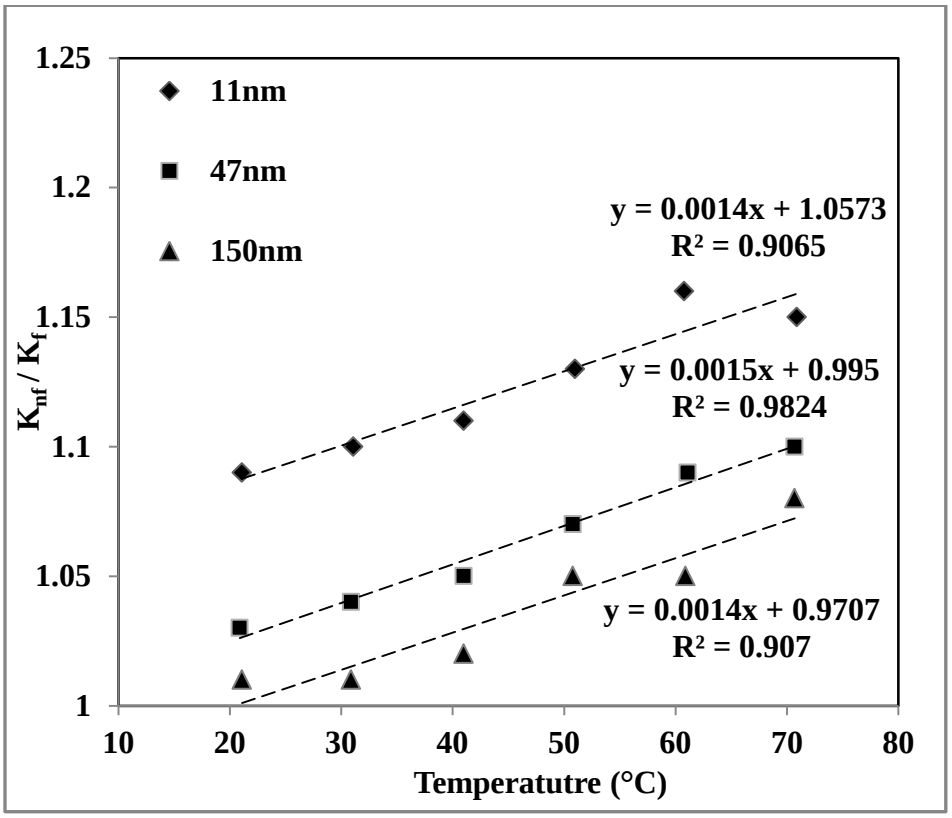


**Figure 3.1:** Comparison of thermal conductivity ratio verses temperature for $Al_2O_3$-water nanofluid (using Chon et al., 2005 data).

Figure 3.1 shows thermal conductivity ratio verses temperature graph at 1% volume concentration with different size of $Al_2O_3$ nanoparticles i.e. 11, 47 and 150 nm diameter dispersed in deionized water. In order to obtain the trend of increase of thermal conductivity

ratio, suitable trend lines are drawn for each particle size with their corresponding equation and $R^2$ (R: correlation coefficient) values. It is concluded from the Figure 3.1 that there may be linear variation of thermal conductivity ratio with temperature. It would have been better if more data points would have been included between temperature range from 20°C to 70°C. So with more data points clear trend can be established with more confidence. It is concluded from Figure 3.1 that with decrease in size of $Al_2O_3$ nanoparticles and increase in temperature thermal conductivity ratio increases and at a fixed temperature and at a fixed volume fraction thermal conductivity ratio increases with decrease in size of nanoparticles.

Experimental data obtain from Murshud et al. (2008) is shown in Figures 3.2, 3.3 and 3.4.

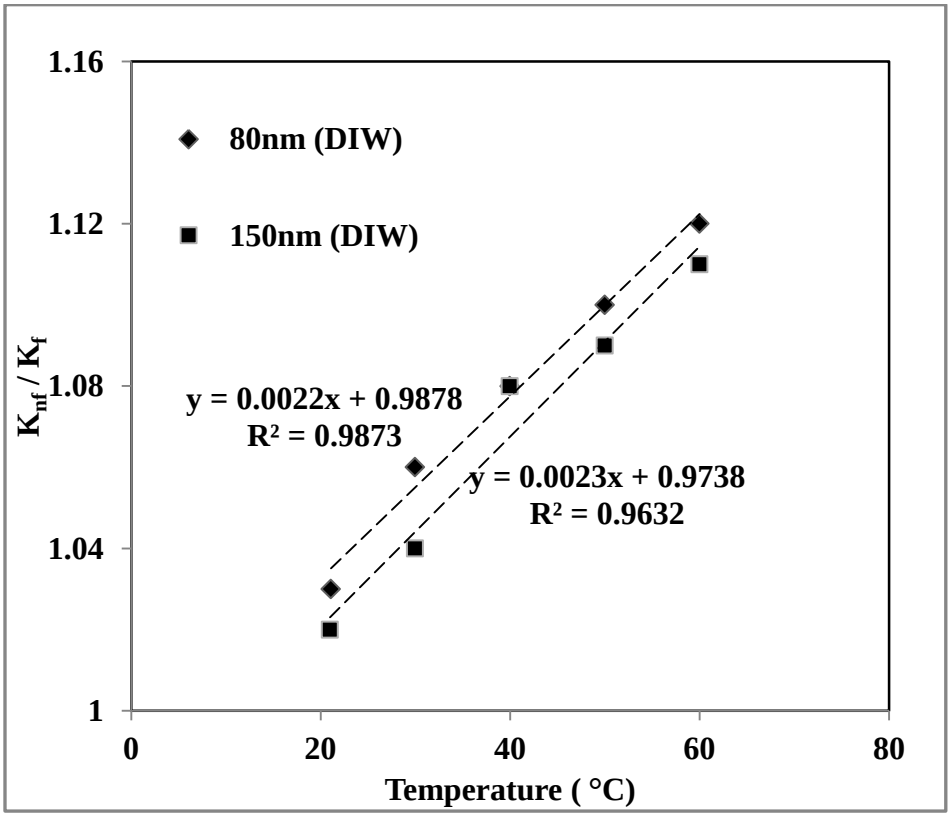


**Figure 3.2:** Comparison of thermal conductivity enhancement with temperature for $Al_2O_3$/water based nanofluids (using Murshud et al., 2008 data).

Figure 3.2 shows consolidated data obtained from different graphs of $Al_2O_3$-water based nanofluids. The variation of thermal conductivity ratio with temperature at 1% volume fraction of $Al_2O_3$ nanoparticles and at different sizes of $Al_2O_3$ nanoparticles i.e. 80 and 150 nm diameter is shown in Figure 3.2. $Al_2O_3$ particles of 80 nm in deionized water show higher enhancement in thermal conductivity ratio $Al_2O_3$ particles of than 150 nm with linear trend. At 40$^oC$ $Al_2O_3$ particles of 80 and 150 nm show same value of thermal conductivity ratio i.e. 1.08.

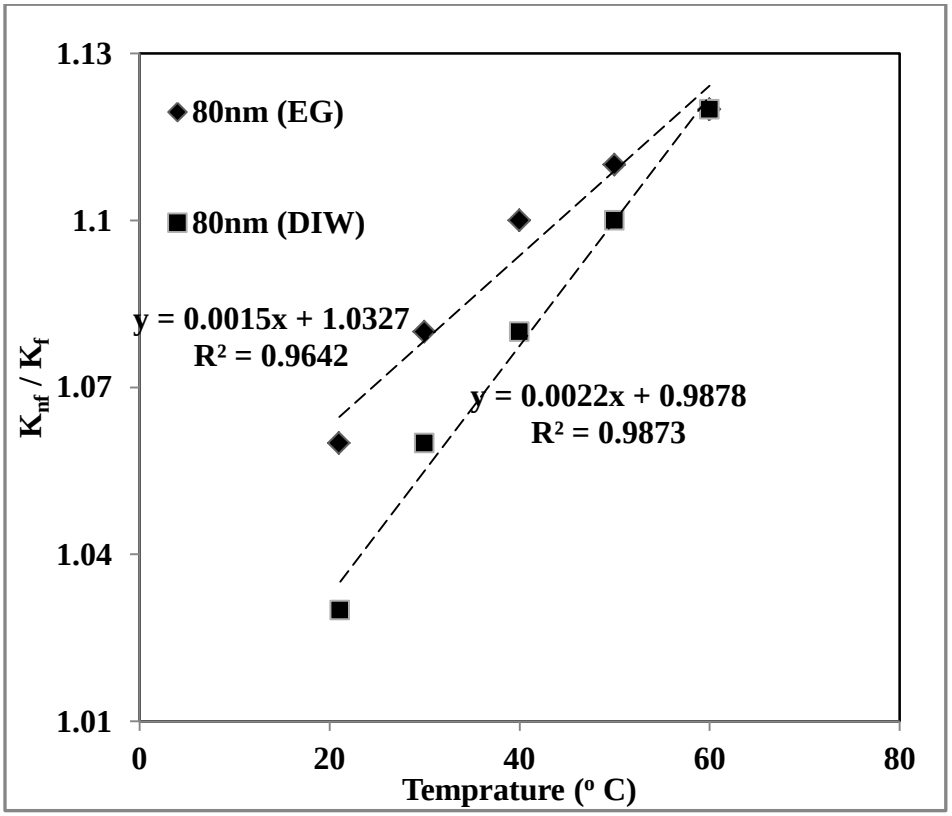


**Figure 3.3:** Comparison of thermal conductivity enhancement with temperature for $Al_2O_3$-water and $Al_2O_3$-ethylene glycol based nanofluids (using Murshud et al., 2008 data).

Figure 3.3 shows consolidated data from different graphs of $Al_2O_3$-water and $Al_2O_3$-ethylene glycol based nanofluids. As shown in Figure 3.3 $Al_2O_3$ particles of 80 nm diameter in ethylene

glycol show higher thermal conductivity ratio than $Al_2O_3$ particles of 80 nm diameter in deionized water at 1% volume fraction with linear trend. As temperature increases, data points of both nanofluid ($Al_2O_3$-water and $Al_2O_3$-ethylene glycol) are coming closer to each other (trend lines are converging) and at 60$^o$C data points of both the fluids ($Al_2O_3$-water and $Al_2O_3$-ethylene) are showing same value of thermal conductivity ratio i.e. 1.12. If there would have been more data points, then the trend could be more clear and results would be predicted with more accuracy.

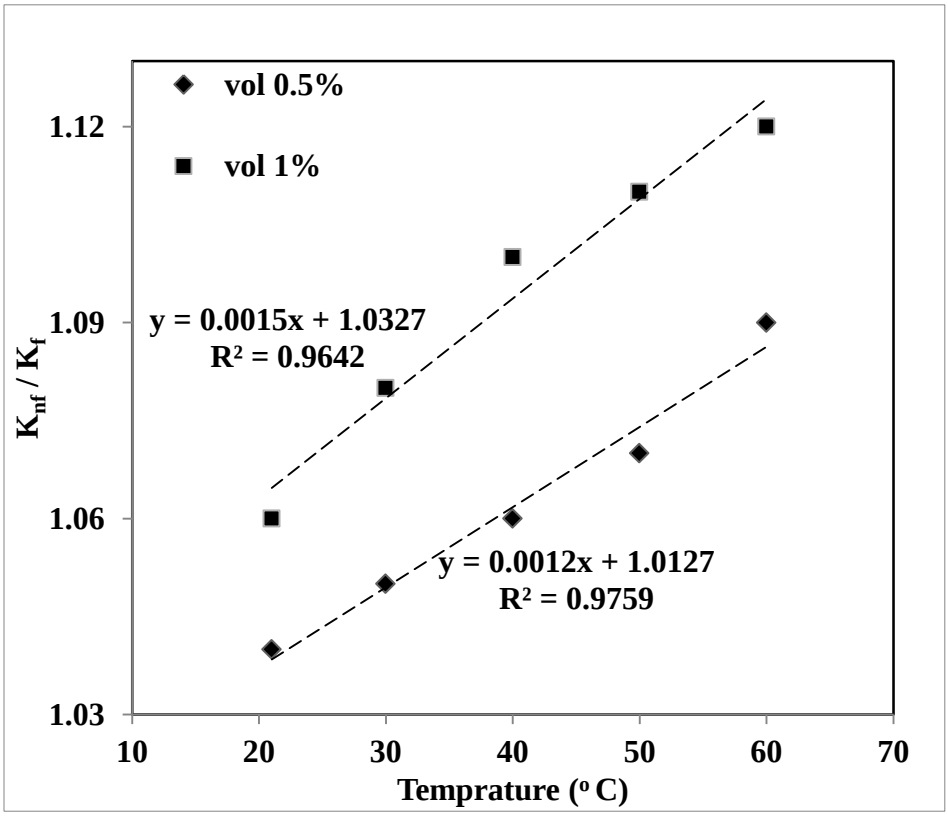


**Figure 3.4:** Comparison of thermal conductivity enhancement with temperature for $Al_2O_3$-ethylene glycol based nanofluids (using Murshud et al., 2008 data).

Figure 3.4 shows that at 1% volume fraction 80 nm diameter $Al_2O_3$ particles in ethylene glycol provides higher thermal conductivity ratio than 0.5% volume fraction with linear trend. So it is concluded that for any particle size thermal conductivity ratio increases with increase in temperature, thermal conductivity ratio increases with decrease in particle size with some discrepancy (Figure 3.2 and Figure 3.3) and $Al_2O_3$-ethylene glycol nanofluid shows more enhancement in thermal conductivity ratio than $Al_2O_3$- water nanofluid for same particle size and with increase volume fraction of $Al_2O_3$ nanoparticles thermal conductivity ratio increases.

Experimental data obtained from Tang et al. (2010) is shown in Figures 3.5, 3.6 and 3.7.

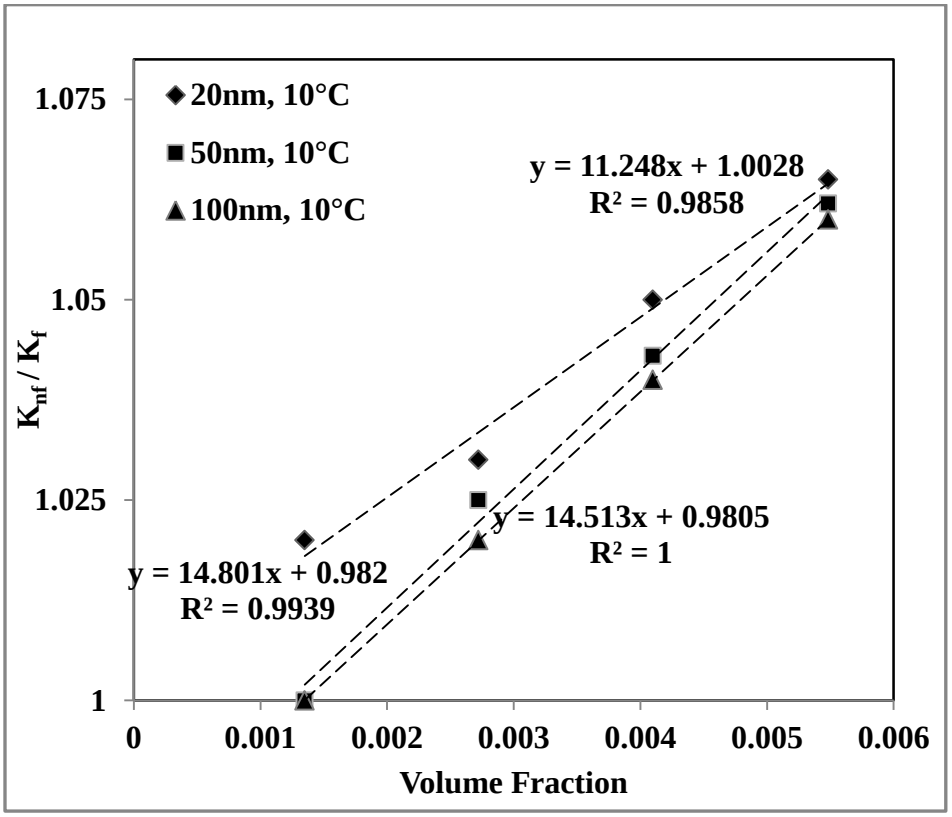


**Figure 3.5:** Comparison of thermal conductivity ratio of $Al_2O_3$-water nanofluid verses volume fraction with different particle sizes at $10^oC$ (using Tang et al., 2010 data).

Figure 3.5 is showing thermal conductivity ratio increases as size of $Al_2O_3$ nanoparticles decreases with linear trend. At volume fraction of 0.135, 0.41 and 0.55% $Al_2O_3$ particles of 50 and 100 nm diameter are overlapping. At volume fraction of 0.55% $Al_2O_3$ particles of 20, 50 and 100 nm diameter are overlapping. Nanoparticles of 50 nm and 100 nm diameter are showing marginal difference in thermal conductivity ratio. Trend of enhancement of thermal conductivity ratio would be more clear if there would have been more data points.

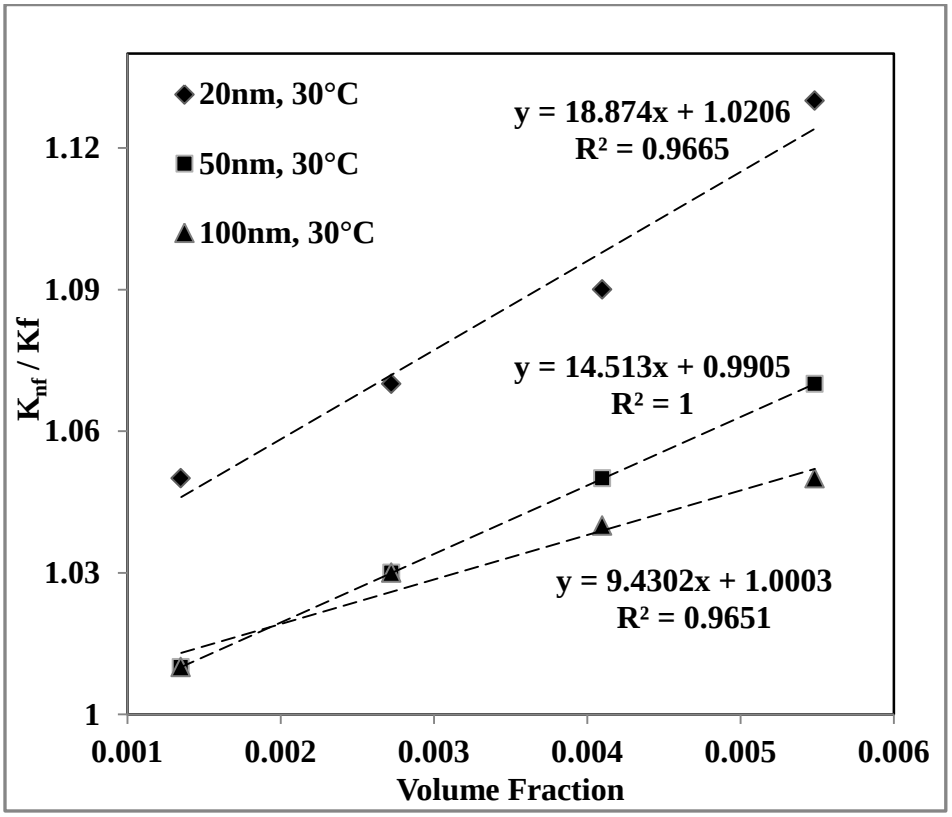


**Figure 3.6:** Comparison of thermal conductivity ratio of $Al_2O_3$-water nanofluid verses volume fraction with different particle sizes at 30$^o$C (using Tang et al., 2010 data).

Figure 3.6 shows $Al_2O_3$ particles of 20 nm diameter gives highest enhancement in thermal conductivity ratio than 50 and 100 nm diameter with linear trend. Data points of 50 and 100 nm diameter are overlapping at volume fraction of 0.135 and 0.2755% and as volume fraction increases, data points of both particles (50 and 100 nm diameter) are divergent from each other,

i.e. trend lines are converging at 0.135% of volume fraction then as volume fraction increases they start diverging.

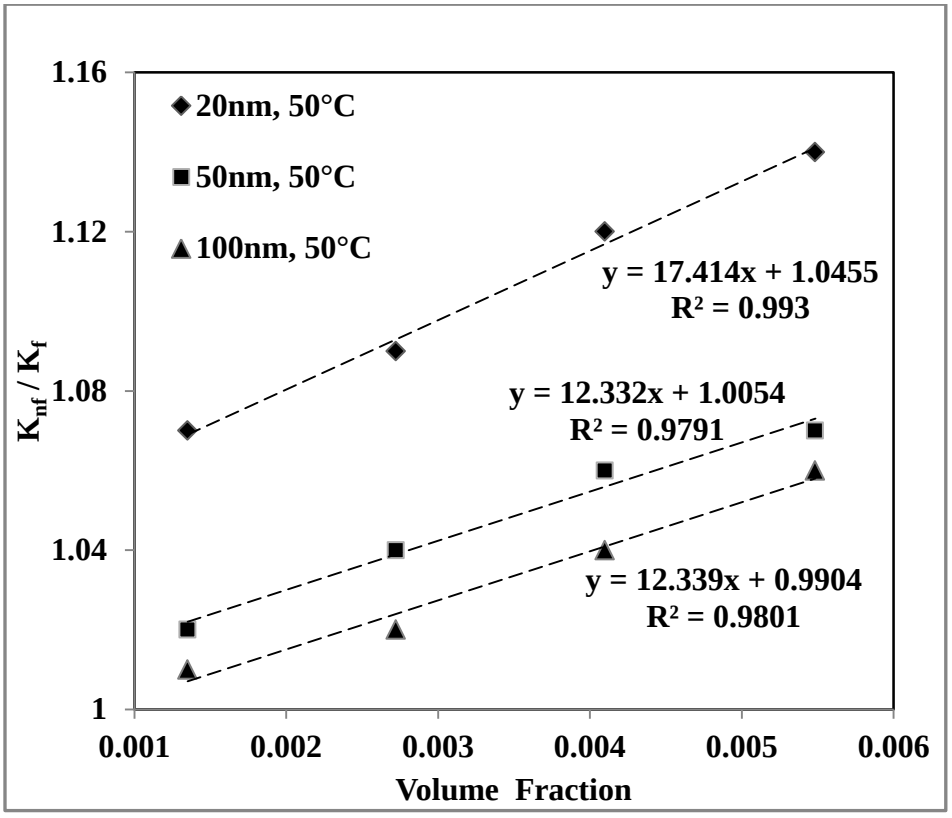


**Figure 3.7:** Comparison of thermal conductivity ratio of $Al_2O_3$-water nanofluid verses volume fraction with different particle sizes at 50$^o$C (using Tang et al. (2010) data).

Figure 3.7 shows thermal conductivity ratio increases with decrease in particle size at 50$^o$C with linear trend. $Al_2O_3$ particles of 20 nm diameter show highest thermal conductivity ratio than $Al_2O_3$ particles of 50 and 100 nm diameter. So, it is concluded that with increase in volume fraction thermal conductivity ratio increases and with decrease in size thermal conductivity ratio increases at particular temperature with some discrepancy (Figure 3.6). It is clearly seen from Figures 3.5, 3.6 and 3.7 that as temperature increases (10, 30 and 50$^o$C), the data pints of thermal

conductivity ratio for different particle sizes 10 nm, 20 nm and 100 nm are going away from each other.

Comparison between experimental data of Murshud et al. (2008) and Chon et al. (2005) is shown in Figure 3.8. At same $Al_2O_3$ particle size (150 nm in diameter), same volume concentration (1%), temperature range between 20$^o$C to 70$^o$C, transient hot wire technique was used to measure thermal conductivity and water as base fluid data obtained from both the papers shows different enhancement in thermal conductivity ratio. This variation in enhancement in thermal conductivity may be due to manufacturing method of nanofluid, different sonification time and different pH.

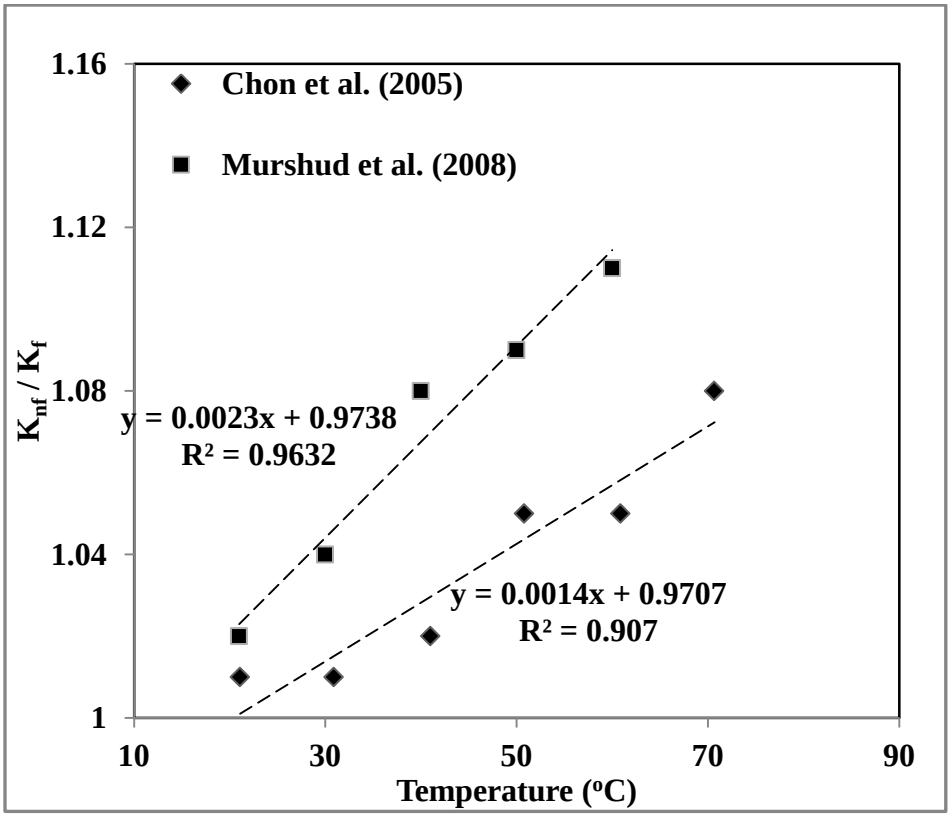


**Figure 3.8:** Comparison of thermal conductivity ratio verses temperature for $Al_2O_3$-water nanofluid (using Murshud et al., 2008 and Chon et al., 2005 data)

Experimental data obtaind from Timofeeva et al. (2007) is shown in Figure 3.9.

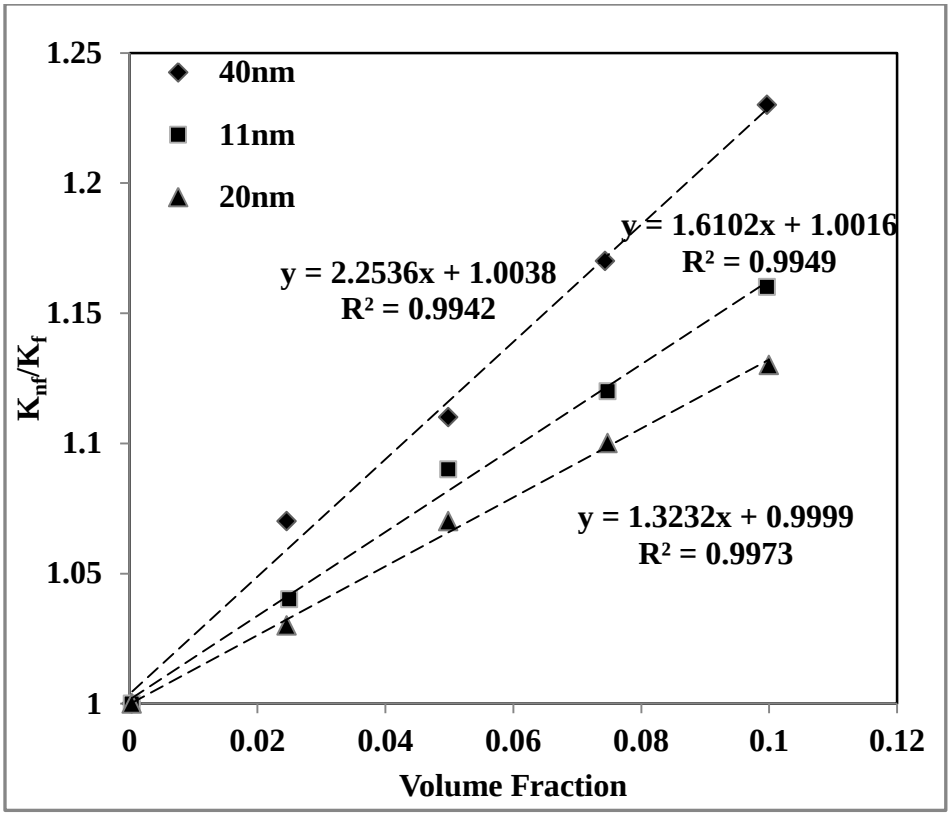


**Figure 3.9:** Comparison of thermal conductivity ratio verses volume fraction of $Al_2O_3$-water nanofluid at 23$^oC$ (using Timofeeva et al., 2007).

Figure 3.9 shows that at fixed volume fraction, particle of 40 nm diameter shows highest enhancement and particles of 20 nm diameter shows smallest enhancement of thermal conductivity and enhancement of thermal conductivity for 11 nm diameter particles lies between 40 and 20 nm particles. Results of Timofeeva et al. (2007) are contradicting from the results of Chon et al. (2005) and Tang et al. (2010) which show that at fixed temperature and at fixed volume fraction with decrease in nanoparticles size thermal conductivity ratio increases.

# Chapter 4: Evaluation of Theoretical and Empirical Models for Thermal Conductivity of Nanofluids

To evaluate the accuracy of the existing theoretical and empirical models of nanofluid thermal conductivity, some theoretical and empirical models have been evaluated in this chapter against a wide range of experimental data for Alumina-water based nanofluids. Towards the letter part of this thesis work, some additional similar work has been done for $Tio_2$-water based nanofluids as done for Alumina-water based nanofluids.

## 4.1 Experimental data of $Al_2O_3$ and $Tio_2$ based nanofluids

For the purpose of evaluating the effects of different particles and base-fluids properties on the thermal conductivity of nanofluids, predictions with of existing models and developing new models (discussed in chapter 5), the following data on $Al_2O_3$-water (DI) nanofluids (table 4.1) and $TiO_2$-water (DI) nanofluids (table 4.2) have been used.

**Table 4.1:** Physical Properties of $Al_2O_3$-Water Nanofluids

| **Reference** | **Particle average diameter (nm)** | **Volume fraction (%)** | **Temperature (°C)** |
|---|---|---|---|
| Das et al. (2003) | 38.4 | 1 to 4 | 21 to 51 |
| Chon et al. (2005) | 11, 47, 150 | 1, 4 | 21 to 71 |
| Yoo et al. (2007) | 48 | 0.3, 0.5, 0.7, 1 | 20 |
| Li and Peterson (2006) | 36 | 2, 6, 4, 10 | 27.5s, 32.5, 34.7 |
| Zhang et al. 2007 | 20 | 3, 14 | 5 to 50 |
| Timofeeva et al. 2007 | 11, 20, 40 | Up to 10 | 23 |

| | | | |
|---|---|---|---|
| Murshed et al. 2008 | 80, 150 | 1 | 20 to 60 |
| Teng et al. 2010 | 20, 50, 100 | 0.1 – 0.5 | 10, 30, 50 |

**Table 4.2:** Physical Properties of $TiO_2$-Water Nanofluids

| **Reference** | **Particle average diameter (nm)** | **Volume fraction (%)** | **Temperature (°C)** |
|---|---|---|---|
| Turgut et al. (2009) | 21 | 0.002 to 0.03 | 23 |
| He et al. (2009) | 21 | 0.000312 to 0.012 | 22 |
| Duangthongsuk and Wongwises (2009) | 21 | 0.002 to 0.02 | 15-35 |
| Yoo et al. (2007) | 25 | 0.001, 0.005,0.0 1 | 20 |
| Murshed et al. (2009) | 15 | 0.01 to 0.04 | 20 |
| Zhang et al. (2007) | 40 | 0.606, 1.24, 2.574 | 30 |

Room temperature: 20 $^{o}$C

## 4.2 Theoretical and empirical models for thermal conductivity of nanofluids

In this section theoretical and empirical models for thermal conductivity of nanofluid are discussed. Theoretical models such as Maxwell (1873); Bruggeman (1935); Jeffrey (1973); Yu and Choi (2003); Koo and Kleinstreuer (2004); Xie et al. (2005) and empirical models such as Chon et al. (2005); Li and Peterson (2006); Mintsa et al. (2009); He et al. (2009);

Duangthongsuk and Wongwises (2009) and Teng et al. (2010) have been used in the present study for comparing the experimental results with predicted values (for evaluating the models for their accuracy). Other discussed models such as Jang and Choi Model (2004); Jung and Yoo Model (20009) and Chandrasekhar et al. (2010) are not evaluated because these models are product specific. Hamilton-Crosser Model (1962) is not evaluated because for spherical shape particles this model becomes same as Maxwell Model (1873). Spherical shape particles of $Al_2O_3$ and $TiO_2$ are used in this study.

*Maxwell Model (1873)*

Maxwell was one of the earlier researchers to analytically investigate the heat conduction phenomenon through suspended particles (Das et al, 2007). This model (equation 4.1) is believed to be more suitable for micro to mm sized particles with low volume concentrations of particles, where the interaction amongst the particles can be neglected (Vajjha and Das, 2009; Das et al., 2008). However, because of its popularity (Das et al, 2007), the model has been selected here for evaluation.

$$K_{nf} = \frac{K_p + 2K_f + 2(K_p - K_f)\phi}{K_p + 2K_f - (K_p - K_f)\phi} K_f \tag{4.1}$$

*Bruggeman Model (1935)*

This model was proposed to analyze the interactions among randomly distributed particles. For a binary mixture of homogeneous spherical inclusions, the Bruggeman model is given by equation (4.2) (Vajjha and Das, 2009).

$$\phi \frac{K_p - K_{nf}}{K_p + 2K_{nf}} + (1-\phi) \frac{K_f - K_{nf}}{K_f + 2K_{nf}} = 0 \tag{4.2}$$

*Hamilton-Crosser Model (1962)*

This model was developed to measure the thermal conductivity of particle-fluid mixture. This model is based on the sphericity of particles, volume fraction of particles and the thermal conductivity of particles and fluid. When the particles are spherical with value of sphericity 1, Hamilton-Crosser equation becomes the same as the Maxwell's equation (Zhang et al., 2007). Hamilton-Crosser model given by equation (4.3) can be used for any shape of particles i.e. arbitrary particles (Yu et al., 2007).

$$\frac{K_{nf}}{K_f} = \frac{K_p + (n'-1)K_f - (n'-1)\phi(K_f - K_p)}{K_p + (n'-1)K_f + \phi(K_f - K_p)} \tag{4.3}$$

Where, n' = 3/ψ

*Jeffrey Model (1973)*

Jeffery (1973) studied the heat conduction through random, stationary and homogenous suspension of spherical shape particles in uniform conductivity matrix. The model (as given equation 4.4, neglecting higher order terms) is reported to be applicable for spherical shaped particles with low volume fraction (Jeffrey, 1973).

$$\frac{K_{nf}}{K_f} = 1 + 3\phi\beta + \phi^2\left\{3\beta^2 + \frac{3\beta^3}{4} + .....\right\} \tag{4.4}$$

*Yu and Choi Model (2003)*

In this model, Maxwell's model (equation 4.1) was modified by considering the effect of ordered liquid nano-layer around the nanoparticles on the thermal conductivity of nanofluids. Nano-layer has an impact on thermal conductivity of nanofluids when diameter of nanoparticles are less than 10 nm (Yu and Choi, 2003). Nanolayer thickness is taken as 1 nm (as employed by Yu and Choi, 2003; Xie et al., 2005; Murshed et al., 2008) for all calculations in this thesis.

$$\frac{K_{nf}}{K_f} = \frac{K_p + 2K_f + 2(K_p - K_f)(1+\gamma)^3\phi}{K_p + 2K_f - (K_p - K_f)(1+\gamma)^3\phi} \tag{4.5}$$

*Jang and Choi Model (2004)*

They derived theoretical model that accounts for the fundamental role of dynamic nanoparticles in nanofluids. Four modes of energy transport in nanofluids were: (i) collision between base fluid molecules, (ii) the thermal diffusion in nanoparticles in fluids, (iii) collision between nanoparticles due to Brownian motion and (iv) thermal interactions of dynamic nanoparticles with base fluid molecules (Jang and Choi, 2004*)*. A derived model for the thermal conductivity of nanofluids is given by equation (4.6):

$$K_{nf} = K_f(1-\phi) + K_p\phi + 3C_1\frac{d_f}{d_p}K_f\,\mathrm{Re}_{dp}^{\,2}\,\mathrm{Pr}\,\phi \qquad (4.6)$$

Where, $C_{R.M} = \frac{D_o}{l_f}, D_o = \frac{K_B T}{3\pi\mu d_p}, \mathrm{Re}_{dp} = \frac{C_{RM} d_p}{\nu}$

Above equation (4.6) includes (i), (ii) and (iv) modes of energy transport in nanofluids.

*Koo and Kleinstreuer Model (2004)*

This model considered the effect of thermal conductivity due to both Brownian motion and conventional static part on the effective thermal conductivity of nanofluids. This model takes into consideration the effects of particle dynamics. For the calculation of thermal conductivity of static part, Maxwell's model is to be used (equation 4.1). Two versions of thermal conductivity models were provided to include Brownian motion of particles, as given by equation (4.8) (version 1) and (4.9) (version 2).

$$K_{nf} = K_{static} + K_{Brownian} \tag{4.7}$$

$$K_{Brownian} = 37.5^2 \times 75\sqrt{\frac{18}{\Pi}} p\psi\phi\rho_p C_p \sqrt{\left(\frac{K_B}{\rho_P}\right)}\sqrt{\frac{T}{d}}\sqrt{\frac{L}{d}} f(T,\phi) \tag{4.8}$$

$$K_{Brownian} = 5\times 10^4 \psi\phi\rho_l C_l \sqrt{\left(\frac{K_B}{\rho_P}\right)}\sqrt{\frac{T}{d}} f(T,\phi) \tag{4.9}$$

Where, $\frac{L}{d} = 1$

$f(T,\phi) = (-6.04\phi + 0.4705)T + (1722.3\phi - 134.63)$

For $Al_2O_3$-water nanofluids and ϕ> 1%, $\psi = 0.0017(100\phi)^{-0.0841}$

Expectation value of particles to move in one direction (p) is 0.197 (Koo, 2004). $f(T,\phi)$ is valid for 1% <ϕ < 4% and 300K<T<325 K.

*Xie et al. Model (2005)*

Xie et al. (2005) considered the effect of interfacial nanolayer at the solid-liquid interface with linear thermal conductivity distribution and proposed a model for the thermal conductivity of nanofluids by including volume fraction, nanolayer thickness at particle-fluid interface, size of nanoparticles, thermal conductivity of nanoparticles and base fluids. The model is given by equation 4.10. The model is used for low volume fractions of nanoparticles in base fluids (Xie et al., 2005). Nanolayer thickness is considered as 1 nm (Yu and Choi, 2003; Xie et al., 2005; Murshed et al., 2008) for the purpose of calculation in this thesis.

$$\frac{K_{nf}-K_f}{K_f}=3\Theta\phi_T+\frac{3\Theta^2\phi_T{}^2}{1-\Theta\Phi_T} \tag{4.10}$$

Where, $$\Theta=\frac{B_{lf}\left[(1+\gamma)^3-\frac{B_{pl}}{B_{fl}}\right]}{(1+\gamma)^3+2B_{pl}B_{lf}};B_{pl}=\frac{K_p-K_l}{K_p+2K_l};B_{fl}=\frac{K_f-K_l}{K_f+2K_l};B_{lf}=\frac{K_l-Kf}{K_l+2K_f}$$

$$K_l=\frac{K_f M^2}{(M-\gamma)\ln(1+M)+\gamma M};\phi_T=\phi(1+\gamma)^3;\gamma=\frac{\delta}{r_p};M=\alpha(1+\gamma)-1$$

*Jung and Yoo Model (20009)*

Jung and Yoo (2009) proposed the expression of nanofluids thermal conductivity. Proposed model consist three modes i.e stationary model, mode of single particle motion and interparticle interaction mode. Stationary mode simply deals with Maxwell model (equation 4.1). Single particle motion mode taken into account the Brownian motion. Interparticle interaction mode deals with the nanofluid thermal conductivity derived from kinetic theory about the motion of particle induced by EDL (electrical double layers). By taking into consideration all the three modes, the expression of thermal conductivity of nanofluid is given in equation 4.11:

$$K_{nf}=K_{Maxwell}+K_{Br\,ownian}\left(1+\frac{K_{EDL}}{K_{Browniian}}\right) \tag{4.11}$$

Where, $K_{Br\,ownian}=\frac{nl_pC}{3}\frac{K_BT}{3\pi\mu d_p l_f}$, $K_{EDL}=\frac{nl_pC}{3}\frac{\sqrt{Aq^2l_p}}{\sqrt{\varepsilon'_f\,m_p(r\phi^{-1/3})^2}}$, $l_p=\frac{1}{\sqrt{2}n\pi d^2{}_p}$

*Murshed et al. Model (2008)*

Murshed et al. (2008) developed the models by considering the contribution of interfacial layer at the solid-liquid interface on the effective thermal conductivity of nanofluids. It was assumed that the liquid (base fluid), interfacial layer and solids collectively form nanofluids; all the nanoparticles which are stationary are separated from each other; there is a continuous heat flux at interfaces like layer/fluid and particle/layer. Following equation (4.12) and equation (4.13) are for the effective thermal conductivity of nanofluids with spherical nanoparticles and cylindrical nanoparticles respectively.. Interfacial layer thickness is taken as 1 nm (Murshed et al., 2008) for the purpose of calculation in this paper. Also, $K_{lr}$ is taken 3 $K_f$ in equation 4.12 and 4.13 (as employed by Murshed et al., 2008)**.**

$$K_{nf} = \frac{(K_p - K_{lr})\phi_p K_{lr}(2\varepsilon_1^{\,3} - \varepsilon^3 + 1) + (K_p + 2K_{lr})\varepsilon_1^{\,3}\{\phi_p \varepsilon^3 (K_{lr} - K_f) + K_f\}}{(K_p + 2K_{lr})\varepsilon_1^{\,3} - (K_p - K_{lr})\phi_p(\varepsilon_1^{\,3} + \varepsilon^3 - 1)} \tag{4.12}$$

$$K_{nf} = \frac{(K_p - K_{lr})\phi K_{lr}(\varepsilon_1^{\,2} - \varepsilon^2 + 1) + (K_p + K_{lr})\varepsilon_1^{\,2}[\phi_p \varepsilon^2 (K_{lr} - K_f) + K_f]}{\varepsilon_1^{\,2}(K_p + K_{lr}) - (K_p - K_{lr})\phi_p(\varepsilon_1 + \varepsilon_2 - 1)} \tag{4.13}$$

$$Where, \varepsilon = 1 + \frac{\delta}{r}; \varepsilon_1 = 1 + \frac{\delta}{2r}$$

*Chandrasekar et al. Model (2010)*

Chandrasekar et al., (2010) proposed a theoretical model of nanofluid thermal conductivity without resorting Maxwell model. It was assuming that the nanoparticles were well dispersed within the base fluid, the thermo-physical properties of the particle-base fluid mixture can be

calculated using equation. Following theoretical model (equation 4.14) had been developed for the measurement of thermal conductivity ratio:

$$\frac{K_{nf}}{K_f} = \left(\frac{C_{nf}}{C_f}\right)^a \left(\frac{\rho_{nf}}{\rho_f}\right)^b \left(\frac{M'_f}{M'_{nf}}\right)^c \tag{4.14}$$

Where, $\rho_{nf} = (1-\phi)\rho_f + \phi\rho_p$, $(\rho C_p)_{nf} = (1-\phi)\rho C_f + \phi\rho_p C_p$, $M'_{nf} = (1-M')M' + \phi M'_p$

Where a, b and c are the exponents, determined from experiments.

*Chon et al. Model (2005)*

This empirical model was developed by using Buckingham-Pi theorem with linear regression analysis with $R^2$ value of 95% for experimental results shown in Chon el al., 2005. Experiment data of $Al_2O_3$ nanoparticles were used with particle size of 11, 47 and 150 nm for $Al_2O_3$-water nanofluids, in the temperature range of 21 to 71°C and with 1 and 4% volume fraction (Chon el al., 2005).

$$\frac{K_{nf}}{K_f} = 1 + 64.7\phi^{0.746}\left(\frac{d_f}{d_p}\right)^{0.369}\left(\frac{K_p}{K_f}\right)^{0.7476} \mathrm{Pr}^{0.9955}\,\mathrm{Re}^{1.2321} \tag{4.15}$$

Where: $\mathrm{Re} = \frac{\rho_f T K_B}{3\pi\mu^2 l_f}$, $\mathrm{Pr} = \frac{\mu C_f}{K_f}$, $l_f = \frac{1}{\sqrt{2}u\pi d^2_f}$, $V_{Br} = \frac{K_B T}{3\pi d_p \mu l_f} = \frac{K_B}{3\pi d_p l_f} \cdot \frac{T}{A'.10^{B'/(T-C')}}$,

$\mu = A'.10^{\frac{B'}{T-C'}}$

Where, *A'*, *B'*, and *C'* are constants

A' = $2.414\times10^{-5}$, B' = 247.8, and C' = 140, for the water and mean free path of base fluid ($l_f$ ) is taken as 0.17 nm for water for the range of temperature mentioned above Chon et al. (2005).

*Li and Peterson Model (2006)*

Empirical model is developed by two factor linear analysis with $R^2$ value of 0.9171. This empirical model is developed by performing the experiments at volume fraction of 2, 4, 6 and 10% and temperature range of 27.5 °C to 34.7 °C for $Al_2O_3$-water nanofluids.

$$\frac{(K_{nf} - K_f)}{K_f} = 0.764\phi + 0.018t - 0.462 \quad (4.16)$$

*Minsta et al. Model (2009)*

This empirical model was developed by simple linear regression analysis with $R^2$ value of 95% for thermal conductivity ratio of $Al_2O_3$-water nanofluids with volume fraction as the influential parameter. This model is derived using experimental data up to a volume fraction of 0.2.

$$\frac{K_{nf}}{K_f} = 1.72\phi + 1.0 \quad (4.17)$$

*Teng et al. Model (2010)*

This empirical model was developed by considering the effect of temperature, nanoparticles size and weight fraction on thermal conductivity ratio of $Al_2O_3$-water nanofluids with the $R^2$ value of regression as 0.9, using experiments data performed with 20, 50 and 100 nm size of nanoparticles, temperature range of 10 to 50 °C and weight fractions of 0.5 to 2%. (Teng et al., 2010).

$$\frac{K_{nf}}{K_f} = C_0 + C_1(100\omega) + C_2(T - 273.15) + C_3 d_p + C_4(100\omega)^2 + C_5(T - 273.15)^2 + C_6 d^2{}_p + C_7(100\omega)^3 + C_8(T - 273.15)^3 \quad (4.18)$$

Where: $C_0 = 0.991$, $C_1 = 0.253$, $C_2 = -0.001$, $C_3 = -0.002$, $C_4 = -0.189$, $C_5 = 6.19 \times 10^{-5}$, $C_6 = 1.317 \times 10^{-5}$, $C_7 = 0.049$, $C_8 = -7.66 \times 10^{-7}$.

*He et al. (2009) model*

He et al. (2009) developed following empirical model for $Tio_2$-water nanoflid.

$$\frac{K_{nf}}{K_f} = 125..62\phi^2 + 4.82\phi + 1.0 \quad (4.19)$$

*Duangthongsuk and Wongwises(2009) model*

Duangthongsuk and Wongwises (2009) developed a new model for $Tio_2$- water nanofluid in the following form:

$$\frac{K_{nf}}{K_f} = a + b\phi \tag{4.20}$$

This equation is limited to temperature range from 15 to 35 $^{o}$C and volume concentration 0.2 to 2%.

For 15, 25 and 35 value of a is 1.0225, 1.0204 and 1.0139 respectively and b is 0.0272, 0.0249, 0.0250 respectively.

### 4.3 Evaluation of Theoritical Models for $Al_2O_3/Tio_2$ Nanofluids

The above models have been evaluated by using them to predict the ratio of thermal conductivity of nanofluids to that of base fluids for a range of experimental conditions and comparing them with available experimental data for the same range of volume fraction, temperature and particle size. Lines of best fit have been drawn through the experimental data to indicate their trends. For the purpose of calculation, the following parameters are considered:

(a) Thermal conductivity of $Al_2O_3$ particles vary from 41.44 W/m K at 0°C to 31.03 W/m K at 100°C;

(b) Thermal conductivity of water varies from 0.57 W/m K at 0°C to 0.67 W/m K at 100°C (Li and Peterson, 2006);

(c) Thermal conductivity of $TiO_2$ at 15 °C, 25 °C and 35 °C are 8.63 W/mK, 8.48 W/mK and 8.32 W/mK, respectively (Duangthongsuk and Wongwises,2009).

(d) Specific heat and density of water are as 4.186 kJ/kgK and 1000 kg/$m^3$, respectively;

(e) Density of $Al_2O_3$ particles were as mentioned in their respective references, such as $\rho_p$: 3965 kg/$m^3$ (Zhu et al., 2009).

(f) Specific heat of $Al_2O_3$ is taken as 880 J/kg K (Rea et al., 2009).

(g) Specific heat of $TiO_2$ is 700 J/kg K (Wang et al., 2007);

(h) Density of $TiO_2$ particles 3950 kJ/kgK.

(i) Molecular diameter of water 0.3 nm (Bhattacharya et al., 2009).

In Figure 4.1, values of experimental thermal conductivity ratio for $Al_2O_3$ nanoparticle diameter of 38.4 nm and at 51$^oC$ temperature have been compared with predictions obtained using theoretical models for a range of nanoparticle volume fractions.

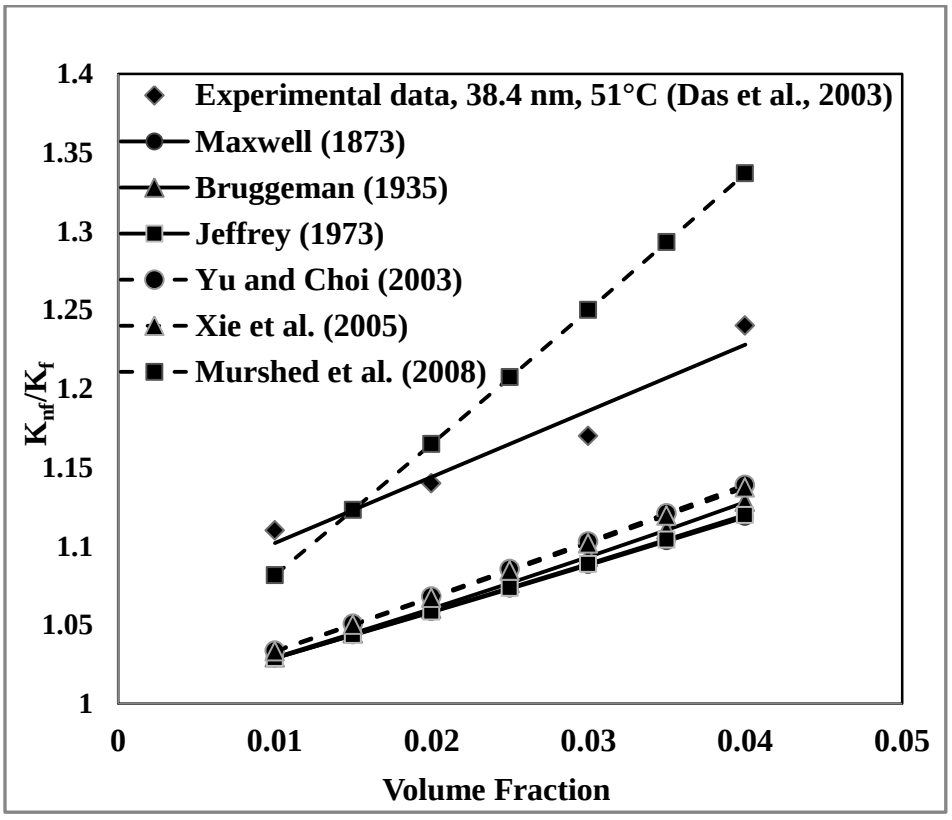

**Figure 4.1:** Experimental versus predicted values of thermal conductivity ratio with increase in volume fraction of $Al_2O_3$ nanoparticles, d: 38.4 nm, T: 51$^oC$.

Figure 4.1 results show that Murshed et al. (2008) model slightly under-predicts the experimental data below a volume fraction of 0.015 and over-predicts from volume fraction of 0.015 to 0.04. The margin of over-prediction increases with increase in volumetric concentrations. The other models (Maxwell, 1873 to Xie et al., 2005) have provided under-predictions and the predictions are found to be almost superimposing on each other. The trends of predictions obtained using Maxwell (1873) to Xie et al. (2005) are almost parallel to the experimental data. Results of The Koo and Kleinstreuer (2004) model are shown in separate Figure 4.2.

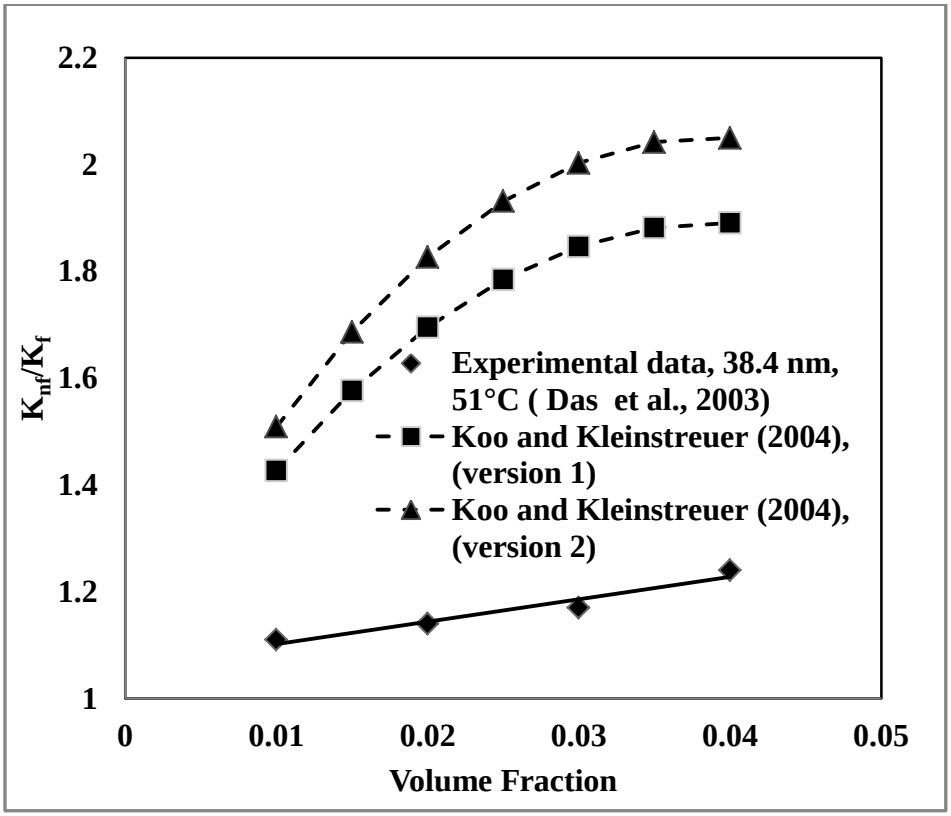


**Figure 4.2:** Experimental versus predicted values of thermal conductivity ratio with increase in volume fraction of $Al_2O_3$ nanoparticles, d: 38.4 nm, T: 51$^oC$.

As shown in Figure 4.2 Koo and Kleinstreuer (2004) model provides great over-predictions. For all the models (Maxwell, 1873 to Murshed et al., 2008), increase in volume fraction has provided increase in thermal conductivity ratio. In Figure 4.3, values of experimental thermal conductivity ratio for $Al_2O_3$ nanoparticle diameter of 11 nm and with 1% nanoparticle volume fraction have been compared with predictions obtained using theoretical models for a range of temperatures.

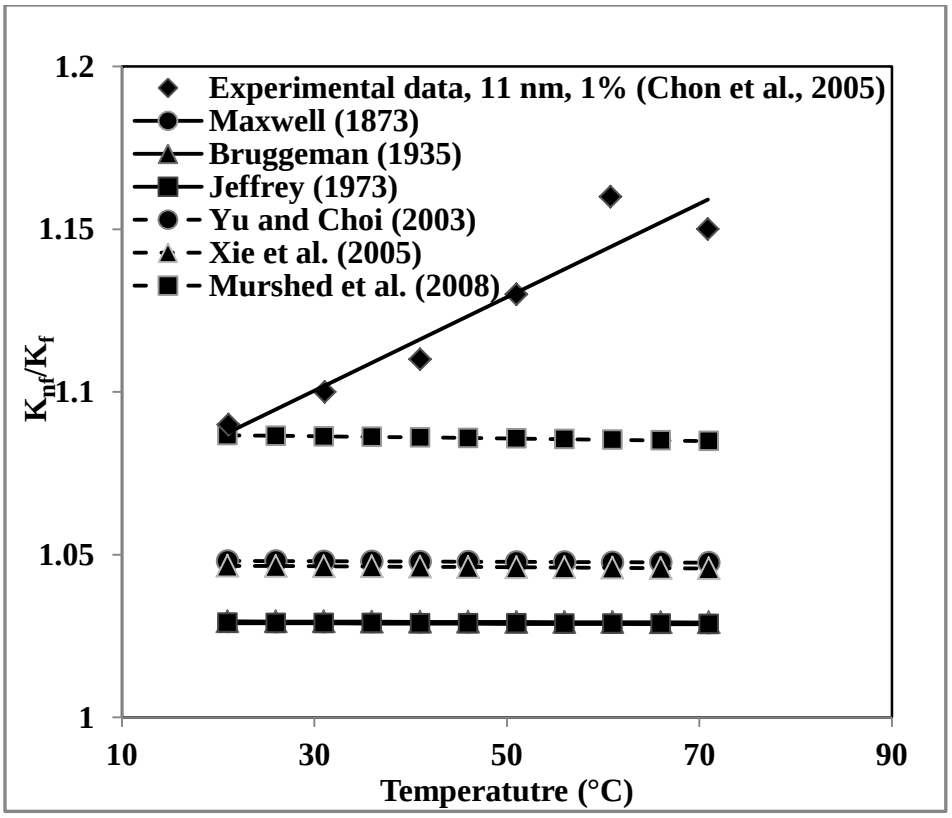


**Figure 4.3:** Experimental versus predicted values of thermal conductivity ratio with increase in temperature, d: 11 nm, $\phi$: 1%.

Figure 4.3 shows that all the models generally under-predict the experimental data, with Murshed et al. (2008) model providing the relatively higher values of predictions. The models do not provide any appreciable changes in predictions with increase in temperature, while the values of experimental thermal conductivity ratio increase rather sharply with increase in temperature.

The inaccuracies in predictions increase with increase in temperature. Results of The Koo and Kleinstreuer (2004) model are shown in separate Figure 4.4.

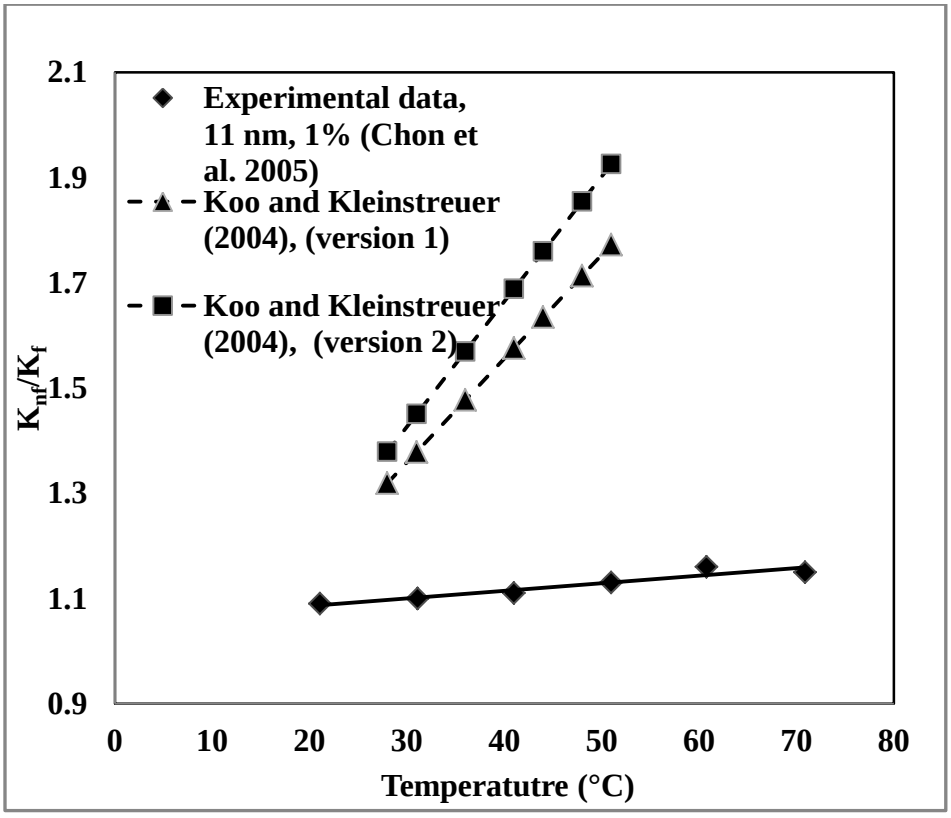


**Figure 4.4:** Experimental versus predicted values of thermal conductivity ratio with increase in temperature, d: 11 nm, $\phi$: 1%.

Once again, the Koo and Kleinstreuer (2004) model provided significant over-predictions. In Figure 4.5 values of experimental thermal conductivity ratio for $Al_2O_3$ nanoparticle diameter of 48 nm and at room temperature have been compared with predictions obtained using theoretical models for a range of volume fraction.

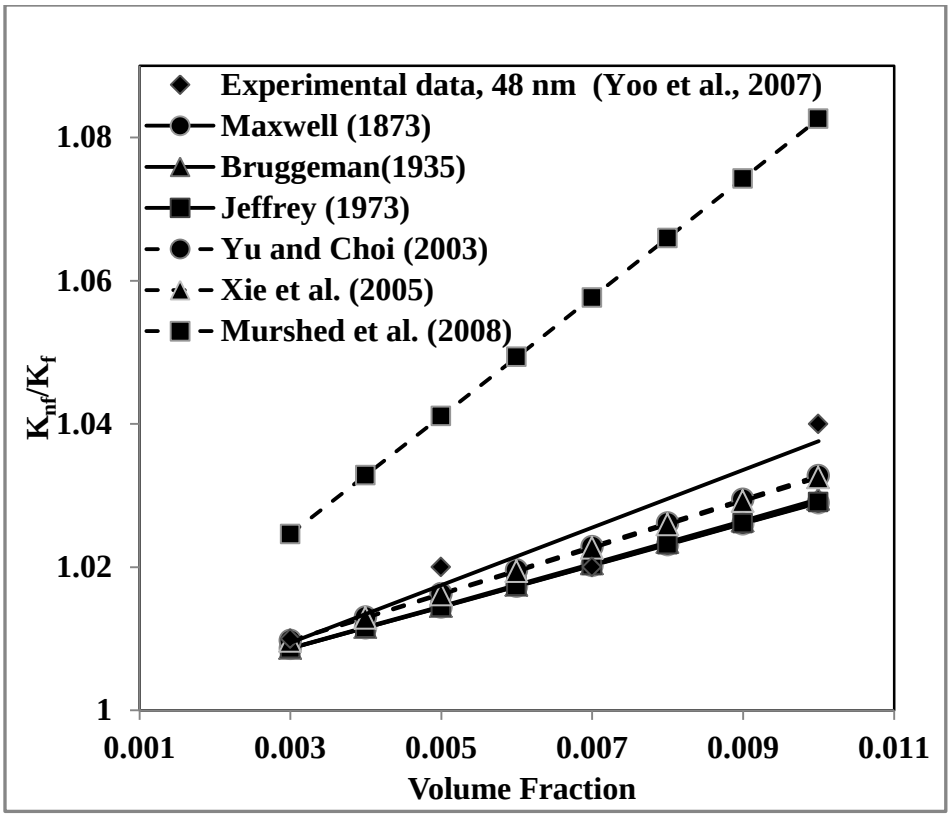


**Figure 4.5:** Experimental versus predicted values of thermal conductivity ratio with increase in volume fraction of $Al_2O_3$ nanoparticles, d: 48 nm, T: 20$^oC$.

In Figure 4.5 all the models, except Murshed et al. (2008) under-predict the experimental data. The trends of predictions obtained using Maxwell (1873) to Murshed et al. (2008) are almost parallel to the experimental data. Results of Murshed et al. (2008) show over prediction. Thermal conductivity ratio increases with increase in temperature. In Figure 4.6, values of experimental thermal conductivity ratio for $Al_2O_3$ nanoparticle diameter of 36 nm and at 34.7 °C have been compared with predictions obtained using theoretical models for a range of volume fraction.

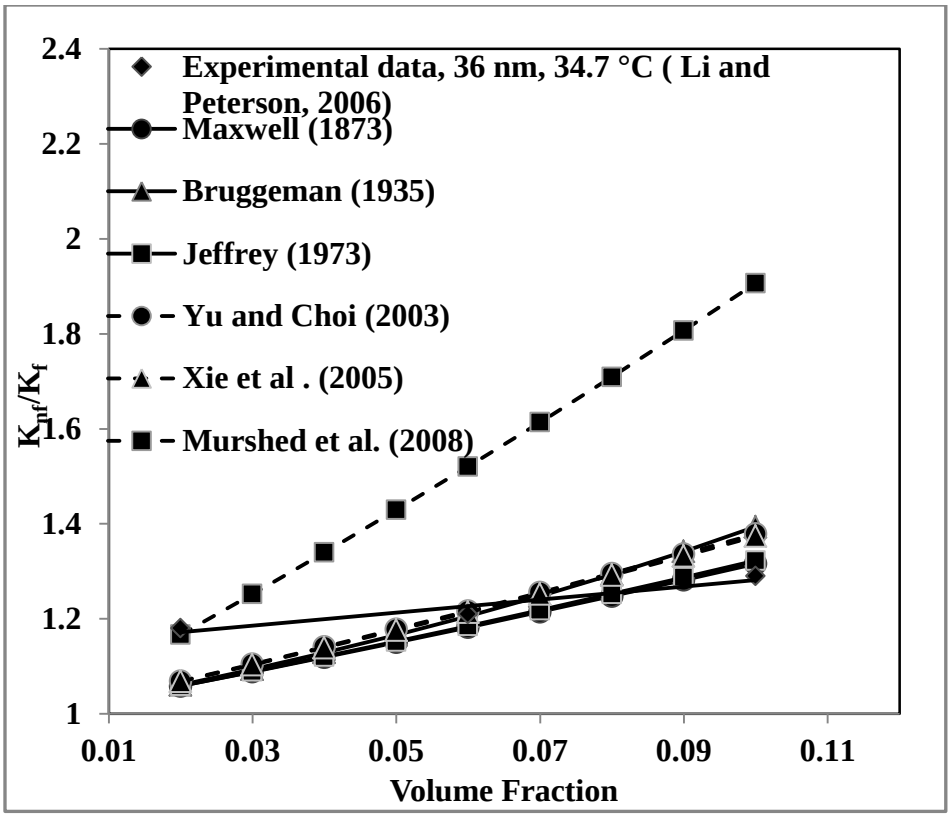


**Figure 4.6:** Experimental versus predicted values of thermal conductivity ratio with increase in volume fraction of $Al_2O_3$ nanoparticles, d: 36 nm, T: 34.7 °C.

In Figure 4.6 models Maxwell (1873) and Jeffrey (1973) under predict the experimental thermal conductivity ratio below 0.07 volume fraction and over predict above 0.07 volume fraction. Bruggeman (1935), Yu and Choi (2003) and Xie et al. (2005) models under predict the experimental thermal conductivity ratio below 0.08 volume fraction and over predict above 0.08 volume fraction. Murshed et al. (2008) are showing over predicted thermal conductivity ratio. Thermal conductivity ratio increases with increase in volume fraction. Once again, the Koo and Kleinstreuer (2004) model provided significant over-predictions; predictions with this model are shown in Appendix A1. In Figure 4.7, values of experimental thermal conductivity ratio for

$Al_2O_3$ nanoparticle diameter of 11 nm and at 23$^oC$ temperature have been compared with predictions obtained using theoretical models for a range of nanoparticle volume fractions.

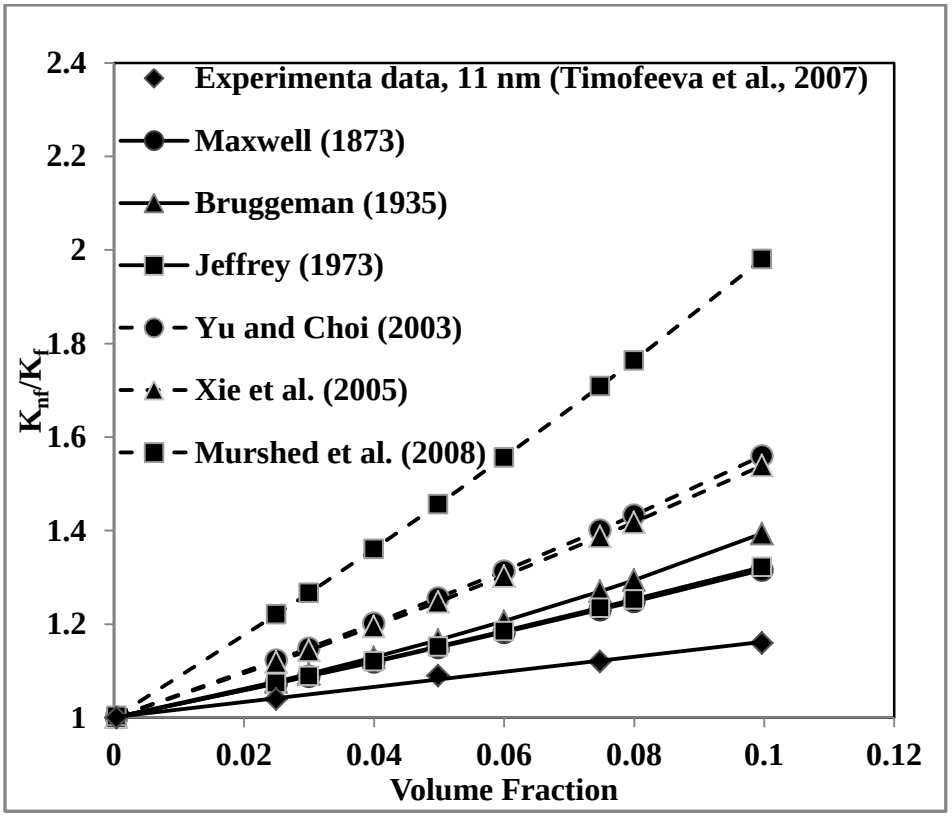


**Figure 4.7:** Experimental versus predicted values of thermal conductivity ratio with increase in volume fraction of $Al_2O_3$ nanoparticles, d: 11 nm, T: 23$^oC$

Figure 4.7 shows that all the models over-predict the experimental data, with Murshed et al. (2008) model providing the largest over-predictions. The amount of inaccuracy increases with increase in volume concentration of nanoparticles. All the models result in increase in thermal conductivity ratio with increase in volume concentrations. In Figure 4.8, values of experimental thermal conductivity ratio for $Al_2O_3$ nanoparticle diameter of 80 nm and with 1% nanoparticle volume fraction have been compared with predictions obtained using theoretical models for a range of temperatures.

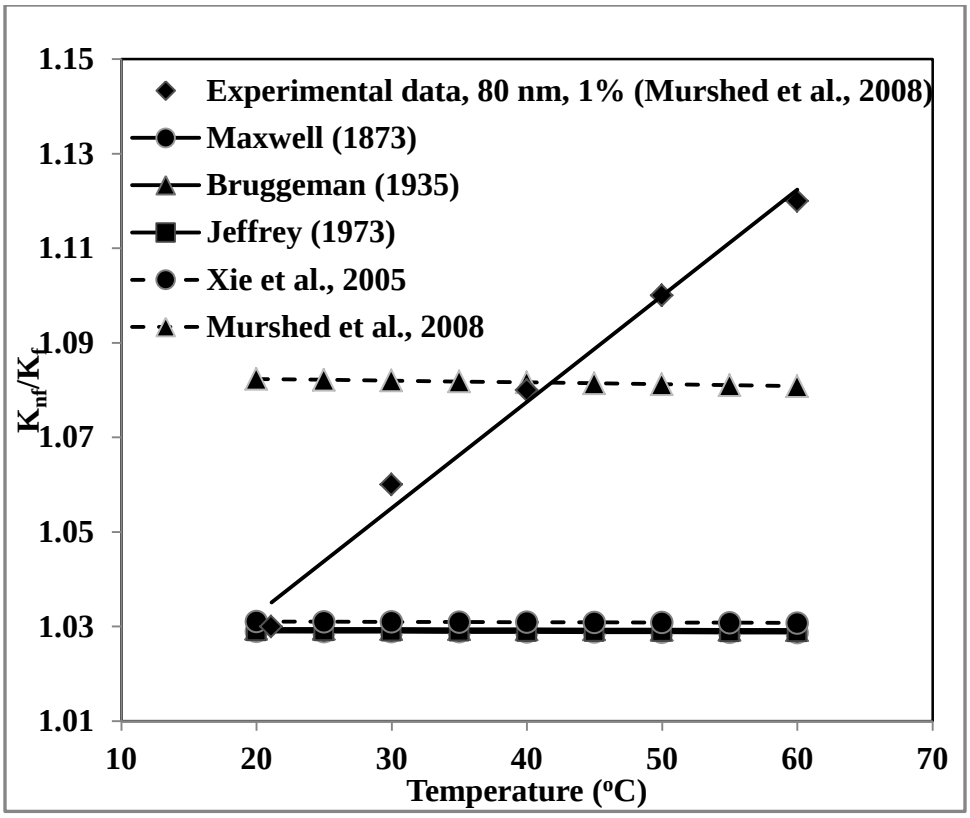


**Figure 4.8:** Experimental versus predicted values of thermal conductivity ratio with increase in temperature, d: 80 nm, $\phi$: 1%.

Figure 4.8 shows that all the models, except Murshed at al. (2008) model under-predict the experimental data. Murshed et al. (2008) model provides over-predictions in the range of 20-40$^{o}$C and under-prediction from 40-60$^{o}$C. Once again, the models do not provide any appreciable changes in predictions with increase in temperature, while the values of experimental thermal conductivity ratio increase with increase in temperature. Once again, the Koo and Kleinstreuer (2004) model provided significant over-predictions; predictions with this model are shown in Figure Appendix A2. In Figure 4.9, values of experimental thermal conductivity ratio for $Al_2O_3$ nanoparticle diameter of 20 nm and at 50$^{o}$C temperature have been compared with predictions obtained using theoretical models for a range of nanoparticle volume fractions.

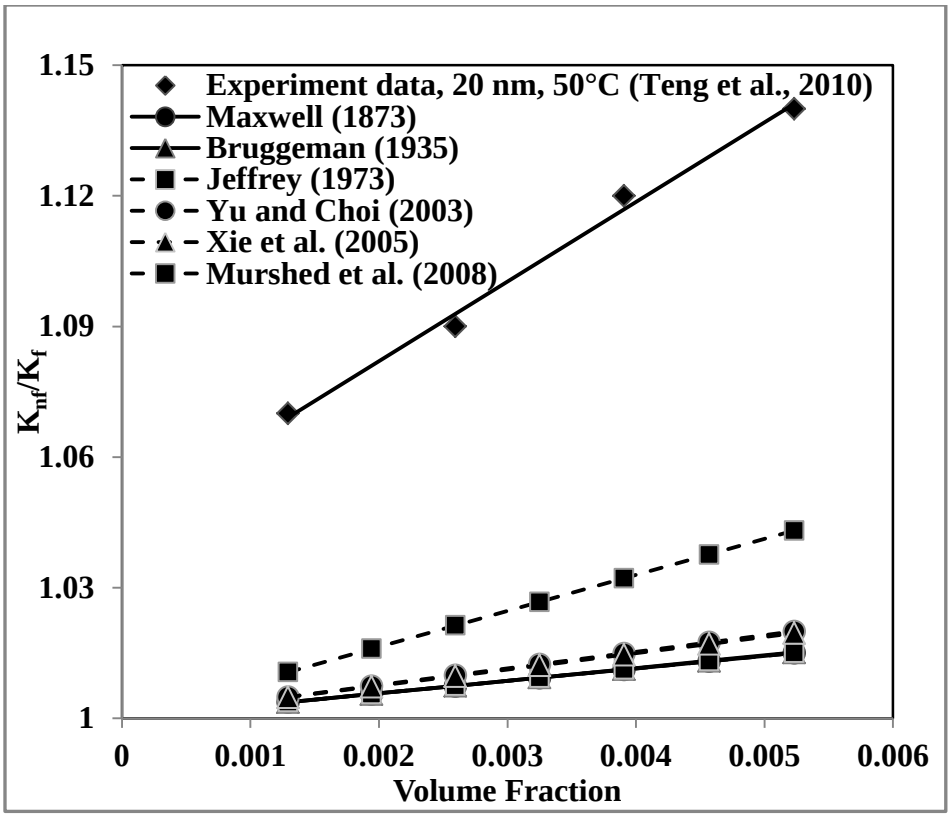


**Figure 4.9:** Experimental versus predicted values of thermal conductivity ratio with increase in volume fraction of $Al_2O_3$ nanoparticles, d: 20 nm, T: 50$^oC$

Figure 4.9 shows that all the models under-predict the experimental data, with Murshed et al. (2008) model providing the relatively higher values of predictions. All the models result in increase in thermal conductivity ratio with increase in volume concentrations. In Figure 4.10, experimental data of Yoo et al. (2007) at $TiO_2$ nanoparticles of diameter 24 nm, room temperature and for a given range of volume fraction is compared with theoretical models.

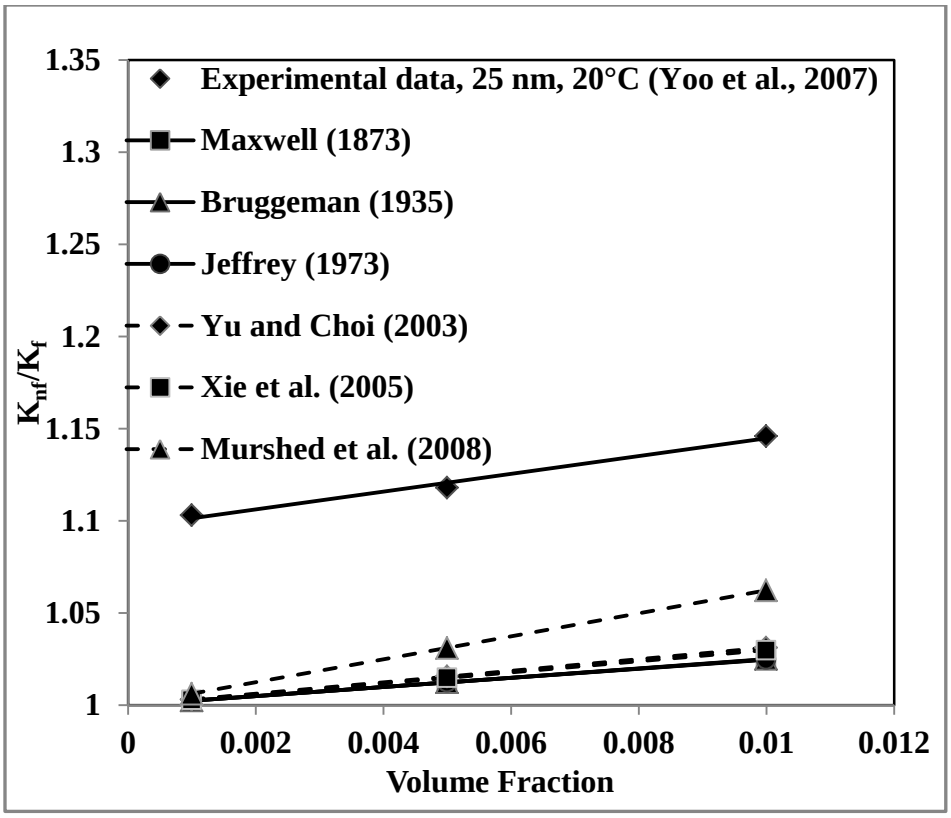


**Figure 4.10:** Experimental versus predicted values of thermal conductivity ratio with increase in volume fraction of $TiO_2$ nanoparticles, d: 25 nm, T: 20$^oC$.

In Figure 4.10 results of Maxwell (1873), Bruggeman (1935), Jeffrey (1973), Yu and Choi (2003) and Xie et al. (2005) models are almost similar. All the theoretical models have provided under-predictions. In Figure 4.11, experimental data of He et al. (2009) at $TiO_2$ nanoparticles of diameter 21nm, 22$^oC$ temperature and for given volume fraction is compared with theoretical models.

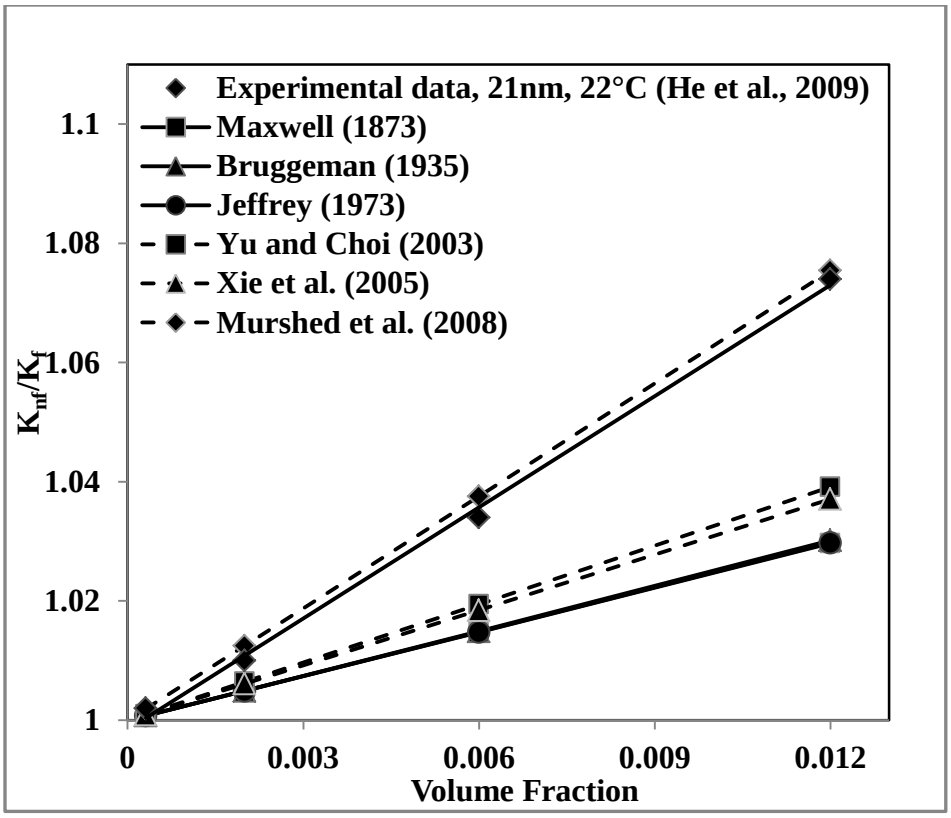


**Figure 4.11:** Experimental versus predicted values of thermal conductivity ratio with increase in volume fraction of $TiO_2$ nanoparticles, d: 21 nm, T: 22$^oC$.

In Figure 4.11 Results of Murshed et al. (2008) are very close to experimental thermal conductivity ratio. Yu and Choi (2003) and Xie et al. (2005) models provide very similar results. Results of Maxwell (1873), bruggeman (1935) and Jeffrey (1973) are overlapping. Maxwell (1873), bruggeman (1935), Jeffrey (1973), Yu and Choi (2003) and Xie et al. (2005) model under-predict the experimental results. In Figure 4.12, experimental data of Turgut et al. (2009) at $TiO_2$ nanoparticles of diameter 21 nm, 23$^oC$ temperature and for a given temperature range is compared with theoretical models.

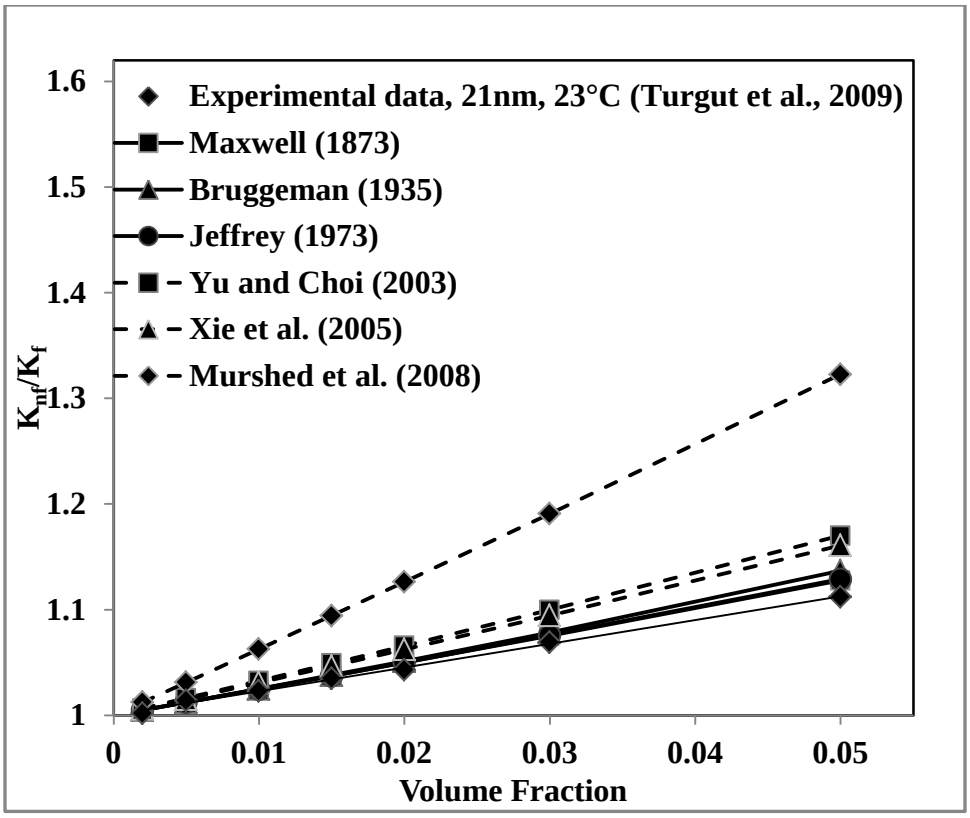


**Figure 4.12:** Experimental versus predicted values of thermal conductivity ratio with increase in volume fraction of $TiO_2$ nanoparticles, d: 21 nm, T: 23$^oC$.

In Figure 4.12 thermal conductivity ratio obtained from of Maxwell (1873) and bruggeman (1935), Jeffrey (1973), Yu and Choi (2003), Xie et al. (2005) are very near to that obtained from experiment. Results of Yu and Choi (2003) and Xie et al. (2005) are almost superimposing. Models over-predict the experimental thermal conductivity ratio as volume fraction increase. In Figure 4.13, experimental data of Murshed et al. (2009) at $TiO_2$ nanoparticles of diameter 15 nm, room temperature and given range of volume fraction is compared with theoretical models.

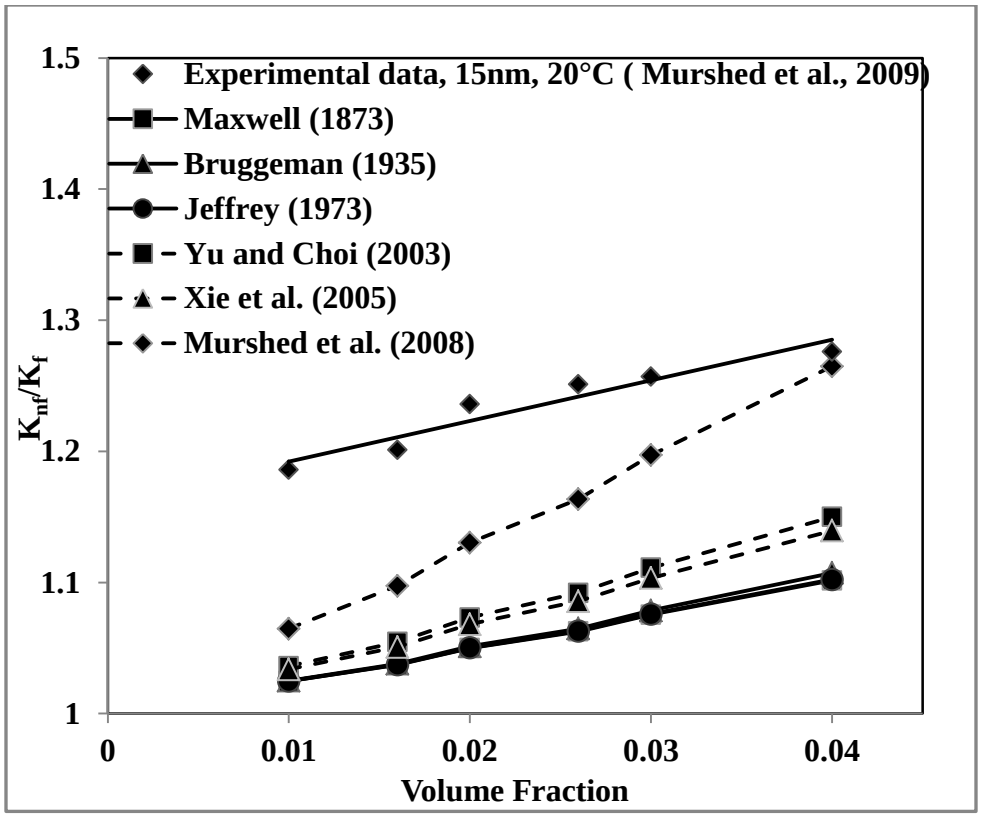


**Figure 4.13:** Experimental versus predicted values of thermal conductivity ratio with increase in volume fraction of $TiO_2$ nanoparticles, d: 15 nm, T: 20$^oC$.

In Figure 4.13, all the models under-predict the thermal conductivity ratio. Results of thermal conductivity ratio obtained from Maxwell (1873), bruggeman (1935) and Jeffrey (1973) models are overlapping. Results of Yu and Choi (2003) and Xie et al. (2005) are very similar.

### 4.4 Evaluation of empirical models for $Al_2O_3/TiO_2$ nanofluids

In Figure 4.14, experimental values of nanofluid thermal conductivity ratio obtained from Das et al. (2003) at $Al_2O_3$ nanoparticle diameter of 38.4 nm, 51$^oC$ temperature and for a range of volume fraction are compared with thermal conductivity ratio predicted with empirical models.

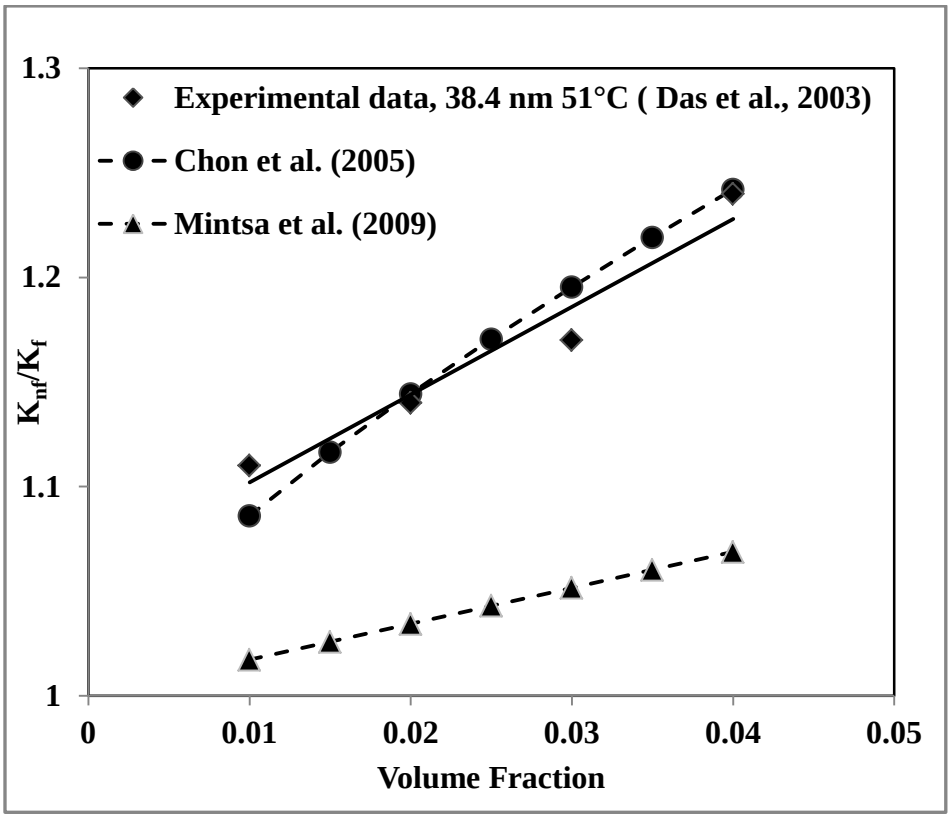


**Figure 4.14:** Experimental versus predicted values of thermal conductivity ratio with increase in volume fraction of $Al_2O_3$ nanoparticles, d: 38.4 nm, T: 51$^oC$.

Figure 4.14 shows that the empirical model Mintsa et al. (2009) under predict the experimental data. Below 0.02 fraction volume Chon et al. (2005) model under predict the experimental thermal conductivity ratio; whereas above 0.02 volume fraction, Chon et al. (2005) model over predict the experimental thermal conductivity ratio. In Figure 4.15, experimental values of

nanofluid thermal conductivity ratio obtained from Li and Peterson (2006) at $Al_2O_3$ nanoparticle diameter of 36 nm, 34.7$^oC$ temperature and for a range of volume fraction are compared with thermal conductivity ratio predicted by empirical models.

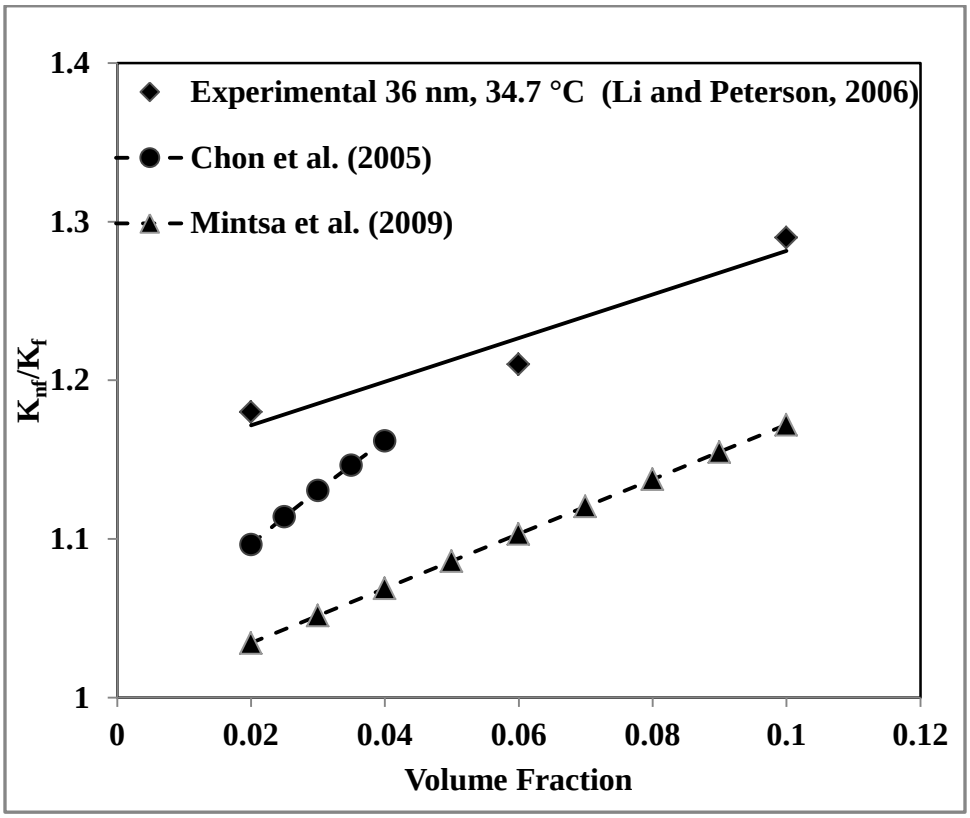


**Figure 4.15:** Experimental versus predicted values of thermal conductivity ratio with increase in volume fraction of $Al_2O_3$ nanoparticles, d: 36 nm, T: 34.7$^oC$.

Figure 4.15 shows that empirical model Chon et al. (2005) and Mintsa et al. (2009) under predict the experimental thermal conductivity ratio. Thermal conductivity ratio increases with increase in volume fraction. In Figure 4.16, experimental values of nanofluid thermal conductivity ratio obtained from Yoo et al. (2007) at $Al_2O_3$ nanoparticle diameter of 48 nm, room temperature and for a range of volume fraction are compared with thermal conductivity ratio predicted by empirical model.

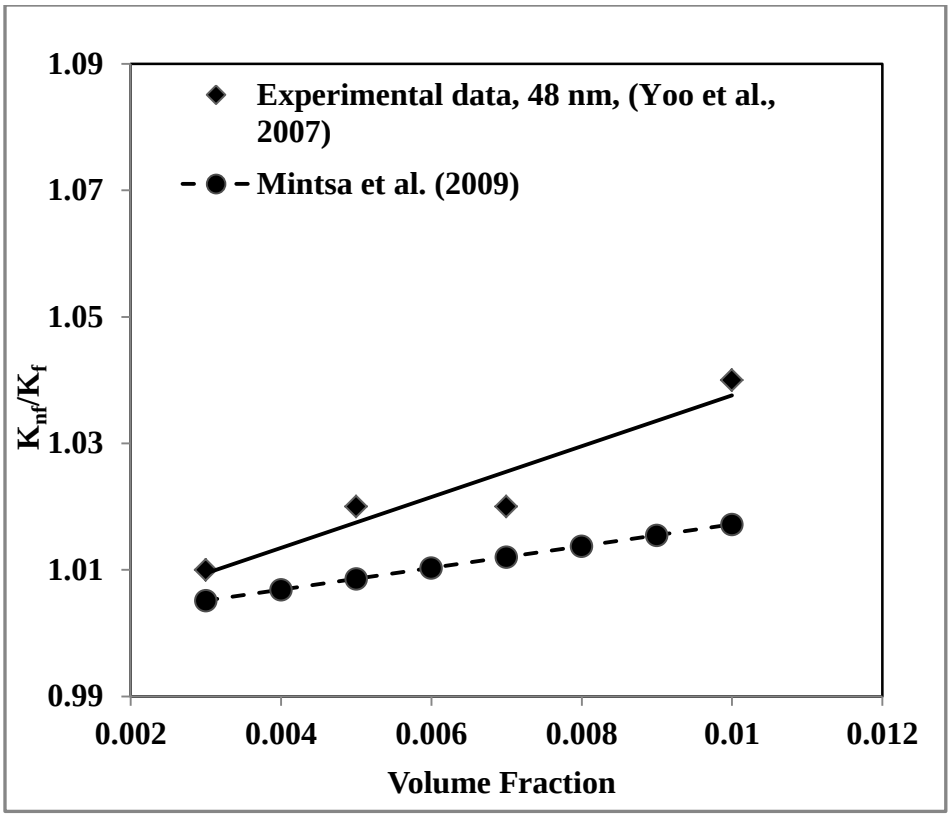


**Figure 4.16:** Experimental versus predicted values of thermal conductivity ratio with increase in volume fraction of $Al_2O_3$ nanoparticles, d: 48 nm, T: 20$^oC$.

Figure 4.16 shows that empirical model Mintsa et al. (2009) under-predict the experimental results. Thermal conductivity ratio increases with an increase in volume fraction. In Figure 4.17, experimental values of nanofluid thermal conductivity ratio obtained from Timofeeva et al. (2007) at $Al_2O_3$ nanoparticle diameter of 11 nm, 23$^oC$ temperature and in he given range of volume fraction are compared with thermal conductivity ratio predicted by empirical models.

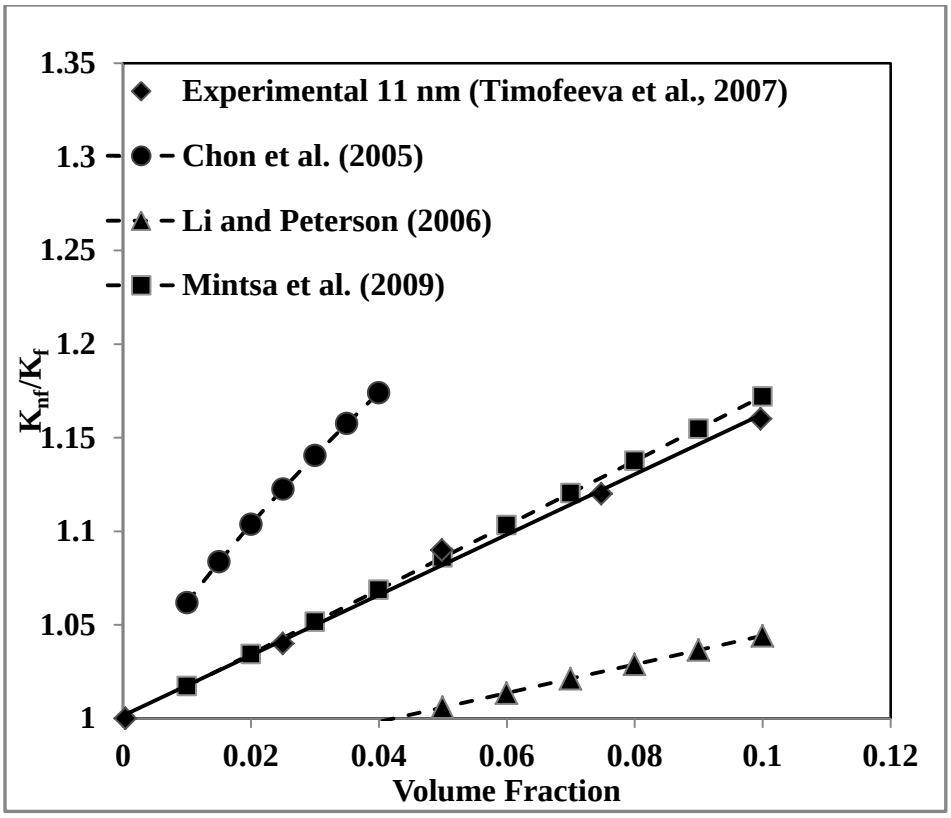


**Figure 4.17:** Experimental versus predicted values of thermal conductivity ratio with increase in volume fraction of $Al_2O_3$ nanoparticles, d: 11 nm, T: 23$^oC$.

Figure 4.17 shows that empirical model Chon et al. (2005) over predict experimental results. Empirical model Li and Peterson (2006) under predict the experimental results. Results of empirical model Mintsa et al. (2009) are superimposing over experimental results. In Figure 4.18, experimental values of nanofluid thermal conductivity ratio obtained from Murshed et al., (2008) with $Al_2O_3$ nanoparticle diameter of 80 nm, 1% volume fraction and for a given range of temperature are compared with thermal conductivity ratio predicted by empirical model.

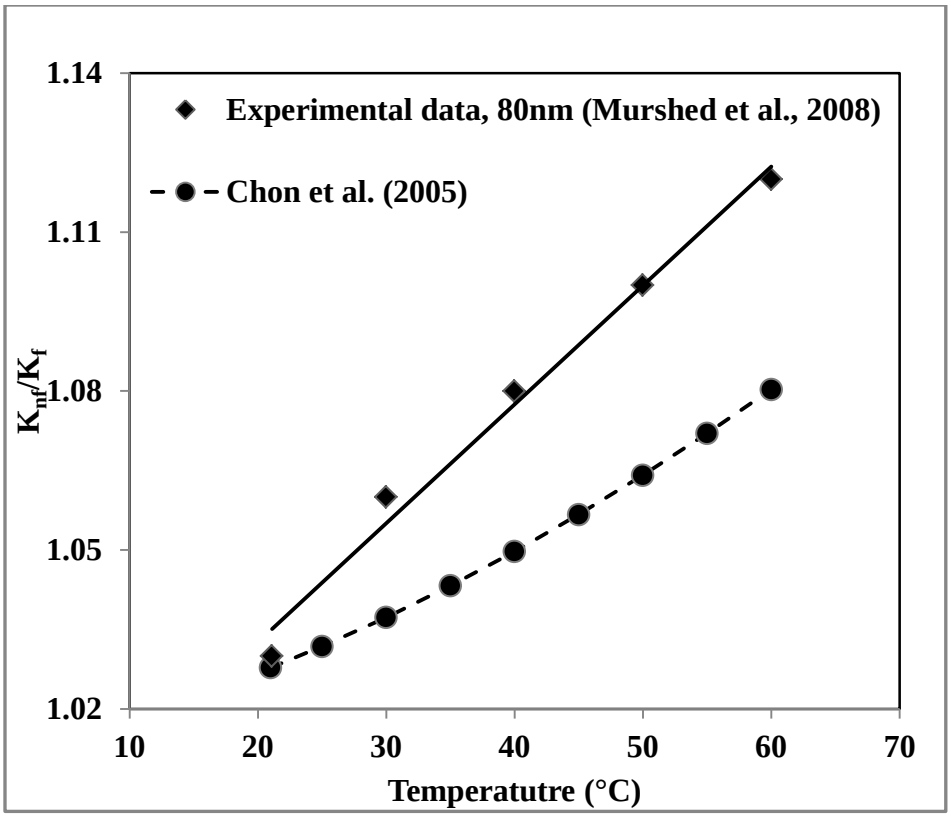


**Figure 4.18:** Experimental versus predicted values of thermal conductivity ratio with increase in temperature, d: 80 nm, $\phi$: 1%.

Figure 4.18 shows that empirical model Chon et al. (2005) under-predict the experimental thermal conductivity ratio. Thermal conductivity ratio increases with increase in temperature. In Figure 4.19, experimental values of nanofluid thermal conductivity ratio obtained from Teng et al. (2010) at $Al_2O_3$ nanoparticle diameter of 20 nm, 50$^oC$ temperature and for a range of volume fraction are compared against the empirical models.

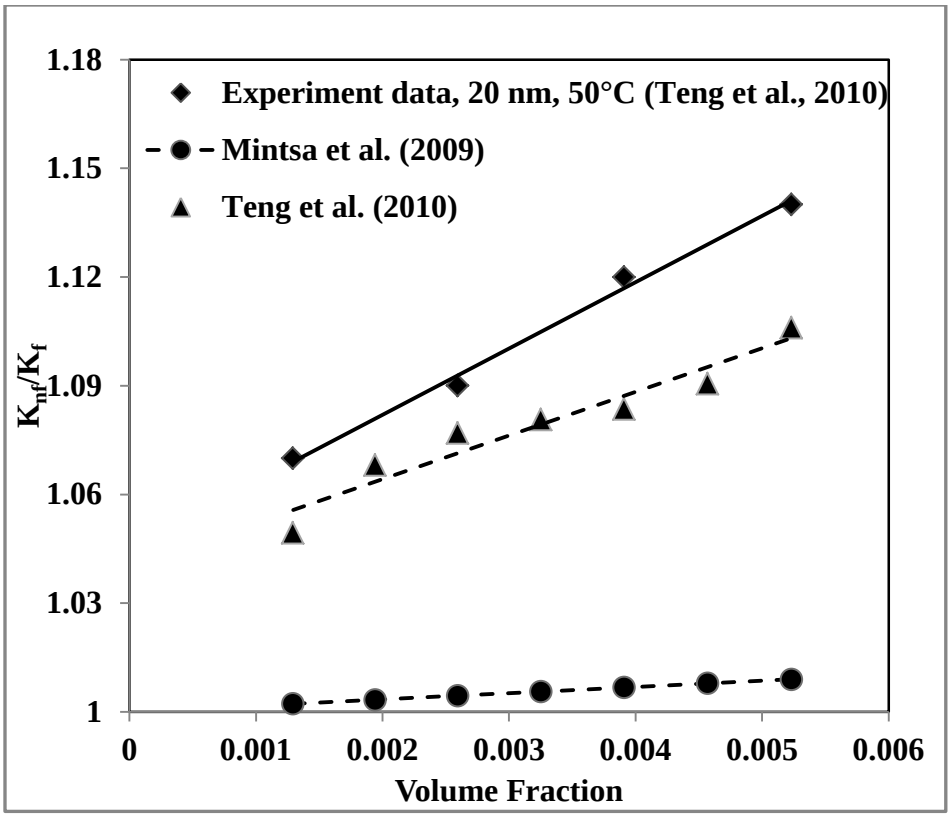


**Figure 4.19:** Experimental versus predicted values of thermal conductivity ratio with increase in volume fraction of $Al_2O_3$ nanoparticles, d: 20 nm, T: 50$^oC$.

Figure 19 shows that empirical models are under predicting the experimental thermal conductivity ratio, with empirical Teng et al. (2010) model providing the highest value of predictions. In Figure 4.20, experimental data of Yoo et al. (2007) at $TiO_2$ nanoparticles of diameter 24 nm, room temperature and for a given range of volume fraction is compared with empirical models.

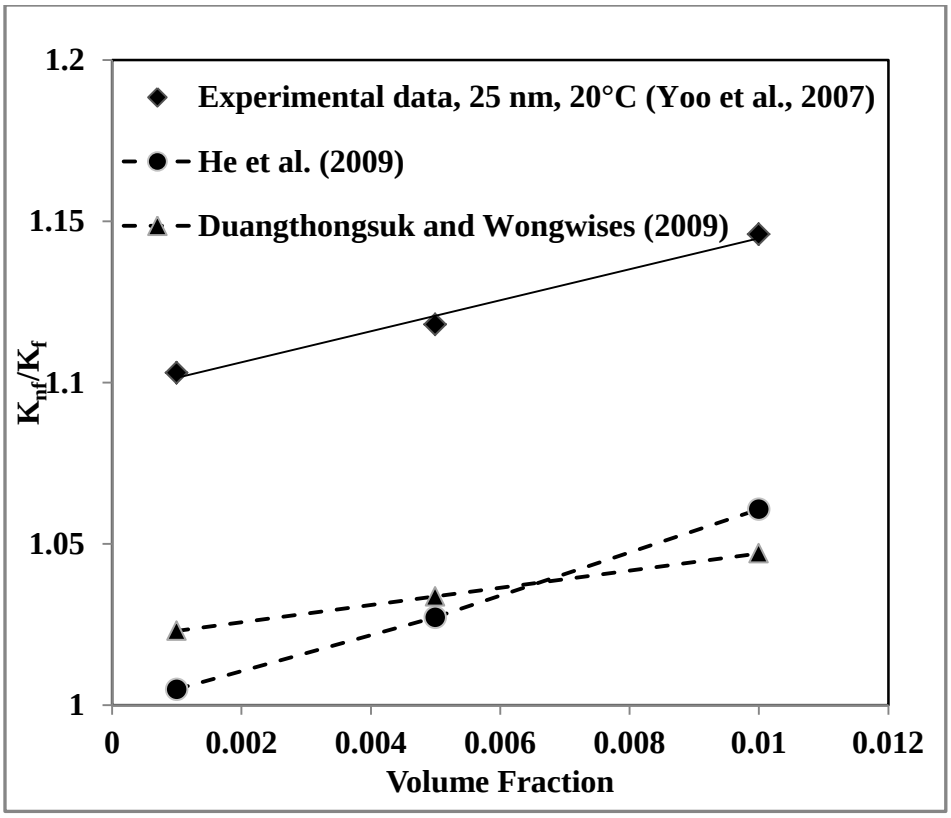


**Figure 4.20:** Experimental versus predicted values of thermal conductivity ratio with increase in volume fraction of $TiO_2$ nanoparticles, d: 25 nm, T: 20$^oC$.

In Figure 4.20 the empirical models He et al. (2009) and Duangthongsuk and Wongwises (2009) have provided under-predictions. In Figure 4.21, experimental data of He et al. (2009) at $TiO_2$ nanoparticles of diameter 21nm, 22$^oC$ temperature and for given volume fraction is compared with empirical models.

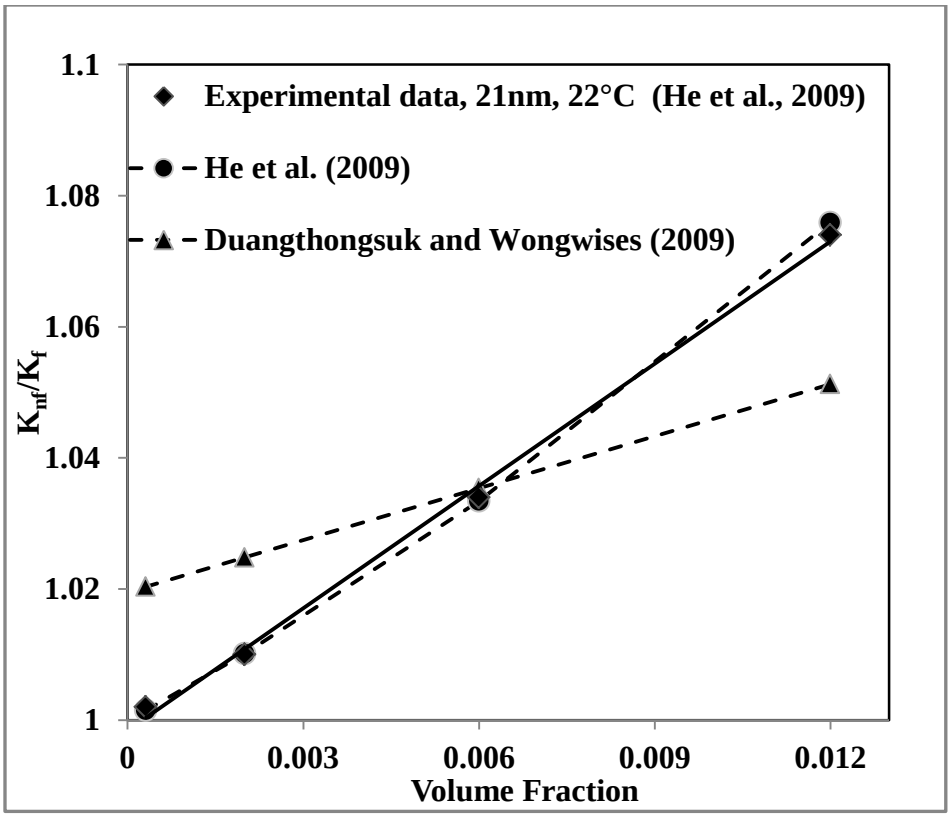


**Figure 4.21:** Experimental versus predicted values of thermal conductivity ratio with increase in volume fraction of $TiO_2$ nanoparticles, d: 21 nm, T: 22$^oC$.

In Figure 4.21 Results of He et al. (2009) are very close to experimental thermal conductivity ratio. Below 0.006 volume fraction Duangthongsuk and Wongwises (2009) model over-predict and above that under-predict the experimental thermal conductivity ratio. In Figure 4.22, experimental data of Turgut et al. (2009) at $TiO_2$ nanoparticles of diameter 21 nm, 23$^oC$ temperature and for a given temperature range is compared with empirical models.

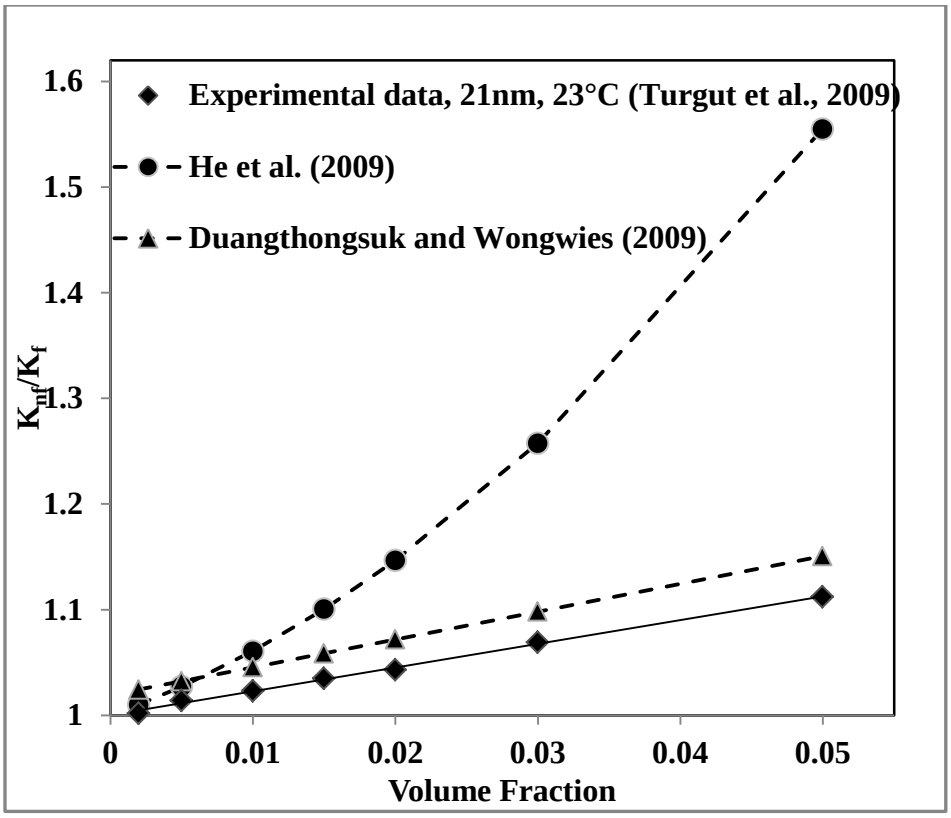


**Figure 4.22:** Experimental versus predicted values of thermal conductivity ratio with increase in volume fraction of $TiO_2$ nanoparticles, d: 21 nm, T: 23$^oC$.

In Figure 4.22 thermal conductivity ratio obtained from Duangthongsuk and Wongwises (2009) are very near to that obtained from experiments. He et al. (2009) model gives highest over prediction. In Figure 4.23, experimental data of Murshed et al. (2009) at $TiO_2$ nanoparticles of diameter 15 nm, room temperature and given range of volume fraction is compared with empirical models.

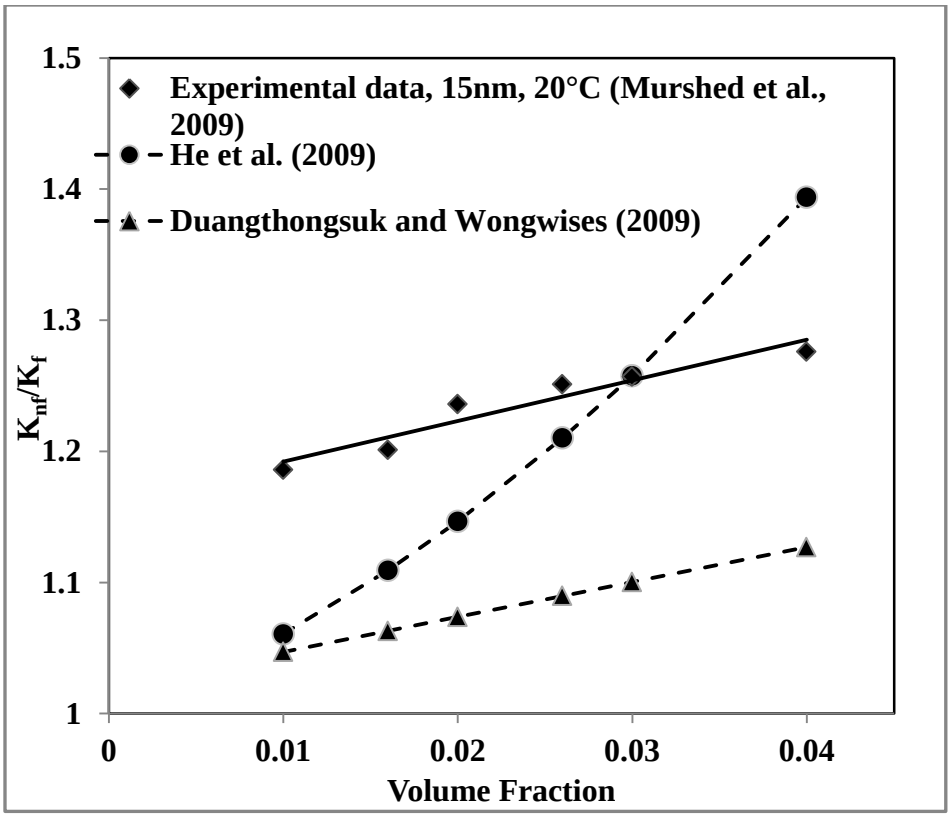


**Figure 4.23:** Experimental versus predicted values of thermal conductivity ratio with increase in volume fraction of $TiO_2$ nanoparticles, d: 15 nm, T: 20$^o$C.

In Figure 4.23 He et al. (2009) model under-predict the thermal conductivity ratio. Results of He et al. (2009) are showing highest over prediction. Below 0.03 volume fraction He et al. (2009) under-predict and above 0.03 volume fraction over-predict experimental values.

Table 4.3 provides average of sum of absolute values of relative error for thermal conductivity ratio (using the formula given below) to indicate the prediction accuracies of the different models (Figure 4.1 to 4.23).

$$\text{Relative error} = \sum_{n} \frac{\text{experimental value} - \text{predicted value}}{\text{experimental value}} \times 100\ \%$$

**Table 4.3:** Relative Errors of Model Predictions (%)

| Figure No. | Maxwell (1873) | Bruggeman (1935) | Jeffrey (1973) | Yu and Choi (2003) | Koo and Kleinstreuer (2004) | Xie et al. (2005) | Chon et al. (2005) | Li and Peterson et al. (2006) | Murshed et al. (2008) | Mintsa et al. (2009) | Teng et al. (2010) | He et al. (2009) | Duangthongsuk and Wongwises (2009) |
|---|---|---|---|---|---|---|---|---|---|---|---|---|---|
| **4.1, 4.2, 4.14** | 8 | 7 | 8 | 7 | Version 1: 47 Version 2: 58 | 7 | 1.22 | - | 4.85 | 10.39 | - | - | - |
| **4.3, 4.4, A5** | 8 | 8 | 8 | 7 | Version 1: 41 Version 2: 52 | 7 | 1.94 | - | 3.29 | - | - | - | - |
| **4.5, 4.16** | 0.44 | 0.43 | 0.44 | 0.34 | | 0.35 | - | - | 2.83 | 1.14 | - | - | - |
| **4.6, 4.15, A1** | 4.88 | 6.18 | 4.97 | 5.61 | Version 1: 19.77, Version 2: 29.65 | 5.44 | - | | 24.88 | 10.10 | - | - | - |
| **4.7, 4.17** | 7 | 9 | 7 | 17 | - | 16 | 7.94 | 1.93 | 34.9 | 0.50 | - | - | - |
| **4.8, 4.18, A2** | 4 | 4 | 4 | | Version 1: 13.31, Version 2: 17.02 | 4 | 2.39 | - | 2.50 | - | - | - | - |
| **4.9,** | 9 | 9 | 9 | 8 | - | 8 | - | - | 7.05 | 8.95 | 2.34 | - | - |

| | | | | | | | | | | | | | |
|---|---|---|---|---|---|---|---|---|---|---|---|---|---|
| **4.19** | | | | | | | | | | | | | |
| **4.10, 4.20** | 9.72 | 9.7 | 9.71 | 9.41 | - | 9.48 | - | - | 8.03 | - | - | 8.15 | 7.81 |
| **4.11, 4.21** | 1.65 | 1.64 | 1.65 | 1.28 | - | 1.36 | - | - | 0.18 | - | - | 0.07 | 1.39 |
| **4.12, 4.22** | 0.49 | 0.69 | 0.53 | 1.89 | - | 1.58 | - | - | 7.24 | - | - | 11.37 | 2.49 |
| **4.13, 4.23** | 14.24 | 14.06 | 14.22 | 12.03 | - | 12.51 | - | - | 6.67 | - | - | 6.33 | 12.23 |
| **A3, A4, A6** | 1.52 | 1.39 | 1.50 | 2.04 | Version 1: 63.62 , Version 2:77.07 | 1.97 | 7.28 | 3.06 | 13.29 | 8.95 | | - | - |
| **Mean of Error** | 5.74 | 5.96 | 5.75 | 6.51 | Version 1: 36.94, Version 2: 46.75 | 6.22 | 4.154 | 2.51 | 9.61 | 6.67 | 2.34 | 6.48 | 5.98 |

# Chapter 5: Development of New Model For Thermal Conductivity of Nanofluids

In this chapter, new models have been developed to measure the thermal conductivity of $Al_2O_3$-water and $TiO_2$-water nanifluids. Models have been developed by considering the fact that thermal conductivity of nanofluid is depends on so many parameters. Prandtl number and a new dimensionless quantity, which is a ratio of Reynolds and Brinkmans number for particle and fluids (to include the effects of micro-convection, Brownian motion of particles and viscous heat dissipation) are used to develop new models of thermal conductivity.

## 5.1 Development of Models for Thermal Conductivity of Nanofluids

The ratio of thermal conductivity of nanofluid to base fluid is believed to be depending on various particle and fluid properties, as given by:

$$\frac{K_{nf}}{K_f} = f(\chi, \rho_p, \rho_f, c_p, c_f, K_p, d, \mu, \phi, T_{abs}) \tag{5.1}$$

Using Buckingham Pi theorem, the following dimensionless groups have been obtained:

$$\Pi_1 = \frac{K_{nf}}{K_f}, \Pi_2 = \chi, \Pi_3 = \phi, \Pi_4 = \frac{\mu c_p}{K_p}, \Pi_5 = \frac{\mu c_f}{K_p}, \Pi_6 = \frac{\rho_p d}{\mu}\sqrt{\frac{K_p T_{abs}}{\mu}}, \Pi_7 = \frac{\rho_f d}{\mu}\sqrt{\frac{K_p T_{abs}}{\mu}}$$

$\Pi_4$ and $\Pi_5$ represents the Prandtl numbers for particles ($Pr_p$) and base fluid ($Pr_f$), respectively.

$\Pi_6$ and $\Pi_7$ can also be represented as:

$$\Pi_6 = \frac{\frac{\rho_p dv}{\mu}}{\sqrt{\frac{\mu v^2}{K_p(T_{abs} - T_0)}}}, \Pi_7 = \frac{\frac{\rho_f dv}{\mu}}{\sqrt{\frac{\mu v^2}{K_p(T_{abs} - T_0)}}}$$

Where, $T_0$: 0 K, $T_{abs}$: absolute temperature in K. Introduction of the 'v' term (conceptualized as the local fluid velocity) in the above dimensionless groupings transforms $\Pi_6$ and $\Pi_7$ as:

$$\Pi_6 = \frac{\mathrm{Re}_p}{\sqrt{N_{BRp}}}, \Pi_7 = \frac{\mathrm{Re}_f}{\sqrt{N_{BRp}}}$$

$$Where, \mathrm{Re}_p = \frac{\rho_p dv}{\mu}, \mathrm{Re}_f = \frac{\rho_f dv}{\mu}, N_{BRp} = \frac{\mu v^2}{K_p(T_{abs} - T_0)}$$

Brinkman number is a dimensionless number signifying the ratio of heat transfer by diffusion to conduction (Yarin et al., 2009).

Using experimental data for $Al_2O_3$-water nanofluids and $TiO_2$-water nanofluids for a wide range of volume fraction, particle size and temperature, the following models has been derived using regression analysis. Model given in equation 5.2 is for $Al_2O_3$-water nanofluids and in equation 5.3 is for $TiO_2$-water nanofluids.

$$\frac{K_{nf}}{K_f} = 0.35\phi^{0.035}\,\mathrm{Pr}_p^{\,0.34}\,\mathrm{Pr}_f^{\,-0.38}\left(\frac{\mathrm{Re}_p}{\sqrt{N_{BRp}}}\right)^{-0.017} \tag{5.2}$$

$$\frac{K_{nf}}{K_f} = 0.103\phi^{0.029}\,\mathrm{Pr}_p^{\,0.88}\,\mathrm{Pr}_f^{\,-0.77}\left(\frac{\mathrm{Re}_p}{\sqrt{N_{BRp}}}\right)^{-0.117} \tag{5.3}$$

The values exponents of $\Pi_2$ and $\Pi_7$ have come equal to zero as $Al_2O_3/TiO_2$ particles have been assumed to be spherical (with aspect ratio:1) and density and specific heat of the base-fluid (DI

water) has been considered to be almost unchanged over the range of experimental conditions (15 to 70$^{o}$C). The values of these exponents are expected to be non-zero if the model were developed using nano-particle of different shapes and base-fluids with different properties. The above models have been used to predict the nanofluid thermal conductivity and the predicted versus experimental values of thermal conductivity of nanofluids are provided in Figure 5.1 (for of $Al_2O_3$-water nanifluids) and Figure 5.2 (for $TiO_2$-water nanifluids). The comparison plots show that the new model generally predicts within $\pm$5% accuracy range for $Al_2O_3$-water nanofluids and $\pm$6% for $TiO_2$-water nanofluids.

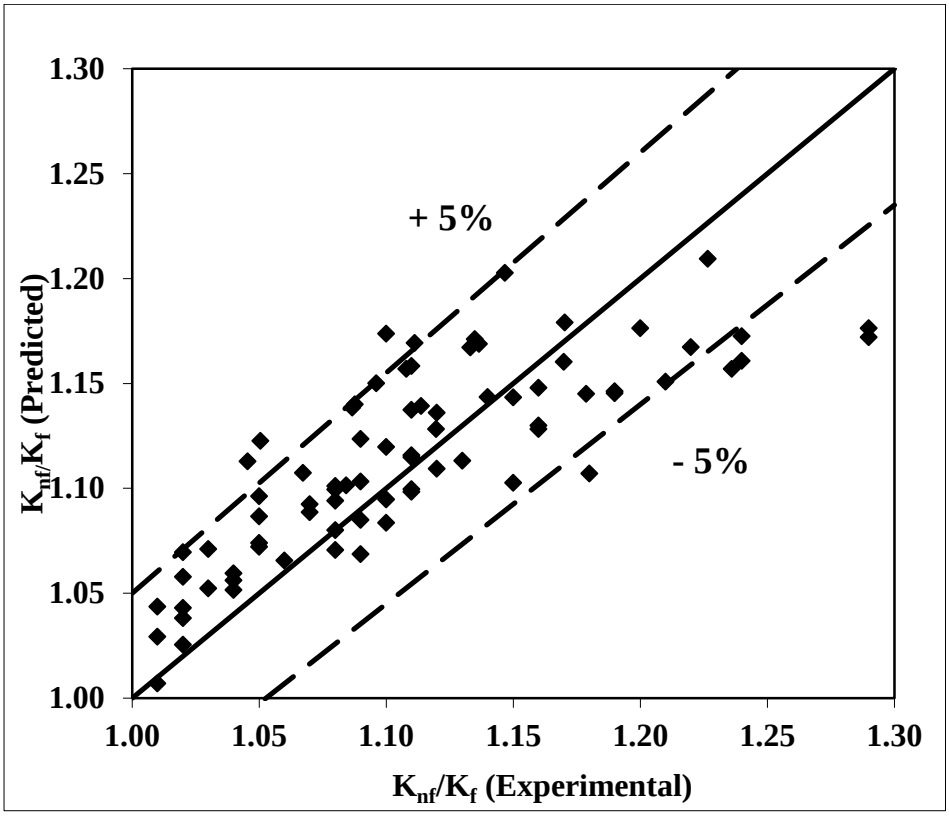


**Figure 5.1:** Experimental versus predicted values of thermal conductivity for $Al_2O_3$-water nanofluids using new model given (equation 5.2).

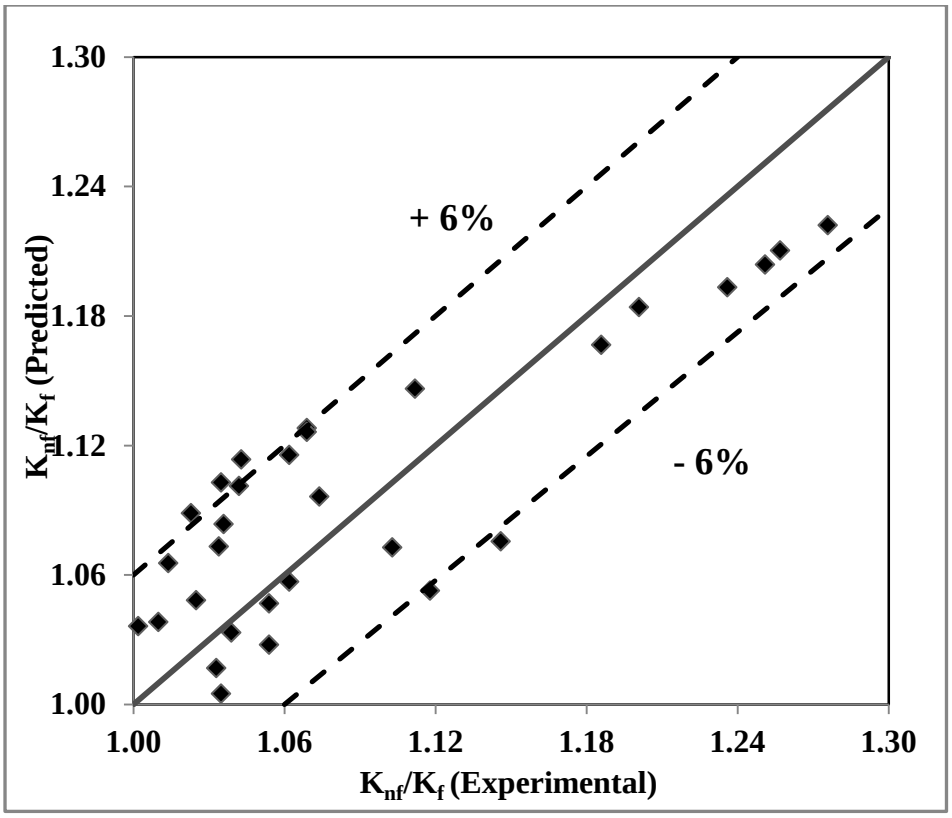


**Figure 5.2:** Experimental versus predicted values of thermal conductivity for $TiO_2$-water nanofluids using new model given (equation 5.3).

## 5.2 Validation of New Developed Models:

The above models (equation 5.2 and 5.3) has been further evaluated by using it to predict the nanofluid thermal conductivity for a range of experimental conditions and by comparing the predicted versus experimental values.

In Figure 5.3, experimental values of thermal conductivity ratio obtained from Li and Peterson (2007) at $Al_2O_3$ nanoparticles of diameter 36 nm, 35.5$^oC$ temperature and given volume fraction range are compared with that obtained from new developed model for $Al_2O_3$ (equation 5.2).

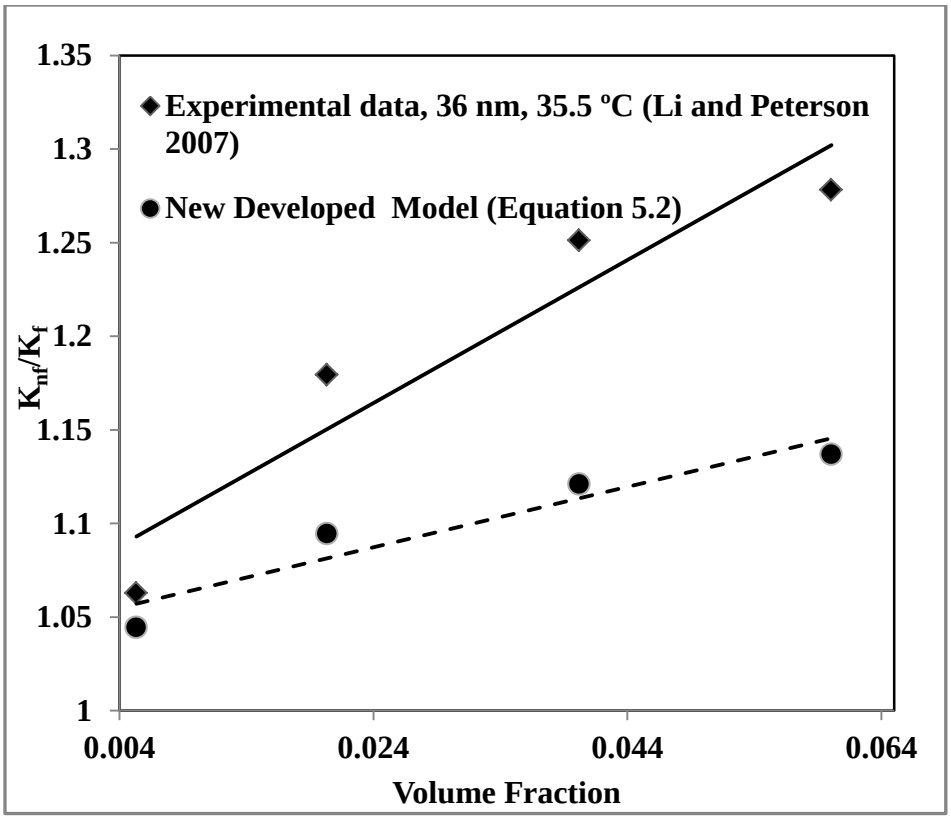


**Figure 5.3:** Experimental versus predicted values (present model) of thermal conductivity ratio with increase in volume, d: 36 nm, T: 35.5$^{o}$C.

Figure 5.3 shows that the thermal conductivity ratio obtained from new developed model under predict the experimental values. The trend of predictions obtained using new developed model is almost parallel to the experimental data. In Figure 5.4, experimental values of thermal conductivity ratio obtained from Mintsa et al. (2009 ) at $Al_2O_3$ nanoparticles of diameter 47 nm, 4% volume fraction and given temperature range are compared with that obtained from new developed model for $Al_2O_3$ (equation 5.2).

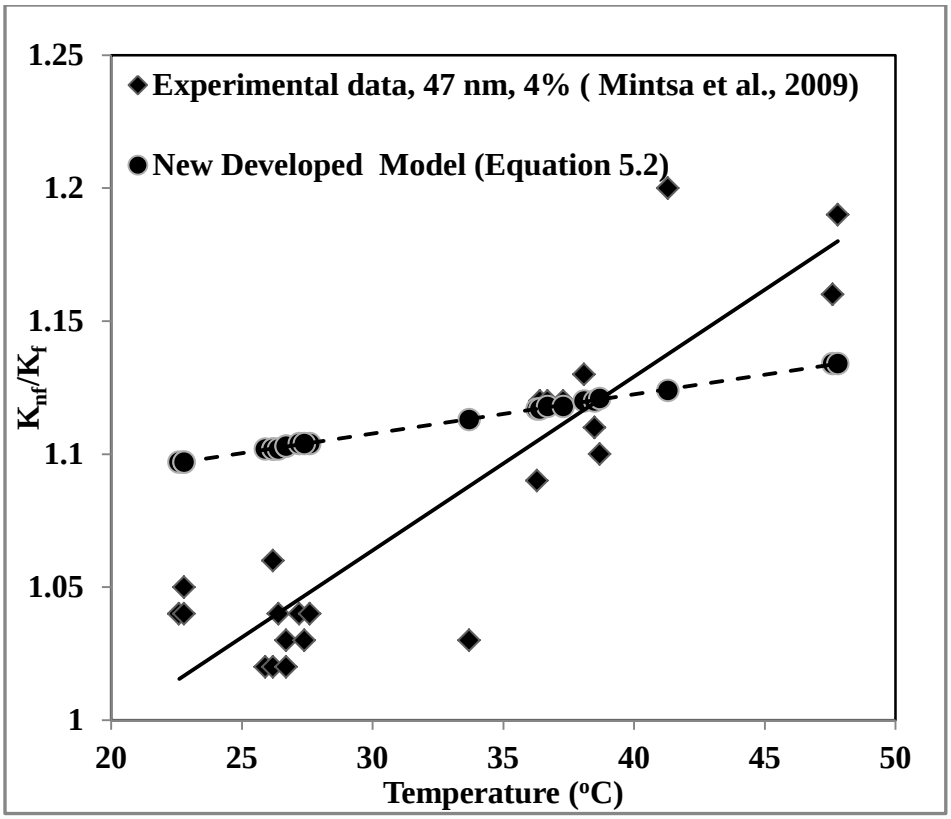


**Figure 5.4:** Experimental versus predicted values (present model) of thermal conductivity ratio with increase in temperature of $Al_2O_3$ nanoparticles, d: 47 nm, $\phi$: 4%.

Figure 5.4 shows that below 40$^o$C new developed model over predict the experimental values and above 40$^o$C model under predict the experimental values. Thermal conductivity ratio obtained from experiment and model increases with increase in temperature. In Figure 5.5, experimental values of thermal conductivity ratio obtained from Chandrasekar et al. (2010) at $Al_2O_3$ nanoparticles of diameter 43 nm, room temperature and given volume fraction range are compared with that obtained from the new developed model for $Al_2O_3$ (equation 5.2).

.

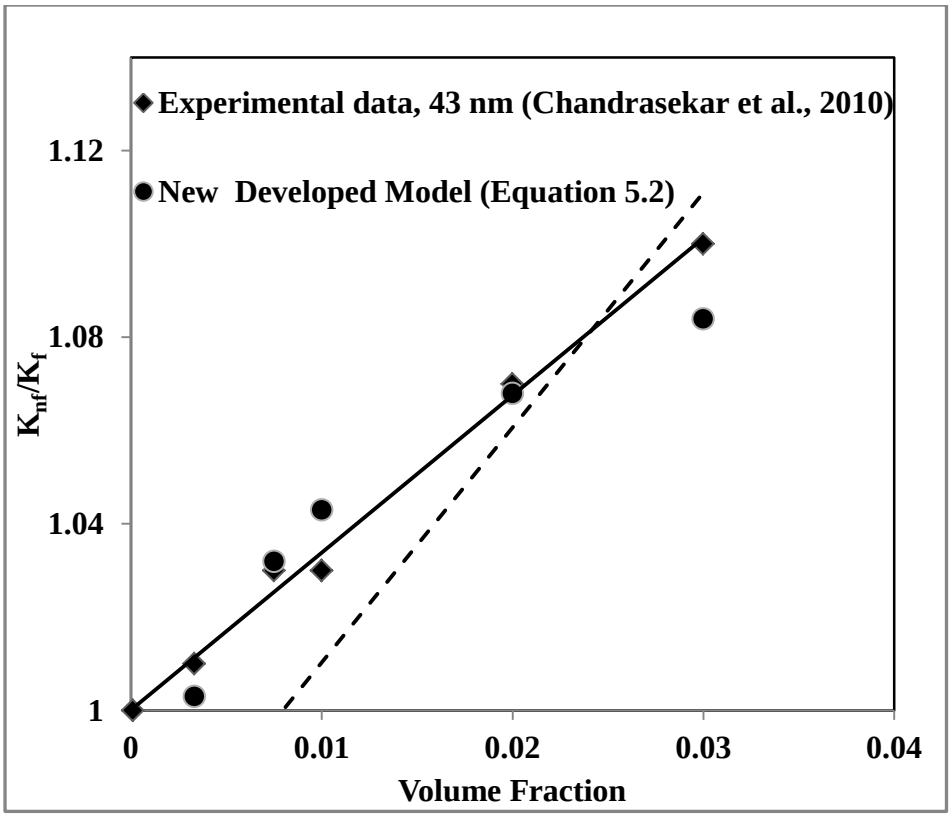


**Figure 5.5:** Experimental versus predicted values (present model) of thermal conductivity ratio with increase in volume fraction of $Al_2O_3$ nanoparticles, d: 36 nm, T: room temperature ($20^oC$).

Figure 5.5 shows that values of thermal conductivity ratio obtained from new developed model are very close to that obtained from experiment. Thermal conductivity ratio increases with increase in volume fraction. Experimental values of thermal conductivity ratio obtained from Wang et al. (1999) at $Al_2O_3$ nanoparticles of diameter 28 nm, $24^oC$ and given volume fraction range are compared with that obtained from new developed model for $Al_2O_3$ (equation 5.2) in Figure 5.6.

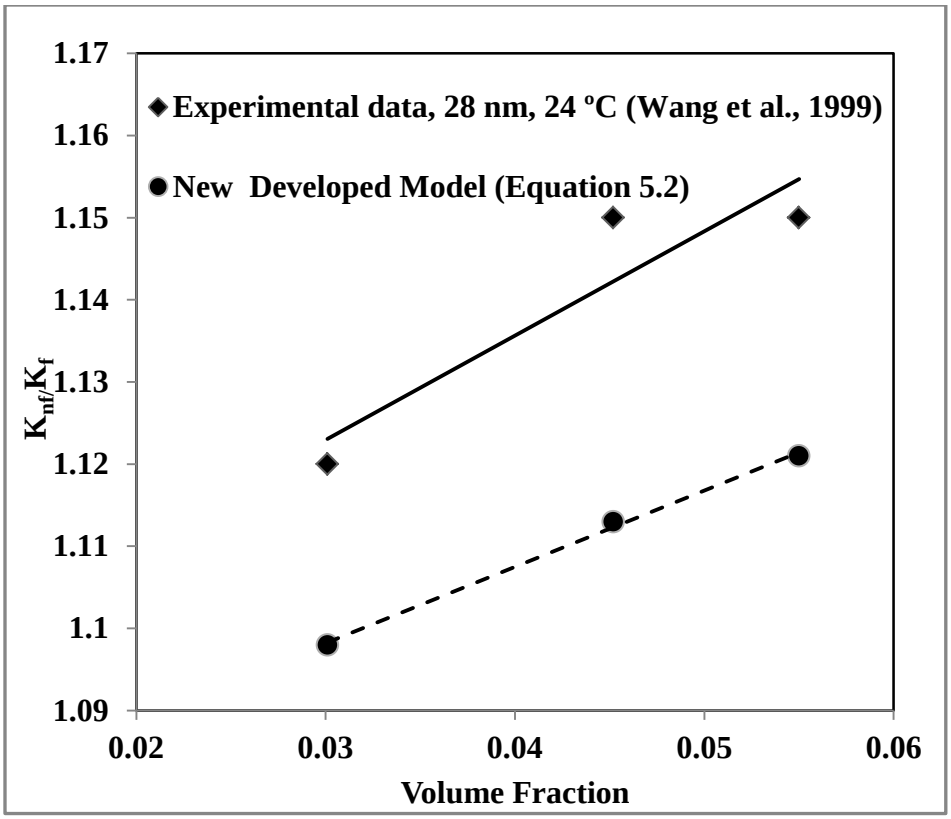


**Figure 5.6:** Experimental versus predicted values (present model) of thermal conductivity ratio with increase in volume fraction of $Al_2O_3$ nanoparticles, d: 28 nm, T: 24$^oC$.

In Figure 5.6 thermal conductivity ratio obtained from model under predicts the experimental values. Thermal conductivity ratio increases with increase in volume fraction. Experimental values of thermal conductivity ratio obtained from Wang et al. (2007) at $TiO_2$ nanoparticles of diameter 26 nm, 18$^oC$ and given volume fraction range are compared with that obtained from new developed model for $TiO_2$ (equation 5.3) in Figure 5.7.

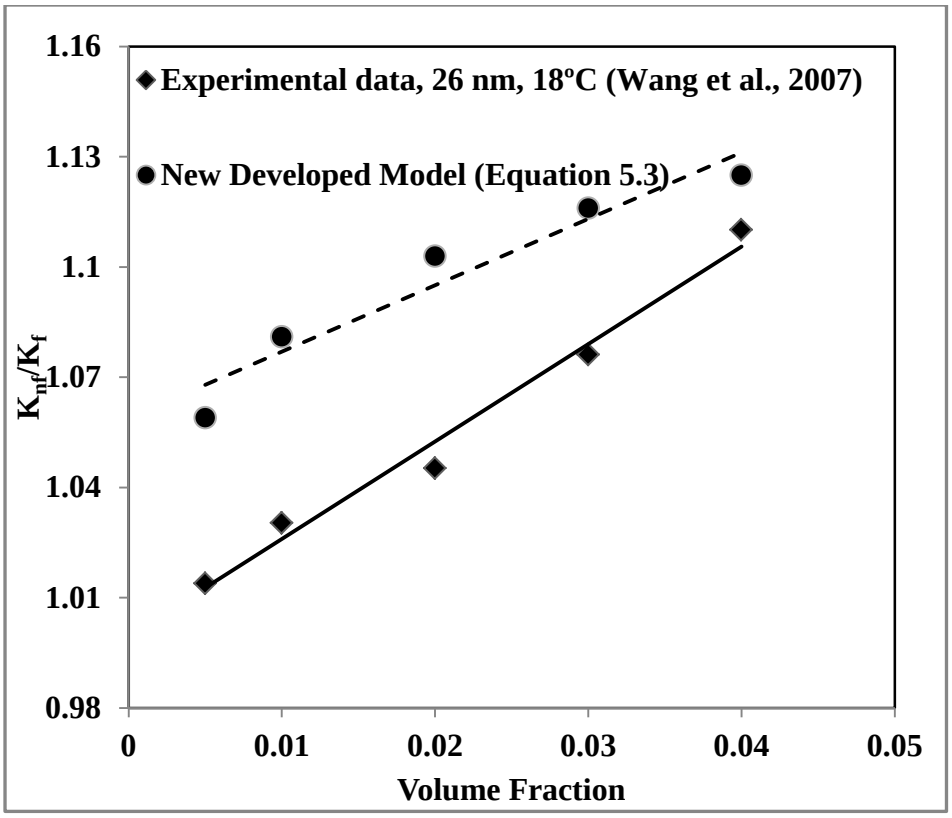


**Figure 5.7:** Experimental versus predicted values (present model) of thermal conductivity ratio with increase in volume fraction of $TiO_2$ nanoparticles, d: 26 nm, T: 18$^o$C.

In Figure 5.7 thermal conductivity ratio obtained from model over predicts the experimental values. Thermal conductivity ratio increases with increase in volume fraction.

Table 5.1 provides average of sum of absolute values of relative error for thermal conductivity ratio (using the formula given below) to indicate the prediction accuracies of the new developed model (Figure 5.3 to 5.7).

$$\text{Relative error} = \sum_{n} \frac{\text{experimental value} - \text{predicted value}}{\text{experimental value}} \times 100\ \%$$

**Table 5.1:** Relative Errors of New Developed Model Predictions (%)

| **Figures** | **New developed model for $Al_2O_3$ (Equation 5.2)** | **New developed model for $TiO_2$ (Equation 5.3)** |
|---|---|---|
| 5.3 | 5.22 | - |
| 5.4 | 4.53 | - |
| 5.5 | 0.79 | - |
| 5.6 | 2.57 | - |
| 5.7 | - | 3.98 |

From the error analysis it is clear that the existing new model for $Al_2O_3$-water nanofluids provides inaccuracies (over/under-predictions) in the range of 0.78-4.53% and existing new model for $TiO_2$-water nanofluids provide inaccuracy (over -predictions) of 3.98%.

# Chapter 6: Conclusion and Future Scope of Work

## 6.1 Conclusion

- Thermal conductivity of nanofluids increases with increase in volume fraction of nanoparticles in base fluid, temperature of nanofluids and decrease in size of nanoparticles,
- Evaluation of accuracy of existing theoretical and empirical models for thermal conductivity of $Al_2O_3$-water/ $TiO_2$-water nanofluids by comparing the predicted versus experimental values have revealed that the existing models provide inaccuracy within 2-47% range.
- A new thermal conductivity models have been developed using dimensionless analysis, which includes Prandtl number and a new dimensionless number that is a ratio to Reynolds number to the square root of Brinkman number for particle and fluids. The new models have been found to generally predict thermal conductivity of nanofluids within $\pm$ 5% accuracy range for $Al_2O_3$-water naofluids and $\pm$6% accuracy range for $TiO_2$-water nanofluids.
- Further studies are required to better understand the mechanism of heat conduction through nanofluids and the influence of different experimental conditions on the thermal conductivity of nanofluids for more accurate modelling.

## 6.2 Future Scope of Work

- More fundamental study has to be carried out for the effect of different parameters on thermal conductivity of nannofluids.

- A standard theoretical model for nanofluid thermal conductivity has to be developed by taking consideration of all the possible mechanisms such as interracial layer, brawnion motion, clustering etc. and effect of all the factors such as size, shape, temperature, volume fraction, ultrasonication time and pH.
- A standard design of experiment for thermal conductivity of nanofluid can be proposed by doing efficient number of experiments over wide range of variables.
- More application based testing is required to evaluate the effect of convection phenomenon and pool boiling.

# List of Publications

**Referred Journals (Under Review) – 2 Nos.**

Mallick S.S., Mishra A. and Kundan L., An Investigation into Modelling Thermal Conductivity for Alumina-Water Nanofluids, Powder Technology (**Accepted**).

Mishra A., Kundan L.and Mallick S.S., Modelling Thermal Conductivity for Alumina-Water Nanofluids, Particulate Science and Technology (Under Review).

**Referred Conferences (Published/Accepted) – 2 Nos.**

Mishra A. and Mallick, S.S., Modelling Thermal Conductivity for Nanopowder Suspension in Fluid (Nanofluid), CHoPS 2012 conference, 10 to 13 September 2012, Germany (Accepted for oral presentaion).

Mishra A. and Mallick, S.S., Modelling Thermal Conductivity of Alumina Nanofluids, National Conference on Emerging Trends in Mechanical & Electrical Engineering (NCETMEE-12), 12-13 June 2012, Lucknow

# Appendix

## Appendix A

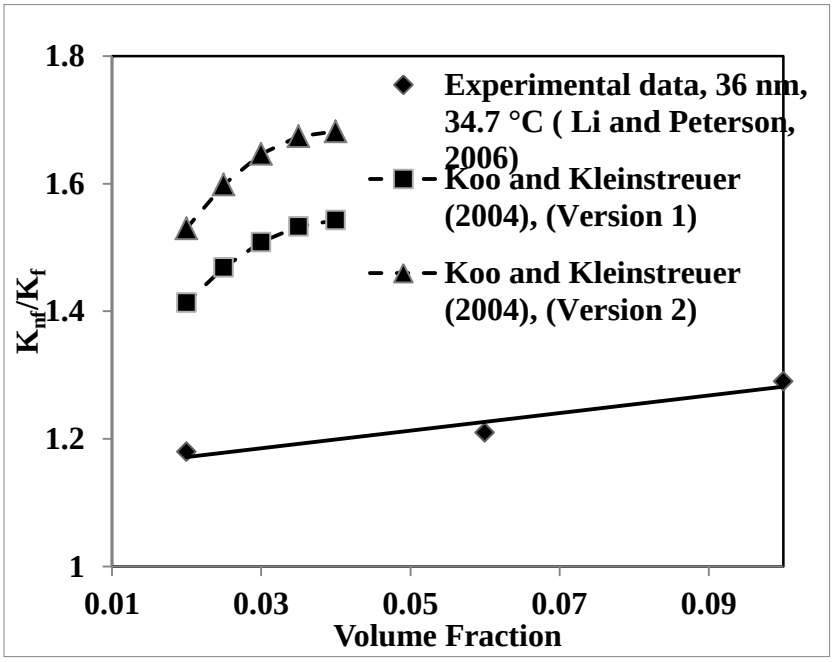


**Figure A1:** Experimental versus predicted values of thermal conductivity ratio with increase in volume fraction, d: 36 nm, T: 34.7 °C.

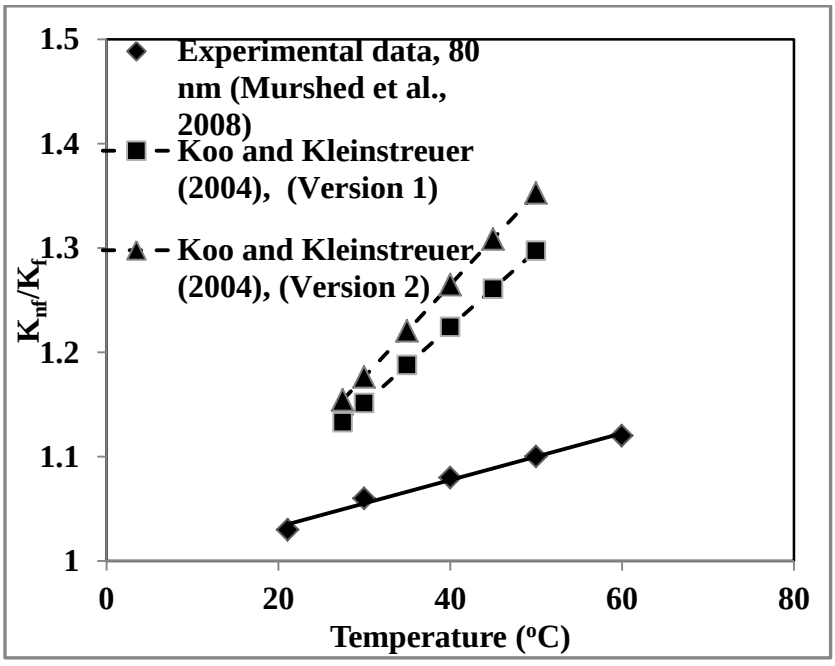


**Figure A2:** Experimental versus predicted values of thermal conductivity ratio with increase in temperature, d: 80 nm, φ: 1%.

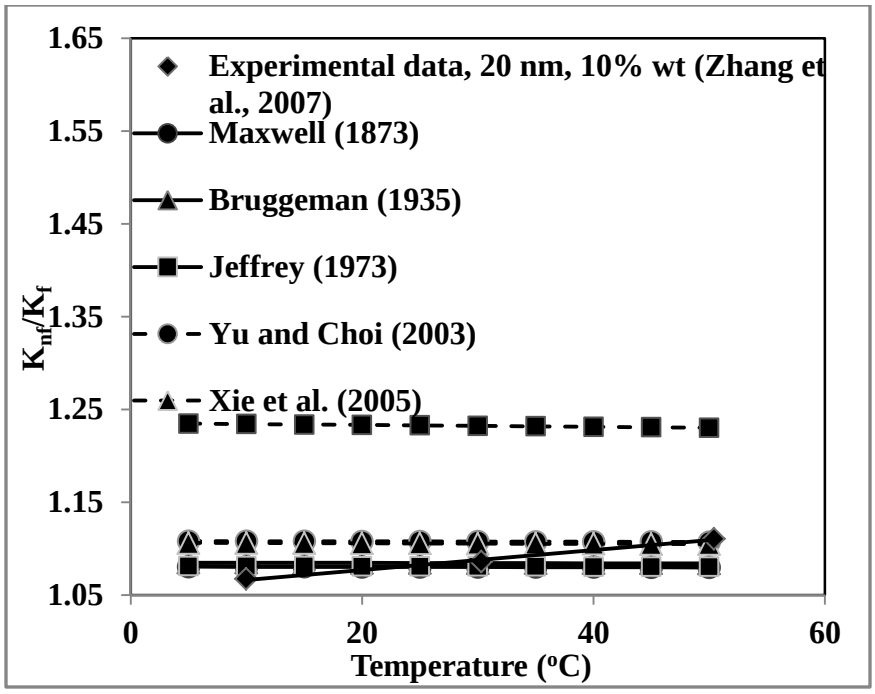


**Figure A3:** Experimental versus predicted values of thermal conductivity ratio with increase in temperature, d: 200 nm, weight fraction: 10%.

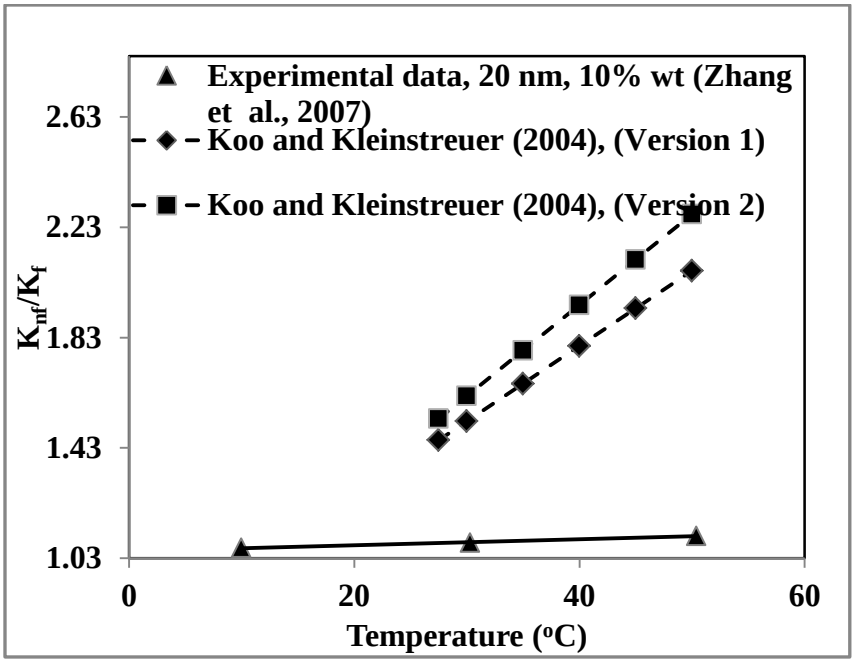


**Figure A4:** Experimental versus predicted values of thermal conductivity ratio with increase in temperature, d: 80 nm, $\phi$: 1%.

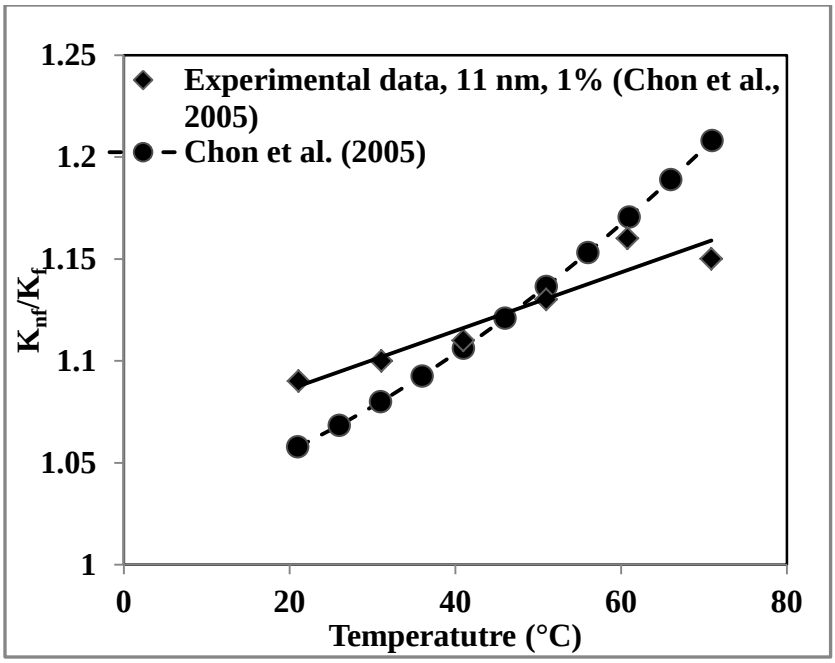


**Figure A5:** Experimental versus predicted values of thermal conductivity ratio with increase in temperature, d: 11 nm, $\phi$: 1%.

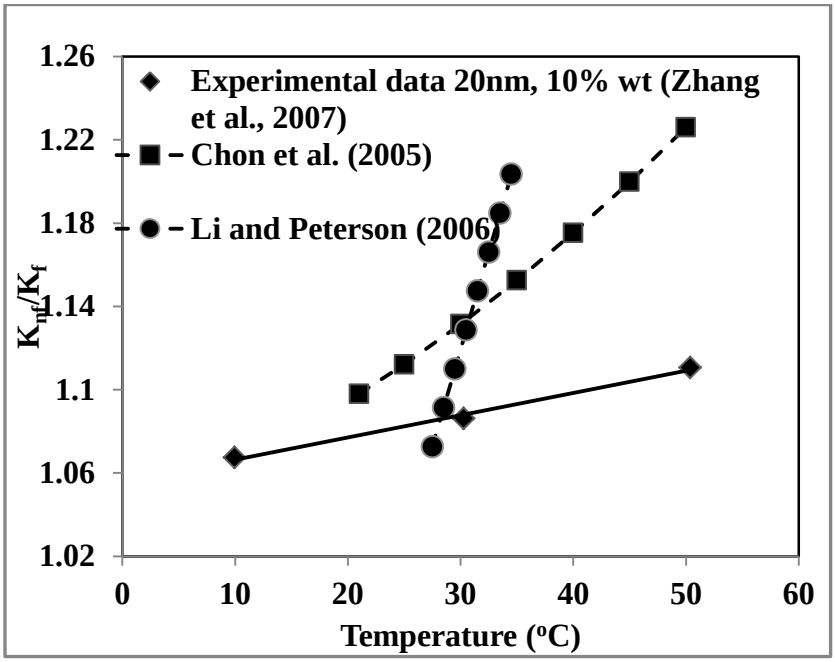


**Figure A6:** Experimental versus predicted values of thermal conductivity ratio with increase in volume fraction of $Al_2O_3$ nanoparticles, d: 20 nm, $\omega$ : 10%.

## Appendix B

A brief discussion on design of experiment (DOE) and Taguchi method is discussed in this section.

### Design of Experiment (DOE)

a) In 1920 R. A. Fisher introduced design of experiments as a statistical technique.
b) Design of Experiments is a powerful statistical based approach to study the effect of multiple variables/factors/parameters simultaneously.
c) Design of experiments is very effective when the performance of the process/experiment is controlled by more than one parameter/factor.

### Design of experiment using Taguchi Method

Taguchi method or Taguchi approach is a modified and standardized form of design experiments with special principles. Taguchi technique in DOE improves the consistency of the performance. Taguchi improved or simplify the DOE by incorporating following in the process of application (Roy, 2001):

a) Standard procedure of analysis.
b) Clear guidelines for results incorporation.
c) Special data transformation to obtain reduce variation.
d) Formal study of uncontrollable factors/parameters/variables through robust design technique.

Overall attempt of design of experiment using Taguchi approach is to improve consistency of the performance.

An attempt has been made to prepare the design of experiment using Taguchi design in minitab 14 for doing experiments for measuring thermal conductivity of nanofluids, whose ultimate aim is to shows how many minimum number of times experiment has to obtain quality results by varying number of variables/factors.

For the design of experiment using Taguchi design for measuring thermal conductivity of nanofluid 5 level design and 6 factors are selected. 6 factors are size of nanoparticles, shape of the nanoparyicles, volume concentration of nanoparticles in base fluid, temperature of nanofluids, ultrasonication time to prepare nanofluid and pH value of nanofluids.

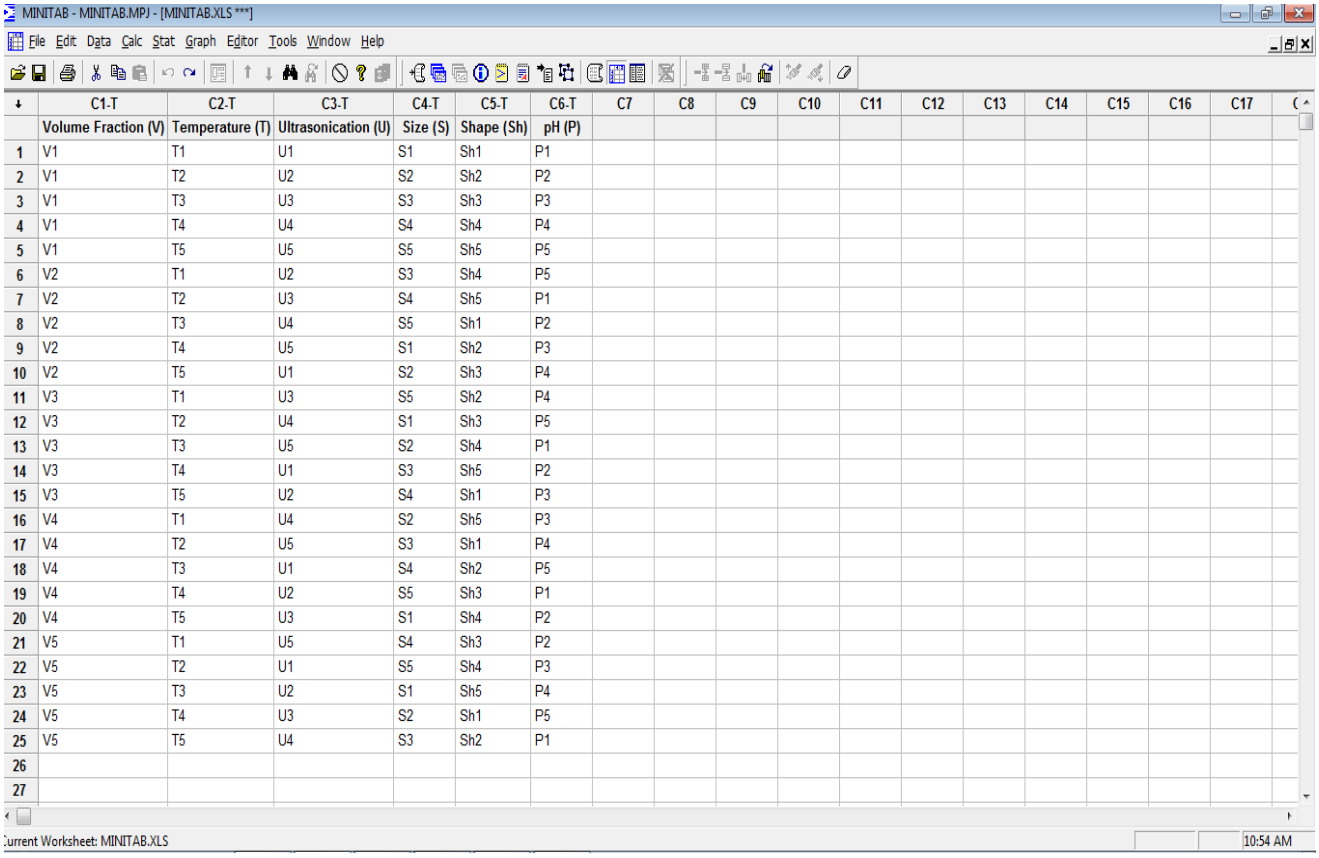


| | C1-T | C2-T | C3-T | C4-T | C5-T | C6-T | C7 | C8 | C9 | C10 | C11 | C12 | C13 | C14 | C15 | C16 | C17 |
|---|---|---|---|---|---|---|---|---|---|---|---|---|---|---|---|---|---|
| | Volume Fraction (V) | Temperature (T) | Ultrasonication (U) | Size (S) | Shape (Sh) | pH (P) | | | | | | | | | | | |
| 1 | V1 | T1 | U1 | S1 | Sh1 | P1 | | | | | | | | | | | |
| 2 | V1 | T2 | U2 | S2 | Sh2 | P2 | | | | | | | | | | | |
| 3 | V1 | T3 | U3 | S3 | Sh3 | P3 | | | | | | | | | | | |
| 4 | V1 | T4 | U4 | S4 | Sh4 | P4 | | | | | | | | | | | |
| 5 | V1 | T5 | U5 | S5 | Sh5 | P5 | | | | | | | | | | | |
| 6 | V2 | T1 | U2 | S3 | Sh4 | P5 | | | | | | | | | | | |
| 7 | V2 | T2 | U3 | S4 | Sh5 | P1 | | | | | | | | | | | |
| 8 | V2 | T3 | U4 | S5 | Sh1 | P2 | | | | | | | | | | | |
| 9 | V2 | T4 | U5 | S1 | Sh2 | P3 | | | | | | | | | | | |
| 10 | V2 | T5 | U1 | S2 | Sh3 | P4 | | | | | | | | | | | |
| 11 | V3 | T1 | U3 | S5 | Sh2 | P4 | | | | | | | | | | | |
| 12 | V3 | T2 | U4 | S1 | Sh3 | P5 | | | | | | | | | | | |
| 13 | V3 | T3 | U5 | S2 | Sh4 | P1 | | | | | | | | | | | |
| 14 | V3 | T4 | U1 | S3 | Sh5 | P2 | | | | | | | | | | | |
| 15 | V3 | T5 | U2 | S4 | Sh1 | P3 | | | | | | | | | | | |
| 16 | V4 | T1 | U4 | S2 | Sh5 | P3 | | | | | | | | | | | |
| 17 | V4 | T2 | U5 | S3 | Sh1 | P4 | | | | | | | | | | | |
| 18 | V4 | T3 | U1 | S4 | Sh2 | P5 | | | | | | | | | | | |
| 19 | V4 | T4 | U2 | S5 | Sh3 | P1 | | | | | | | | | | | |
| 20 | V4 | T5 | U3 | S1 | Sh4 | P2 | | | | | | | | | | | |
| 21 | V5 | T1 | U5 | S4 | Sh3 | P2 | | | | | | | | | | | |
| 22 | V5 | T2 | U1 | S5 | Sh4 | P3 | | | | | | | | | | | |
| 23 | V5 | T3 | U2 | S1 | Sh5 | P4 | | | | | | | | | | | |
| 24 | V5 | T4 | U3 | S2 | Sh1 | P5 | | | | | | | | | | | |
| 25 | V5 | T5 | U4 | S3 | Sh2 | P1 | | | | | | | | | | | |
| 26 | | | | | | | | | | | | | | | | | |
| 27 | | | | | | | | | | | | | | | | | |

Above table specified that at what value of parameters each experiment has to conduct.

## Appendix C

During the thesis work $Al_2O_3$ nanoparticles are synthesis by method proposed by Zhai et al. (2006) i.e."combustion synthesis of the nano-structured alumina powder". Steps performed to synthesis $Al_2O_3$ nanoparticles are shown in Figure C1.

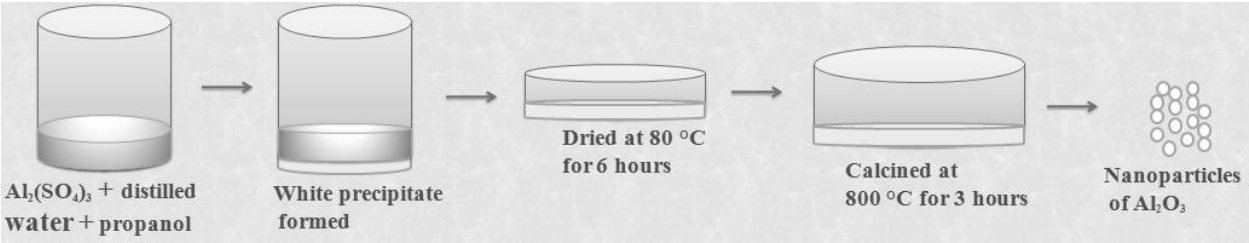


**Figure C1:** Steps in synthesis of $Al_2O_3$ nanoparticles (using Zhai et al., 2006 method).

X-Ray diffraction result and SEM image of prepared $Al_2O_3$ nanoparticles sample is shown in Figure C2. Average size of prepared $Al_2O_3$ nanoparticles is 136 nm.

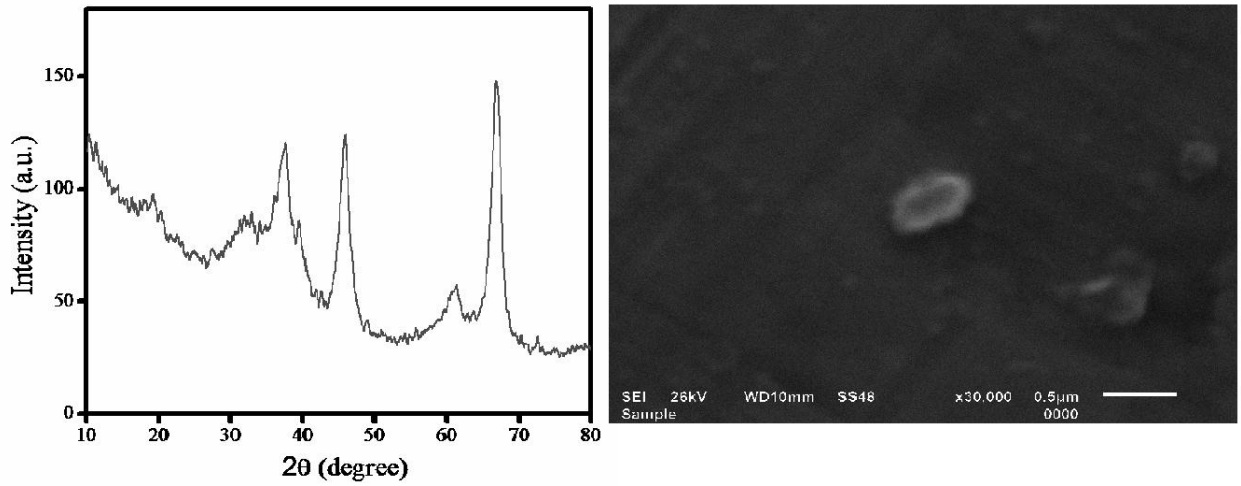


**Figure C2:** X-Ray diffraction analysis and SEM of prepared $Al_2O_3$ nanoparticles

**List of Symbols**

A : Coulomb constant ($9 \times 10^{9} Nm^2 C^{-2}$)

a : Cross section area ($m^2$)

C : Specific heat (J/kg K)

$C_1$ : Proportionality constant

$C_{R.M}$ : Random motion velocity

d : Particle diameter (m/nm)

h : Length of wire (m)

i : Time (Sec)

I : Current (A)

K : Thermal conductivity (W/mK)

$K_B$ : Boltzmann constant ($1.3807 \times 10^{-23}$ J/K)

L : Average distance for a particle to travel along one direction due to the particle Brownian motion (m)

$l$ : Mean free path (nm)

M' : Molecular weight (Kg/Kmol)

m : Mass (Kg)

$N_{BR}$ : Brinkman number

n : Particle concentration ($m^{-3}$)

P : Input power (Watt)

P : Probability for a particle to travel along any direction

Q : Heat flux ( $W/m^2$)

q : Electric charge (C)

Pr : Prandtl number

Re : Reynolds number

r : Particle radius (nm)

T : Temperature (K)

$\Delta T$ : Temperature difference

t: Temperature ($^oC$)

u : Molecular number density

$V_{Br}$ : Brownian velocity of nanoparticles

V : Voltage (V)

X : Thickness of the glass spacer between the two copper plates (m)

: Distance along copper bar/ two cell surfaces

**Greek symbols**

Φ : Volume fraction of nanoparticles

Ψ : Sphericity

α : Thermal diffusivity ($m^2$/sec)

$\kappa$ : Ratio of thermal conductivity of particle to that of base fluid

β : ($\kappa$ - 1) / ($\kappa$ +2)

ρ : density ($kg/m^3$)

γ : Ratio of nanolayer thickness to radius of nanoparticles

$\mu$ : Viscosity (Pa.s)

$\upsilon$ : Kinematic viscosity (Stoke)

$\varepsilon'$ : Dielectric constant of medium

$\delta$ : Nanolayer/interfacial layer thickness (nm)

$\chi$ : Shape factor

$\omega$ : Weight fraction (%)

**Subscript**

c : Top copper plate

g : Glass spacers

p : Particle/nanoparticle

f : Base fluid

*l* : Liquid phase (for base fluid)

lr : Interfacial layer

nf : Nanofluid

EDL : Electrical double layer

**Abbreviation**

DI : Deionized water

R : Correlation coefficient

**References**

Akoh H., Tsukasaki Y., Yatsuya S., and Tasaki A., 1978, Magnetic Properties of Ferromagnetic Uhrafine Particles Prepared by a Vacuum Evaporation on Running Oil Substrate, J Cryst. Growth, Vol. 45, PP. 495-500.

Ashly S., 1994, Small-Scale Structure Yields Big Property Payoffsfl, Mechanical Engineering, Vol. 116, Issue. 2, PP. 52-57.

Bruggeman D.A.G., 1935, Berechnung verschiedener physikalischer Konstanten von heterogenen Substanzen. I. Dielektrizitätskonstanten und Leitfähigkeiten der Mischkörper aus isotropen Substanzen, Annalen der Physik, Vol. 416, Issue 7, PP. 636–664.

Buhr E., Senftleben N,, Klein T., Bergmann D., Gnieser D., Frase C. G. and Bosse H., 2009,Characterization of Nanoparticles by Scanning Electron Microscopy in Transmission Mode, Measurement Science and Technology, Vol. 20, Issue. 084025, PP. 1-9.

Beck M.P., Yuan Y., Warrier P. and Teja A.S., 2009, The Effect of Particle Size on the Thermal Conductivity of Alumina Nanofluids, Nanopart Res, Vol. 11, PP. 1129–1136.

Bhattacharya P., Samanta A.N. and Chakraborty S., 2009, Numerical Study of Conjugate Heat Transfer in Rectangular Microchannel Heat Sink With $Al_2o_3/H_2O$ Nanofluids, Heat Mass Transfer, Vol. 45, PP. 1323–1333.

Choi S.U.S., 1995, Developments and Applications of Non-Newtonian Flows, Fed Vol. 231/Md Vol. 66, pp. 99–105.

Choi S. U. S., 1999, Nanofluid Technology: Current Status and Future Research, Stephen U.S. Choi Energy Technology Division Argonne National Laboratory Argonne, Il 60439.

Cullity B.D. and Stock S.R., 2001, Elements of X-Ray Diffraction, Third Edition, Pub. Prentice Hall.

Chon C.H., Kihm K.D., Lee S.P. and Choi S.U.S., 2005, Empirical Correlation Finding The Role of Temperature and Particle Size for Nanofluid ($Al_2O_3$) Thermal Conductivity Enhancement, Physics Letter, Vol. 87, Issue. 153107, PP. 1-3.

Chopkar M., Sudarshan S., Das P.K., and Manna I., 2008, Effect of Particle Size on Thermal Conductivity of Nanofluid, Metals & Materials Society, Volume 39 A, PP. 1535-1542.

Chandrasekar M., Suresh S. and Bose A.C., 2010, Experimental Investigations and Theoretical Determination of Thermal Conductivity and Viscosity of $Al_2O_3$/Water Nanofluid, Experimental Thermal and Fluid Science, Vol. 34, PP. 210-216.

Das S.K., Putra N., Thiesen P. and Roetzel W., 2003, Temperature Dependence of Thermal Conductivity Enhancement for Nanofluids, Heat Transfer, Vol. 125, PP. 567-574.

Das S.K., Choi S.U.S., Yu W. and Pradeep K., 2007, Nanofluids Science and Technology, Publ. Wiley Interscience.

Eastman J. A., Choi U. S., Li S., Thompson L. J., and Lee S., 1997, Enhanced Thermal Conductivity through the Development of Nanofluids, Y Proc. of the Symposium on Nanophase and Nanocomposite Materials H, Materials Research Society, Boston, Vol. 457, PP. 3-11.

Granqvisq C. G., and Buhrrnan, R. A., 1976, Ultrtilne Metal Particles, J Applied Physics, Vol.47, PP. 2200.

Gabriel B.L., 1985, SEM: A User Manual For Material Science, American Society For Metals.
Gleiter, H., 1989, Nanocrystalline Materials, Prog. Material Science, Vol. 33, PP. 223-315.

Gallego M.J.P., Lugo L., Legido J.L. and Pineiro M.M., 2011, Thermal conductivity and viscosity measurements of ethylene glycol-based Al2O3 nanofluids Nanoscale Research Letters, Vol. 6:211, PP. 1-11.

Hamilton R.L. and Crosser O.K., 1962, Thermal Conductivity of Heterogeneous Two-Component, I & EC Fund, Vol. 1, PP. 187-191.

He Y., Men Y., Zhao Y., Lu H., Ding Y., 2009 Numerical Investigation into The Convective Heat Transfer of $Tio_2$ Nanofluids Flowing Through a Straight Tube Under the Laminar Flow Conditions, Applied Thermal Engineering, Vol. 29, PP. 1965–1972.

Jeffrey D. J., 1973, Conductionthrough A Random Suspension of Spheres, Royal Society of London, Series A, Vol. 335, Issue. 1602, PP. 355–367.

Jang S.P. and Choi S.U.S., 2004, Role of Brownian Motion in The Enhanced Thermal Conductivity of Nanofluids, Applied Physics Letters, Vol. 84, Issue. 21, PP. 4316-4318.

Jang S.P., Hwang K.S., Lee J.H., Kim J.H., Lee B.H. and Choi S.U.S., 2007, Effective Thermal Conductivities and Viscosities of Water-based Nanofluids Containing $Al_2O_3$ with Low Concentration, 7th IEEE International Conference on Nanotechnology, PP. 1011-1014.

Jung J. Y. and Yoo J.Y., 2009, Thermal conductivity enhancement of nanofluids in conjunction with electrical double layer (EDL), Heat and Mass Transfer, Vol. 52, PP. 525–528.

Koo J. and Kleinstreuer C., 2004, A New Thermal Conductivity Model for Nanofluids, Nanoparticle Research, Vol. 6, PP. 577–588.

Kimoto K., Kamilaya Y., Nonoyama M., and Uyeda R., 1963, An Electron Microscope Study on Fine Metal Particles Prepared by Evaporation in Argon Gas at Low Pressure, Jpn. J. Appi. Phys., Vol. 2, PP. 702.

Koo J., 2004. Computational Nanofluid Flow and Heat Transfer Analyses as Applied to Micro-syslems, PhD Thesis. North Carolina State University, Raleigh, NC.

Kwak K. and Kim C., 2005, Viscosity and Thermal Conductivity of Copper Oxide nanofluid Dispersed In Ethylene Glycol, Korea-Australia Rheology , Vol. 17, Issue. 2, PP. 35-40.

Khanafer K., Vafai K., 2011, A Critical Synthesis of Thermophysical Characteristics of Nanofluids, Heat and Mass Transfer, Vol. 54, PP. 4410-4428.

Li C.H. and Peterson G.P., 2006, Experimental Investigation of Temperature and Volume Fraction Variations on The Effective Thermal Conductivity of Nanoparticle Suspensions (Nanofluids), Applied Physics, Vol. 99, Issue. 08314, PP. 1-8.

Li C. H. and Peterson G. P., 2007, The effect of particle size on the effective thermal conductivity of $Al_2O_3$-water nanofluids, Applied physics, Vol. 101, Issue. 044312, PP. 1-5.

Lin C.Y., Wang J.C. and Chen T.C., 2011, Analysis of Suspension and Heat Transfer Characteristics of Al2O3 Nanofluids Prepared Through Ultrasonic Vibration, Applied Energy, Vol. 88, PP. 4527-4533.

Maxwell J.C., 1873. A Treatise on Electricity and Magnetism, 2nd Ed., Clarendon Press, Oxford, United Kingdom.

Mintsa H.A., Roy G. and Nguyen C.T., 2007, New Temperature Dependent Thermal Conductivity Data of Water Based Nanofluids, 5th IASME/WSEAS Int. Conference on Heat Transfer, Thermal Engineering and Environment, Athens, Greece, PP. 290-294.

Murshed S.M.S., Leong K.C. and Yang C., 2005, Enhanced thermal conductivity of TiO2—water based nanofluids, International Journal of Thermal Sciences, Vol. 44, PP. 367–373.

Murshed S.M.S., Leong K.C. and Yang C., 2008, Investigations of Thermal Conductivity and Viscosity of Nanofluids, Thermal Sciences, Vol. 47, PP. 560–568.

Murshed S.M.S., Leong K.C., Yang C., 2009, A combined model for the effective thermal conductivity of nanofluids, Applied Thermal Engineering,Vol. 29, PP. 2477–2483.

Mintsa H.A., Roy G., Nguyen C.T. and Doucet D., 2009, New Temperature Dependent Thermal Conductivity Data for Water Based Nanofluids, Thermal Sciences, Vol. 48, PP. 363–371.

Roy R.K., 2001, Design of Experiment Using Taguchi Approach 16 Steps to Product & Process Improvement.

Rea U., McKrell M., Hu L.W. and Buongiorno J., 2009, Laminar Convective Heat Transfer and Viscous Pressure Loss of Alumina–Water and Zirconia–Water Nanofluids, Heat and Mass Transfer, Vol. 52, PP. 2042–2048.

Sundar L. S., Ramanathan S., Sharma K.V. and Babu P. S., 2007, Temperature Dependent Flow Charecteristics of Al2o3 Nanofluid, International Journal of Nanotechnology and Applications ,Vol. 1, Issue 2, PP. 35-44.

Stadtlander C. T. K.H., 2007, Scanning Electron Microscopy and Transmission Electron Microscopy of Mollicutes: Challenges and Opportunities, Modern Research and Educational Topics in Microscopy.

Suryanarayana C., Norton M.G., 1998, X-Ray Diffraction: A Practical Approach, Pub. Springer.

Waseda Y., Matsubara E. and Shinoda K., 2001, X-Ray Diffraction Crystallography, Pub. Springer.

Timofeeva E.V., Gavrilov A.N., McCloskey J.M., Tolmachev Y.V., Sprunt S., Lopatina L.M. and Selinger J.V., 2007, Thermal Conductivity and Particle Agglomeration In Alumina Nanofluids: Experiment And Theory, Physical Review E, Vol. 76, Issue. 061703, PP. 1-16.

Turgut A., Tavman I., Chirtoc M., Schuchmann H. P., Sauter C., Tavman S., 2009, Thermal Conductivity and Viscosity Measurements of Water-Based TiO2 Nanofluids, Thermophys, Vol. 30, PP. 1213–1226.

Teng T.P., Hung Y.H., Teng T.C., Moa H.E. and Hsu H.G., 2010, The Effect of Alumina/Water Nanofluid Particle Size on Thermal Conductivity, Thermal Engineering, Vol. 30, PP. 2213-2218.

Vajjha R.S. and Das D.K., 2009, Experimental Determination of Thermal Conductivity of Three Nanofluids and Development of New Correlations, Heat and Mass Transfer, Vol. 52, PP. 4675–4682.

Wagener M., Murty B. S., and Giinther B., 1997, Preparation of Metal IWmosuspensions by High-Pressure DC-Sputtering on Running Liquids; in Nanocrystalline and Narzocomposite

Malerials Z, eds. Komarnenl S., Parker J. C., and Wollenberger H. J. (Materials Research Society, Pittsburgh), Vol. 457, PP. 149-154.

Wang X., Xu X. and Choi S.U.S., 1999, Thermal Conductivity of Nanoparticle- Fluid Mixture, Thermo Physics and Heat Transfer, Vol. 13, Issue. 40, PP. 474-480.

Waseda y., Matsubara E. and Shinoda K., 2001, X-Ray Diffraction Crytalbgaphy, Publ. Springer.

Wang Z. L., Tang D.W., Liu S., Zheng X. H., Araki N., 2007, Thermal-Conductivity and Thermal-Diffusivity Measurements of Nanofluids by $3\omega$ Method and Mechanism Analysis of Heat Transport, Thermophys, Vol. 28, PP. 1255–1268.

Xie H.Q., Wang J.C., Xi T.G., Liu Y., Ai F. and Wu Q.R., 2002 , Thermal Conductivity Enhancement of Suspensions Containing Nanosized Alumia Particles, Applied Physics, Vol. 91, PP. 4568-4572.

Xie H., Fujii M. and Zhang X., 2005, Effect of Interfacial Nanolayer on The Effective Thermal Conductivity of Nanoparticle-Fluid Mixture, Heat and Mass Transfer, Vol. 48, PP. 2926–2932.

Yu W. and Choi S.U.S., 2003, The Role of Interfacial Layers in The Enhanced Thermal Conductivity of Nanofluids: A renovated Maxwell model, Nanoparticle Research, Vol. 5, PP. 167–171.

Yu W., France D.M., Choi S.U.S., and Routbort J.L., 2007, Review and Assessment of Nanofluid Technology for Transportation and Other Applications, Argonne National Laboratory.

Yoo D.H., Hong K.S. and Yang H.S., 2007, Study of Thermal Conductivity of Nanofluid for The Application of Heat Transfer Fluids', Thermochimic Ata, Vol. 455, PP. 66-69.

Yarin L.P., Mosyak A. and Hestroni G., 2009, Fluid Flow Heat Transfer and Boiling in Micro-Channels. Publ. Springer.

Zhang X., and Fujii M., 2000, Simultaneous Measurements of the Thermal Conductivity and Thermal Diffusivity of Molten Salts with a Transient Short-Hot-Wire Method International Journal of Thermophysics, Vol. 21, Issue. 1, PP. 71-84.

Yu W., Xie H., Chen L. and Li Y., 2009, Investigation of Thermal Conductivity and Viscosity of Ethylene Glycol Based Zno Nanofluid, Thermochimica Acta Vol. 491, Vol. 92–96.

Zhang X. and Fujii M., 2000, Simultaneous Measurements of The Thermal Conductivity and Thermal Diffusivity of Molten Salts with A Transient Short-Hot-Wire Method, Thermo physics. Vol. 21, Issue 1, PP. 71–84.

Zhu H., Zhang C., Liu S., Tang Y. and Yin Y., 2006, Effects of nanoparticle clustering and alignment on thermal conductivities of Fe3O4 aqueous nanofluids, Applied Physics Letters, Vol. 89,Issue. 023123, PP. 1-3.

Zhai X., Fu Y. and Chu G., 2006, Combustion synthesis of nano-structure alumina powder, Nanoscience, Vol. 11, Issue. 4, PP. 286-292.

Zhang X., Gu H. and Fujii M., 2007, Effective Thermal Conductivity and Thermal Diffusivity of Nanofluids Containing Spherical and Cylindrical Nanoparticles, Experimental Thermal and Fluid Science, Vol. 31, PP. 593–599.

Zhu D. , Li X., Wang N., Wang X., Gao J. and Li H., 2009, Dispersion behavior and thermal conductivity characteristics of Al2O3–H2O nanofluids, Current Applied Physics, Vol. 9, PP. 131–139.